

**“NUMERICAL AND EXPERIMENTAL STUDY  
OF OPEN CHANNEL FLOW WITH AND  
WITHOUT BAFFLE”**

THESIS SUBMITTED IN PARTIAL FULFILMENT OF THE  
REQUIREMENTS FOR AWARDDING THE DEGREE OF MASTER  
OF MECHANICAL ENGINEERING IN FACULTY OF  
ENGINEERING AND TECHNOLOGY

**JADAVPUR UNIVERSITY**

Submitted By,

**SANCHARI GHOSH**

Regd. No. 129397 of 2014-2015

Examination Roll No. M4MEC1619

**UNDER THE SUPERVISION OF**

**DR. DEBASISH ROY**

**&**

**DR. SNEHAMOY MAJUMDER**

**DEPARTMENT OF MECHANICAL  
ENGINEERING**

**JADAVPUR UNIVERSITY**

**KOLKATA-700032**

**INDIA**

**2016**

DEDICATED  
To  
MY PARENTS  
And *lovely* SISTER

**FACULTY OF ENGINEERING & TECHNOLOGY**  
**DEPARTMENT OF MECHANICAL ENGINEERING**  
**JADAVPUR UNIVERSITY**  
**KOLKATA**

**DECLARATION OF ORIGINALITY**  
**AND**  
**COMPLIANCE OF ACADEMIC ETHICS**

*I hereby declare that this thesis contains literature survey and original research work, by the undersigned candidate, as part of her **Master of Mechanical Engineering** studies.*

*All information in this document have been obtained and presented in accordance with academic rules and ethical conduct.*

*I also declare that, as required by these rules and conduct, I have fully cited and referenced all material and results that are not original to this work.*

Name: Sanchari Ghosh

Examination Roll Number: M4MEC1619

Thesis Title: **NUMERICAL AND EXPERIMENTAL STUDY OF OPEN CHANNEL FLOW WITH AND WITHOUT BAFFLE.**

Signature:

Date:

**FACULTY OF ENGINEERING & TECHNOLOGY**  
**DEPARTMENT OF MECHANICAL ENGINEERING**  
**JADAVPUR UNIVERSITY**  
**KOLKATA**

**CERTIFICATE OF RECOMMENDATION**

*We hereby recommend that this thesis under our supervision by **Sanchari Ghosh**, entitled, “**NUMERICAL AND EXPERIMENTAL STUDY OF OPEN CHANNEL FLOW WITH AND WITHOUT BAFFLE**” be accepted in partial fulfillment of the requirements for awarding the degree of Master of Mechanical Engineering under Department of Mechanical Engineering of Jadavpur University.*

.....  
Dr. Debasish Roy  
Thesis Advisor  
Dept. of Mechanical Engineering  
Jadavpur University, kolkata

.....  
Dr.Snehamoy Majumder  
Thesis Advisor  
Dept. of Mechanical Engineering  
Jadavpur University, kolkata

.....  
Dr.Dipankar Sanyal  
Professor and Head  
Dept. of Mechanical Engineering  
Jadavpur University, Kolkata

.....  
Prof. Sivaji Bandyopadhyay  
Dean  
Faculty Council of Engineering & Technology  
Jadavpur University, Kolkata

**Faculty of Engineering and Technology**  
**Department Of Mechanical Engineering**  
**Jadavpur University**  
**Kolkata**

**CERTIFICATE OF APPROVAL**

*The foregoing thesis entitled “**NUMERICAL AND EXPERIMENTAL STUDY OF OPEN CHANNEL FLOW WITH AND WITHOUT BAFFLE**“ is hereby approved as credible study of Fluid Mechanics and Hydraulics Engineering and presented in a manner satisfactory to warrant its acceptance as a pre-requisite to the degree for which it has been submitted. It is understood that by this approval, the undersigned, do not necessarily endorse or approve any statement made, opinion expressed or conclusion drawn therein, but approve the thesis only for the purpose for which it is submitted.*

Committee of final examination for evaluation of thesis:

.....

.....

.....

.....

## ACKNOWLEDGEMENT

I would like to record here my gratitude to all who supported me and gave constructive suggestions during the completion of this paper. In presenting this thesis report, I would like to express my sincere gratitude and indebtedness to my Thesis Advisers **DR. DEBASISH ROY & DR. SNEHAMOY MAJUMDER** Professor, Department of Mechanical Engineering, Jadavpur University, Kolkata for their valuable suggestion and requisite guidance in various aspects of this project work. It was a great pleasure for me to work under their supervision.

I would like to convey sincere thankfulness to my senior Mr. Arindam Mandal, and Debojit Saha, Shouvik Chaudhari, Research Scholar, Department of Mechanical Engineering, Jadavpur University for their constant inspiration and remaining as a constant catalyst throughout the course of entire project work. They also guided me to learn skills and different approaches towards the work by helping me with discussions on important areas of the project.

I am thankful to **Prof. Dipankar Sanyal**, Head of Mechanical Engineering Department, Jadavpur University and **Prof. Sivaji Bandyopadhyay**, Dean Faculty Council of Engineering & Technology, Jadavpur University for their support in academic matters. I pay my sensible thanks to all the faculties of Fluid Mechanics and Hydraulics specialization for their supporting needs.

I would like to thank my parents and sister and like to express how grateful I am for all the sacrifices that they made on my behalf. Their prayer was what sustained me to this far.

I would also like to thank all my other lab mates-Avanish Rai, Rishi Roy, Ravi Kumar, Sawan Kumar & Souvik Mukhopadhyay for their co-operation, help, motivation and supported me in writing, and incented me to strive towards my goal.

I also like to pay my sensible appreciation to all those who submitted their invaluable database of information in internet and also to those who are maintaining such an invaluable database record by which all scientific future in the field of Engineering relies upon.

Lastly I would like to thank all who have assisted me directly or indirectly to accomplish this work.

Date:

With Regards

Jadavpur University

Kolkata-700032

.....

Sanchari Ghosh

---

# Contents

ABSTRACT.....	i
NOMENCLATURE.....	iii
LIST OF FIGURES.....	v
Chapter 1 .....	1
General Introduction and Literature Review .....	1
1.1 General Introduction .....	2
1.1.1 Objective.....	4
1.1.2 Practical uses.....	4
1.2 Literature Survey .....	8
1.2.1 Open channel flow: A Brief Literature Survey .....	8
Chapter 2 .....	17
Numerical Modeling .....	17
2.1 Mathematical Formulation .....	18
2.2 Numerical Algorithm .....	18
2.2.1 Control- Volume Formulation .....	19
2.2.2 The Power Law Model.....	19
2.2.3 The Staggered Grid .....	19
2.2.4 SIMPLE Algorithm.....	20
2.2.5 SIMPLER Algorithm .....	25
Chapter 3 .....	27
Experimental Setup and Procedure .....	27
3.1 General description of Experiment .....	28
3.2 Experimental Setup.....	31
3.3 Measurements of different experimental quantities: .....	33
3.4 Measurement of average velocity and flow rate through the channel .....	33
3.5 Measurement of velocity through the channel with Current Meter.....	35
3.5.1 Current Meter.....	35
3.5.2 Types of Current Meters.....	35
3.5.3 Current Meter working principle .....	36



---

□ Electromagnetic Induction .....	36
□ Tilt.....	37
3.5.4 Measurement of velocity and flow rate through the channel with Propeller type current meter.....	38
Chapter 4 .....	42
Result and Discussion .....	42
4.1 Numerical Result & Discussion .....	43
4.2 Experimental result and Discussion.....	51
Conclusion.....	77
5.1 CONCLUSION .....	78
5.2 FUTURE SCOPE OF WORK.....	78
References .....	79
ANEXTURE.....	85

# ABSTRACT

The fluid flow analysis through an open channel flow is important for the real life problems like the oil and other fluid transportation, flow through the drainage system, molten metal flow in isothermal condition, canal flow and lot of other industrial applications encountered in practice. The incorporation of the baffle makes the problem more realistic owing to the fact that there are restrictions right from the small size to the large size always present in the flow passages incorporated artificially or automatically generated due to siltation formations or presence of rocky substances while the flow is on. An experimental analysis of open channel flow with baffle placed in the course of the flow from wall to wall inside the channel will suffice the velocity and the recirculation zones in detail. The primary objective is to calculate the velocity field and the flow visualization of the fluid flow. A numerical analysis supported by the experimental results would be very meaningful to carry out the research work in such a physical condition. In the Numerical method a CONTROL VOLUME FORMULATION with power law scheme has been used to study the flow considering the laminar conditions. The grid generated will be both uniform and non-uniform and the turbulent model considered will be the modified  $k - \epsilon$  model with the streamline curvature correction for capturing the recirculatory flow conditions. The recirculatory flow around the baffle is an indication of the low pressure zone where the siltation or the precipitation is largely augmented. Hence estimation of the recirculation size and strength as well as the reattachment point is important to know this important physical phenomenon which is presence in almost all of such open channel flows. Determination of the drag force as well as the drag coefficient is very useful for the design and manufacturing of such construction for industrial purposes. A detailed analysis of the pressure and velocity distributions will suffice

the flow visualization for tracking the fluid flow and will provide the information for the design and selection of pumping devices. A major objective will be to investigate the Hydraulic Jump particularly in case of the water flow through the canals etc. using the experimental procedures. Flow resistance in open channels is usually estimated by applying the approach that is developed originally for pipe flows. Such estimates may be useful for engineering applications, but they always differ to some extent from measurements. This paper first summarize empirical approaches that have been proposed in the literature to reconcile the resistance difference, which include various modifications of the pipe friction for applications to rectangular ducts and open channel flows. Comparisons are made with experimental data reported by previous researchers and those collected in the present study experimentally. It is shown that for both narrow and wide channels the velocities will be different. Based on both of these applications, the present thesis has been carried out considering two different case studies. In the first one case, baffle wall has been considered and the combined effect of upstream and downstream on the fluid flow in open channel flow and the effect of the presence and size of the baffle has been investigated. In the next cases, extensive study has been done without baffle on the channel have been analyzed. In both the case, a numerical study has been presented.

## Nomenclature

2-D	Two Dimensional	
3-D	Three Dimensional	
CFD	Computational Fluid Dynamics	
Re	Reynolds number	
VOF	Volume of Fluid method	
x, y, z	Rectangular coordinates	
U	Horizontal velocity	cm/s, m/s
V	Vertical Velocity	cm/s, m/s
s	Second	
n	Number of revolution	
t	Time	
cm	Centimeter	
m	Meter	
kg	Kilogram	

fps	Feet per Second	
$p$	Pressure	Pa
%	Percentage	
H	Depth of water level in the Supply Tank	
B	Width of the channel	
L	Length of the channel	

### **Greek Symbols**

$\sim$	Coefficient of viscosity	Pa-s
$\dagger$	Surface Tension	N/m
...	Density of fluid	kg/m <sup>3</sup>
$\hat{\sim}$	Velocity	m/s

<b>Figure No</b>	<b>Caption</b>	<b>Page no</b>
Figure 1.1.1	Concrete Baffled Culvert	6
Figure 1.1.2	Baffle Flume	6
Figure 1.1.3	Typical Fish ladder Profile	7
Figure 1.1.4	Typical Fish way or Fish Ladder	7
Figure 1.1.5	Natural fish way in river and canal	8
Figure 1.1.6	Aerial view of Meziadin Fish Ladders-1995	8
Figure 1.1.7	Conceptual layout of a bypass fishway	9
Figure 1.1.8	Salmon jumping weir at Meziadin Fish Ladders-2006	9
Figure 2.2.1	Control Volume Formulation	21
Figure 2.2.2	staggered grid arrangements in three dimensions	22
Figure 2.2.3	staggered grid in two dimensions	22
Figure 2.2.4	Control Volume for u	23
Figure 3.1.1	Rectangular Channel Setup	30
Figure 3.1.2	Schematic Diagram of the Rectangular Channel Set Up	32
Figure 3.1.3	Point gauge mounted on moving trolley	33
Figure 3.1.4	End of Channel	34
Figure 3.1.5	A view of pump system in ground floor	34
Figure 3.1.6	Rectangular notch in return channel	36
Figure 3.1.7	Top view of Rectangular Channel bed	36
Figure 3.1.8	Bucket wheel current meter	38
Figure 3.1.9	Propeller type current Meter	38

	Tilt current meter	39
Figure 3.1.10		
	mechanism of tilt current meter	39
Figure 3.1.11		
	Propeller 3a used in our experiment	40
Figure 3.1.12		
	View of current meter placed in open channel	41
Figure 3.1.13		
	Top view of current meter	42
Figure 3.1.14		
	Close up view of propeller	42
Figure 3.1.15		
	Different type of propeller and instruments	42
Figure 3.1.16		
	Instrument that are used in the Experiment	43
Figure 3.1.17		
	Grid independent study	45
Figure 4.1.1		
	Flow and grid structures with single baffle	46
Figure 4.1.2		
	Flow and grid structures with single baffle	47
Figure 4.1.3		
	3-Dimensional Back step flow analysis	48
Figure 4.1.4		
	3-Dimensional back step result	49
Figure 4.1.5		
	Mid plane back step result	50
Figure 4.1.6		
	3-D and 2-D velocity vector result	51
Figure 4.1.7		
	Stream traces result	52
Figure 4.1.8		
	Different types of Baffle	53
Figure 4.2.1		
	flow pattern of water in the channel	54
Figure 4.2.2		
	a sketch of side view channel with baffle	54
Figure 4.2.3		
Figure	3-D view of type A baffle	55
4.2.4(a)		
Figure	Plan of type A baffle	55
4.2.4(b)		
	a typical geometric drawing for type A shown the position of measurement	55
Figure 4.2.5		

	Velocity Distribution at X= -1 cm	56
Figure 4.2.6		
	Velocity distribution at X=-32cm	56
Figure 4.2.7		
	Velocity distribution at X= -71cm	57
Figure 4.2.8		
	Velocity distribution at X= -90cm	57
Figure 4.2.9		
	Velocity distribution at X= -123cm	58
Figure 4.2.10		
	Velocity distribution at X= -156cm	58
Figure 4.2.11		
	a typical geometric of type B drawing shown the position of measurement	59
Figure 4.2.12		
	velocity distribution at X= -14 cm	59
Figure 4.2.13		
	velocity distribution at X= -32cm	60
Figure 4.2.14		
	velocity distribution at X=-71cm	61
Figure 4.2.15		
	Velocity distribution at X= -90cm	61
Figure 4.2.16		
	velocity distribution at X= -123cm	62
Figure 4.2.17		
	velocity distribution at X= -156cm	62
Figure 4.2.18		
	A typical geometric drawing shown the position of measurement	63
Figure 4.2.19		
	Side view of type C baffle	63
Figure 4.2.20		
	Plan of type C baffle	63
Figure 4.2.21		
	3 dimensional view of C Type Baffle	64
Figure 4.2.22		
	elocity distribution at X=-14cm	64
Figure 4.2.23		
	Fig 4.2.24, velocity distribution at X= -32cm	65
Figure 4.2.24		



	velocity distribution at X= -71cm	65
Figure 4.2.25		
	velocity distribution at X= -90cm	65
Figure 4.2.26		
	velocity distribution at X=-123cm	66
Figure 4.2.27		
	velocity distribution at X=-156cm	66
Figure 4.2.28		
	velocity distribution at y= -7cm	67
Figure 4.2.29		
	velocity distribution at y= -11cm	67
Figure 4.2.30		
	velocity distribution at y= -17cm	67
Figure 4.2.31		
	velocity distribution at y=1cm	68
Figure 4.2.32		
	velocity distribution at y=7cm	68
Figure 4.2.33		
	velocity distribution at y=10cm	68
Figure 4.2.34		
	velocity distribution at y=17cm	69
Figure 4.2.35		
Figure 4.2.36	Horizontal variation of velocity along the width of type B	69
Figure 4.2.37	Plan view of the measurement of type A baffle	70
Figure 4.2.38	Horizontal variation of velocity along the width of type A plan view of measurement	71 71
Figure 4.2.39		
	velocity distribution at x=-15cm	72
Figure 4.2.40		
	velocity distribution at x=-3cm	72
Figure 4.2.41		

	velocity distribution at $x=0$	72
Figure 4.2.42		
	velocity distribution at $x=+19\text{cm}$	73
Figure 4.2.43		
	typical geometric drawing shown the position of measurement	73
Figure 4.2.44		
	velocity distribution at $y=-15\text{cm}$	74
Figure 4.2.45		
	velocity distribution at $y=0$	74
Figure 4.2.46		
	velocity distribution at $y=+15\text{cm}$	74
Figure 4.2.47		
	velocity distribution at $y=19\text{cm}$	75
Figure 4.2.48		
	velocity distribution at $X= -14\text{cm}$	75
Figure 4.2.49		
	velocity distribution at $X= 0$	76
Figure 4.2.50		
	Comparison of velocity profile for flow with and without baffle	76
Figure 4.2.51		

# Chapter 1

---

## General Introduction and Literature Review

## 1.1 General Introduction

Fluid flows are broadly classified into two categories: laminar flow and turbulent flow. The difference between them can still be best illustrated by the well-known experiment Osborne Reynolds 1883. Laminar flow occurs at relatively low flow velocity and is envisaged as a layered flow in which fluid layers smoothly slide over each other, thus maintain a differential flow velocity in fluid layers (normal to the flow direction), without any exchange of fluid mass in between the layers. As the flow velocity exceeds a certain limiting value, the laminar flow becomes unstable, resulting in the formation of eddies which spread throughout the fluid medium. Such highly irregular, random and fluctuating flow is termed turbulent flow.

An open channel always has two sides and a bottom where flow velocity has to satisfy no-slip condition. Therefore, even a straight channel has a three-dimensional velocity with complex velocity profiles due to turbulence. The maximum velocity is seen typical at about 20% of the depth below the free surface in the middle of the channel (51). In very broad shallow channels, the maximum velocity is near the surface and the velocity profile is nearly logarithmic from the bottom of the free surface. In non-circular channels, a secondary flow also exists, which intensifies in case the channel is curved or meandered.

Some general similarities exist between the flow through pipes and the flow through open channels, certain factors such as the presence of a free surface, three-dimensional nature of flow due to noncircular cross section of the channel, and no uniform distribution of shear along the wetted perimeter, distinguish the open channel flow from pipe flow.

However, in wide open channels the nature of flow is two-dimensional and the shear stress is constant along the bed. Thus, the formulas for pipes can be applied to those channels by changing the constants suitably to include the free surface effects. The velocity distribution in the middle region of a channel is not influenced by the presence of side walls, and the flow in that region may be considered as two-dimensional in nature.

The ideal flow conditions generally do not exist in real situations, especially in small hydro electric power stations. The irregularity of the open channel is one of the major factors that increase the measurement uncertainty. The velocity profiles developed in various geometries of open channel are found to be very complex, such that accurate measurement of these profiles

becomes a tedious and challenging job (52). The study of free surface water flow in channels has many important applications. One of the most significant being in the area of river modeling. With major river engineering projects such as flood prevention measures becoming ever more common and ambitious, there is an increasing need to be able to model and predict the far ranging consequences on the environment as a whole of any potential project. A major part of this process is to predict the new hydraulic characteristics of the system. For example constricting the river at some point may result in an increased risk of flooding at a point upstream. The basic equations expressing hydraulic principles were formulated in the 19th century by de St Venant and Boussinesq. Properties of these relationships were studied in the first half of this century but application to real river engineering projects awaited the advent of electronic computers. The hydraulic equations are also of great importance in the modeling and design of networks of artificial channels, as for example may occur in industrial plants or sewage systems.

Understanding of flows over obstacles is important due to their relevance to many practical and theoretical problems. For example, separated flows produced by an abrupt change in geometry are of great importance in many engineering application (53). Also use of baffles or deflectors in settling tanks to improve the flow field has been investigated by several researchers such as Lyn & Rodi (54). Also to investigate the structure of flows as well as effects of a standing baffle on spatial and temporal structure of flow in rectangular open channel.

Due to baffles the variation of turbulent intensity over the depth is strong and its value has been increased in the upper deviation of the structure of the flow from uniformly and strong variation of turbulent intensity over depth after baffle due to presence of baffle. Comparison of stream wise velocity profiles along the channel that existence of baffle causes the flow pattern deviates from uniformity.

Presence of baffle has caused the inherent periodicity in the temporal structure of flow to be destroyed in the downstream of baffle. Baffles can interrupt short circuiting; giving rise to a modified flow field and potentially, improved the tank performances. However, prediction of the effect of baffles is a challenging numerical simulation problem.

The backward facing step flow was already of interest even when fluid mechanical problems used to be addressed only by potential flow theory.

## ■ Objective

- To study laminar three dimensional fluid flow in open channel flow and measure the velocity experimentally.
- To investigate three dimensional laminar fluid flow with a baffle on the channel numerically and experimentally

## ■ Practical uses

The practical natural barriers may also be assessed for fish passage, however they are not prioritized for correction the most common fish way types encountered include:

- Baffled Culvert (BC). A culvert with baffles installed. They are designed to pass fish by creating streaming flow during high-water conditions, reduce the average cross section velocity inside the culvert, or by increasing flow depth throughout the culvert.
- Baffled Flume (BF). A stream reach confined in a concrete flume with baffles installed for fish passage.

A baffle fishway uses a series of symmetrical close-spaced baffles in a channel to redirect the flow of water, allowing fish to swim around the barrier. Baffle fishways need not have resting areas, although pools can be included to provide a resting area or to reduce the velocity of the flow. Such fishways can be built with switchbacks to minimize the space needed for their construction. Baffles come in variety of designs. The original design for a Denil fish way was developed in 1909 by a Belgian scientist, G. Denil; it has since been adjusted and adapted in many ways



*Fig 1.1.1, Concrete Baffled Culvert*



*Fig1.1.2, Baffle Flume*

A fish ladder, also known as a fishway, fish pass or fish steps, is a structure on or around artificial barriers (such as dams and locks) to facilitate diadromous fishes natural migration. Most fishways enable fish to pass around the barriers by swimming and leaping up a series of relatively low steps (hence the term ladder) into the waters on the other side. The velocity of water falling over the steps has to be great enough to attract the fish to the ladder, but it cannot be so great that it washes fish back downstream or exhausts them to the point of inability to continue their journey upriver.

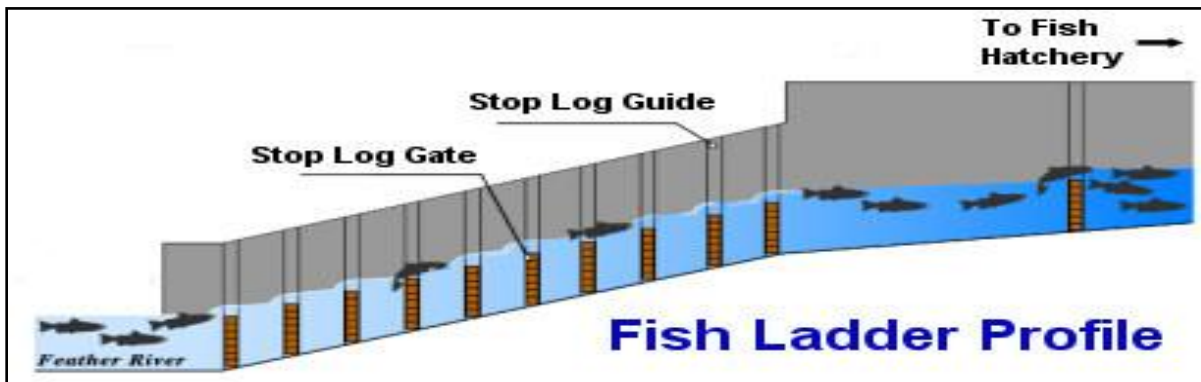


*Fig 1.1.3, Typical Fish ladder Profile*



*Fig 1.1.4, Typical Fish way or Fish Ladder*

Barriers are defined as any obstacle that prevents or impedes fish from successful passage upstream or downstream [Evans and Johnson 1972; (55)], and can be natural or man-made. Some examples of natural barriers are waterfalls, debris jams, or temperature barriers. Artificial, or man-made, barriers for fish migration include stream crossings (culverts, bridges, and fords), irrigation diversions and dams.



*Fig1.1.5, Natural fish way in river and canal*



*Fig.1.1.6, Aerial view of Meziadin Fish Ladders-1995*



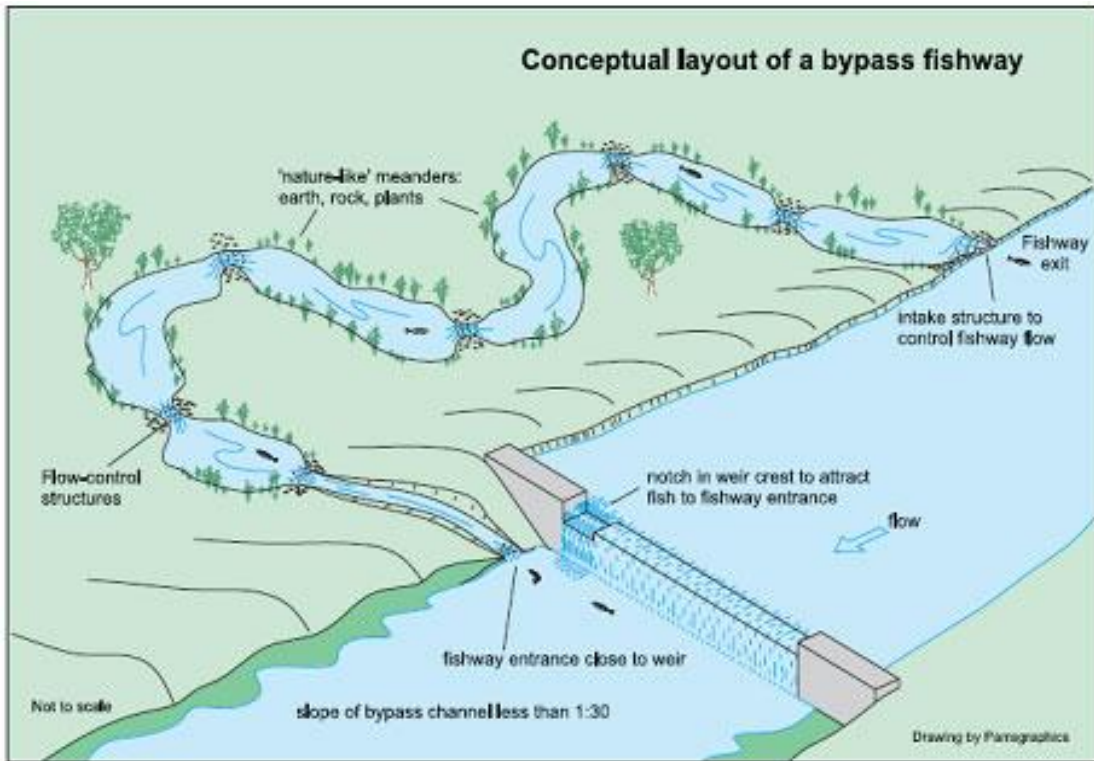


*Fig.1.1.7, Conceptual layout of a bypass fishway*



*Fig .1.1.8, Salmon jumping weir at Meziadin Fish Ladders-2006*

## 1.2 Literature Survey

The intent of this section is to study and analyze published works, unpublished works which deals about open channel flow & Backward-Facing Step Flow to get a better insight of the subject and understand latest development in these fields.

### 1.2.1 Open channel flow: A Brief Literature Survey

The theoretical of **Prandtl** (1) and **Von Karman** (2, 3) on flow through pipes, and experiment studies of **Nikuradse** (4) have led to rational formulas for velocity distribution and hydraulic resistance for turbulent flows over flat plates and circular pipes. These formulas have been extended to open channel flow. Some general similarity exists between the flow through pipe and the flow through open channel.

**Vanoni** (5) reported that in reference to two dimensional channels, the logarithmic velocity distribution was justified by his data to be far below the free surface. He observed that maximum velocities occurred below the free surface.

**Tracy and Leaster** (6) studied the velocity distribution in wide rectangular open channels and drew the following general conclusions:

- i) The flow is symmetrical about the vertical plane equidistant from the two sidewalls of the flume.
- ii) Each half section may be divided into two regions, one in the central portion of the channel and the other in the vicinity of the wall
- iii) Each vertical curve in the central region of the flow is logarithmic from the surface to a point very close to the floor
- iv) Within the limits of experiment accuracy, the vertical velocities curves appear to be identical over the width of the central region, and are logarithmic
- v) The phenomenon of dip occurs near the vicinity of the sidewalls
- vi) There always exists a central region for the channels of aspect ratio greater than 5.

The wall function approach outlined by **Launder and Spalding** (7) was used. This, in effect, means that the boundary conditions are not specified right at the wall but at a point, outside the viscous sub-layer, where the logarithmic law of the wall prevails.

The secondary currents are induced mainly due to the inequality of the normal turbulent stresses at different locations in the cross-sectional plane **Perkins** (8). These secondary currents affect the primary mean flow field and cause the maximum velocity to occur below the free surface (dip phenomenon). It is important to investigate their influence in the developing flow region of a channel. The developing flow is a complex three-dimensional flow influenced by the secondary currents and free surface effects.

**Jing YAN** *et al.* (9) experimentally studied on influence of boundary on location of maximum velocity in open channel flow. It has been proposed that the flow field may be divided into two regions, the relatively strong sidewall region and relatively weak sidewall region. In former region, the distance to the side wall greatly affects the location of maximum velocity, and in the latter region, both the distance to the sidewall and the aspect ratio influenced the location of the maximum velocity.

**Bonakdari** *et al.* (10) theoretically showed a parametric study on developed turbulent flows in rectangular channels. The main aim of the study was the impact of three key hydraulic parameters (relative roughness, the Froude number and the Reynolds number) on the establishment length using computational fluid dynamics (CFD). The establishment length was determined by comparing the modeled velocity fields. The results obtained from this study proved that the effect of the Froude number on the establishment length is negligible. And also the establishment length was found to decrease with the increase in the channel roughness.

**J. H. Burger, R. Haldenwang, and N. J. Alderman** (11) experimentally observed Laminar and Turbulent Flow of Non-Newtonian Fluids in Open Channels for Different Cross-Sectional Shapes. The test work was carried out in a 10-m-long tilting flume designed and built by the Flow Process and Rheology Centre at the Cape Peninsula University of Technology provides further details of this flume. This flume can be hydraulically tilted at various angles of up to  $5^\circ$  from the horizontal. The width of this rectangular flume can be changed from 300 to 150 mm by placing a partition midsection lengthways down the flume. By inserting an appropriate cross-sectional insert, the rectangular flume can be changed into a flume with a triangular,

semicircular, or trapezoidal cross section. These models are compared with three previously published models for laminar flow and five previously published models for turbulent flow using a recently extended experimental database for non-Newtonian flow in open channels of different cross-sectional shapes. Flow of three different fluids (aqueous carboxymethyl cellulose solutions and kaolin and bentonite suspensions) was investigated in open channels of four different cross sections (rectangular, semicircular, trapezoidal, and triangular) at slopes varying from 1 to 5°. The new model for predicting the laminar flow of power law fluid in open channels of different cross-sectional shapes gave good agreement between the measured and predicted values when compared on a velocity basis. A particular advantage of both of these new models for laminar and turbulent open channel flow is that they are applicable for all the non-Newtonian fluids tested and four cross-sectional shapes.

**B. K. Gandhi** *et al.* (12) has been made an effort through the present investigation to determine the velocity profiles in both the directions under different real flow conditions, as ideal flow conditions rarely exist in the field. 'Fluent', a commercial computational fluid dynamics (CFD) code, has been used to numerically model various situations. The flow-velocity profile in rectangular open channels has been numerically modeled. The CFD model has been validated by comparing the results with actual measurement carried out with ADCP. The proposed numerical modeling can be used for determining the optimum number and locations of flow sensors (propeller current meters or transducers of ultrasonic transit-time flow meter, as the case may be) for the measurement of discharge in a given open channel. The CFD model can be expanded to include the effects of silt and larger floating bodies.

In the open channel flow, the velocity distribution along the vertical direction (depth) is theoretically represented by a logarithmic function of the depth of flow (13). It is very difficult to describe the velocity distribution along the width theoretically. However, some of the investigators have proposed empirical equations for the velocity distribution based on experimental and field data (14-17).

**Rafik Absi** (18) showed that the velocity distribution in open channel flows is presented based on an analysis of the Reynolds-Averaged Navier-Stokes equations and a log-wake modified eddy viscosity distribution. This equation allows predicting the velocity-dip-phenomenon, i.e. the maximum velocity below the free surface. Two different degrees of approximations are

presented, a semi-analytical solution of the proposed ordinary differential equation, i.e. the full dip-modified-log-wake law and a simple dip-modified-log-wake law.

**Abinash Mohanta et al.** (19) Water surface prediction is an important task in flood risk management in urban area. In this paper based on the principle of the momentum balance, a one dimensional method is investigated to predict the water surface elevations in non prismatic compound channels. The numerical method is then applied to calculate water surface elevation in non-prismatic compound channel configurations, the results of calculations show good agreement with the experimental data. The results show that the CFD predictions accurately predict the velocity and depth average velocity for les turbulence model. In both the cases velocity was over predicted when smooth walls were applied as expected. In this paper the flow velocity profile in non prismatic compound channel has been numerically modeled.

**S. Patil et al.** (20) validate STAR-CD commercial CFD software for the bridge hydraulics research. This study simulates limited scaled experimental data conducted elsewhere for bridge flooding in open channel flow with Froude number,  $Fr=0.22$ , and dimensionless inundation height ration,  $h=1.5$ . Two approaches are used to simulate two-dimensional open channel turbulent flow with six different turbulence models. It is observed that transient VOF free-surface simulations are much more unstable than usual steady-state single-phase simulations, and thus VOF may amplify solution instability and compromise accuracy with regard to other modeling and solution parameters, namely spatial and time discretization size and non-uniformity transitions, and especially turbulence modeling.

**A.M. Razmi et al.** (21) showed that the hydraulic efficiency of sedimentation basins is reduced by short-circuiting, circulation zones and bottom particle-laden jets. Baffles are used to improve sediment tank performance. In this study, laboratory experiments were used to examine the hydrodynamics of several baffle configurations. An accompanying numerical analysis was performed based on the 2D Reynolds-Averaged Navier-Stokes equations along with the  $k-\varepsilon$  turbulence closure model. A series of experimental measurements as well as numerical modeling were carried out to investigate the effect of baffle positions on the performance of the baffled ST. The model was able to simulate free-surface tracking, sediment distribution and velocity profiles, and gave predictions that agreed well with laboratory data. The simulation results demonstrated that the baffle configuration created significantly different flow fields in the tank and that proper baffle placement improved the ST performance. The location of baffle near the entrance

dissipates the inlet jet energy more efficiently. It diminishes the maximum velocity magnitude along the tank and reduces sediment re-suspension after the baffle position.

Sedimentation tanks are important components of any water purification plant, and account for approximately a third of the infrastructure cost (22). Their task is to remove suspended particles from the flow field, so their efficiency affects the performance of other parts of the plant (23).

Effects of baffle height and position were not considered. The effect of baffle angles and position were examined using a 2D model applied to a small-scale, 2-m long laboratory setup (24, 25, 26). Right-angled (to the tank base) baffles were most favorable for sedimentation. In addition, it was concluded that, to get high settling performance, the baffle should be somewhere close to the inlet. However the effects of baffle height and optimal baffle configuration were not considered.

**Hamidreza Jamshidnia & Yasushi Takeda** (27) experimentally showed the effect of standing baffle on the flow structure in a rectangular open channel to investigate the structure of flows as well as effect of a standing baffle on spatial and temporal structure of flow in a rectangular open channel. Experiments were conducted in a glass sided rectangular open channel 8m x0.2m x 0.4m in length and height ( $x, y, z$  with  $x=0$  at upstream end,  $y=0$  in centre of channel= $0$  at the bed) respectively, with a smooth bottom. The depth was controlled by sharp-edged weir of height 32 cm, located at the downstream end of channel the baffle located at  $x=4$ m and height is 8cm.the velocities were measured by 3D Acoustic Doppler Velocimeter (ADV) which makes it possible to observe the flow field at each point. Due to baffle the variation of turbulent intensities over the depth is strong and its value has been increased in the upper deviation of the structure of flow from uniformly and strong variation of turbulent intensity over depth after baffle due to presence of baffle. Baffle having height range  $8\text{cm} \leq h \leq 12\text{cm}$ . in spatial structure Mean velocities, Turbulence intensities, effect of inlet, Effect of baffle are shown. In temporal structures power spectrums, Methodology, Effect of baffle on power spectra has been observed. From this experiment,

- i) The flow was observed in the upstream of baffle and far from inlet.
- ii) Comparison of stream wise velocity profiles along the channel that existence of baffle causes the flow pattern deviates from uniformity.
- iii) Presence of baffle has caused the inherent periodicity in the temporal structure of flow to be destroyed in the downstream of baffle.

**J.H.Pu** (28) proposed law was derived to concrete in representing the velocity profile at the outer region of velocity Universal Velocity Distribution for Smooth and Rough Open Channel Flow

**Macharia Karimi, et al.** (29) numerically modeled fluid flow in an open Rectangular channel with lateral inflow channel to show that a 5 ft x5 ft x49 ft open-return test section is powered by a 30 hp motor. At a distance of 3.75 ft from the inlet, a plenum chamber pressurized by four fans surrounds the test section. Twelve rows of 23 holes in the walls of the test section form turbulence-generating jets lateral to the main flow. This jet apparatus is referred to as a “turbulence-generating box. Pressure distributions measured on a rectangular cylinder in flows of constant turbulence intensity and varying scales have shown that scales do have significant effects on the flow structure. Up to a critical value, increases of integral scale, with the attendant decreases in small-scale content necessary to maintain constant turbulence intensity, altered mean, rms, and negative peak pressure distributions. With increasing integral scale, the peaks of these distributions moved closer to the leading edge and the shapes of the distributions grew narrower on either side of the peaks. Integral scales above some critical value between 2.8D and 7.8D resulted in flows with pressures distributions trending back toward the results of smooth flow tests.

**Chao- Lin Chiu et al.** (30) theoretically showed in velocity distribution in open channel flow that the entropy concept in selecting the probability distribution of velocity. The geometric technique in modeling the  $\xi$  coordinate, with which the velocity develop and also the basic hydrodynamic concerning the rates of transport of mass, momentum and kinetic energy by the flow through an open channel cross section. Also they used a probabilistic formulation of the velocity distribution problem.

**Fan and Li** (31) formulated the diffusive wave equations for open channel flows with uniform and concentrated lateral inflow. In their formulation, they were able to present continuity and momentum equations of an open channel with a lateral inflow channel that joins the main open channel at a varying angle.

The cross-section of a channel may be closed or open at the top. The channels that have an open top are referred to as open channels while those with a closed top are referred to as closed conduits. The forces at work in open channels are the inertia, gravity and viscosity forces. Chezy equation was one of the earliest equations developed for average computations of the velocity of

a uniform flow. (32). However, the formula that is mostly used in open channel problems is the Manning formula (33). This Manning formula is highly considered and desirable because it takes into account the coefficient of roughness (34).

### 1.2.1 Backward-Facing Step Flow: A Brief Literature Survey

The backward-facing step flow was already of interest even when fluid mechanical problems used to be addressed only by potential flow theory. As shown by **Lee and Smith** (35), potential flow theory permits the treatment of the backward-facing step flow yielding a streamline pattern which does not indicate any separation or recirculation region behind the step.

Hence potential theory does not provide the generally expected separation of the flow at the upper corner of the step, nor does the lower corner yield a region of vortices as expected from the considerations of **Moffatt** (36). Moffatt predicted under specified conditions the existence of a sequence of vortices near corners for  $Re \rightarrow 0$ . Early numerical predictions of backward-facing step flows, e.g., **Roache** (37), **Taylor and Ndefo** (38) and **Durst and Pereira** (39), did not show any separation at the upper corner of the step for low Reynolds numbers. However, a separated region was predicted at the lower corner that contained a single vortex only.

However, a separated region was predicted at the lower corner that contained a single vortex only. A careful analysis of the flow in sudden expansions was carried out by **Alleborn et al.** (40) and it was indicated that, at least at low Reynolds numbers, the lower corner contains a sequence of Moffatt vortices. It was concluded by Alleborn et al. (40) that the earlier numerical predictions were carried out with insufficient numerical grid resolution to resolve the smaller vortices at the lower corner. Hence high-performance computers are needed to carry out detailed studies of backward-facing step flows, even at low Reynolds numbers.

**Kim and Moin** (41) computed the flow over a backward-facing step using a method that is second-order accurate in both space and time. They found a dependence of the reattachment length on Reynolds number in good agreement with the experimental data of **Armaly et al.** (42) up to about  $Re$  500. At  $Re$  600 the computed results of Kim and Moin (41) started to deviate from the experimental values. The difference was attributed to the three-dimensionality of the experimental flow around a Reynolds number of 600.



**Gartling** (43) developed a solution procedure using a Galerkin based finite-element method for steady incompressible flow over backward-facing step geometry. His results compared well, especially with respect to the bottom wall separation zone, with the results of Kim and Moin (41).

**Lee and Mateescu** (44) performed an experimental and numerical investigation of air flow over a two-dimensional backward facing step for  $\mathbf{Re} \leq 3000$ . The hot film sensor measurements at  $\mathbf{Re} = 805$  and expansion ratio  $\mathbf{H/h} = 52$  were found to be in agreement with their numerical predictions with respect to the locations of the separation and reattachment points on the upper and lower walls.

**Le et al.** (45) conducted direct numerical simulations of turbulent flows over a backward-facing step at a Reynolds number of  $\mathbf{Re}_s = 5100$  based on step height  $S$  and inlet free-stream velocity, and an expansion ratio of 1.2. The instantaneous velocity fields reveal the variation of reattachment length in the span wise direction that oscillates about a mean value of  $6.28 S$ . The flow exhibits strong stream wise vertical structures.

**Heenan and Morrison** (46) conducted experiments for a Reynolds number ( $\mathbf{Re}$ ) based on the step height  $S$  of  $1.9 \times 10^5$  and suggested that while the flow is likely to be convectively unstable over a large region, the global unsteadiness, driven by the impingement of large eddies at reattachment is the cause of low frequency oscillations called flapping

**Williams and Baker** (47) investigated laminar flow over three dimensional backward-facing step geometry. The full three dimensional simulation of the geometry of Armaly *et al.* (42) for  $100 \leq \mathbf{Re} \leq 800$  correctly predicts the reattachment lengths and confirms the effect of three-dimensionality. They also found that the side walls result in the creation of a wall jet, located at the lower channel wall and pointing from the side wall towards the channel mid-plane.

Recently, **Barkley et al.** (48) carried out a three-dimensional linear stability analysis for the backward-facing step flow with an expansion ratio of 2. They showed that the primary bifurcation of the steady, two-dimensional flow is a steady, three-dimensional instability. Furthermore, the critical Eigen mode is localized to the primary recirculation region consisting of a flat roll.

**G.Biswas et al.** (49) is concerned with the behavior of flows over backward-facing step geometry for various expansion ratios  $\mathbf{H/h}$  1.9423, 2.5 and 3.0. The study of backward-facing

step flows constitutes an important branch of fundamental fluid mechanics. The interest in such a flow was intensified with the experimental and numerical work of Armaly *et al.* (42). They presented a detailed experimental investigation in backward-facing step geometry for an expansion ratio  $H/h$  1.9423, an aspect ratio  $W/h$  35 and Reynolds numbers up to  $Re = 500 - 600$ . The flow appeared to be three-dimensional above Reynolds numbers close to 400. Around this Reynolds number, they observed a discrepancy in the primary recirculation length between the experimental results and the numerical predictions. Also, around this Reynolds number, a secondary recirculation zone was observed at the channel upper wall. Armaly *et al.* (42) conjectured that the discrepancy between the experimental measurements and the numerical prediction was due to the secondary recirculation zone that perturbed the two-dimensional character of the flow. The normalized value of the reattachment length showed a peak at  $Re$  1200. The decrease in recirculation length beyond a Reynolds number of 1,200 was attributed to the effect of Reynolds stresses.

**P. Fan** *et al.* (50) studied and describes the experimental results of continuous flow measurements Using electromagnetic (EM) current meters and an acoustic Doppler current profiler (ADCP) meter during the 1983-1985 period. A record ice jam in the Clair River occurred in April 1984 and provide<sup>4</sup> an excellent opportunity for testing the current meter program. Verification of current meter results was provided by flows transferred from the Detroit River, which was ice-free and permitted accurate flow simulation. The current meter flow measurement program illustrated high consistency of exponential (logarithmic) vertical distribution of velocities.

**Gaston E. Ferrari** *et al.* (51) developed a model for better understands the complex flow field inside a free surface fish bypass constructed at Rocky Reach Dam. This consists of two identical parallel channels, with fish screens on the walls of each channel, and a pump station recirculating 96% of incoming flows into the forebay. This is very complex, characterized by 3D effects, free surface elevation. A 1D model porous media is used to model the fish screens. The comparison of the numerical model results with measured depth averaged velocity data and water surface differential between the channel and wet well shows very good agreement. In this paper a 3D model presented a better understanding of the flow field inside the fish passage.

## Chapter 2

---

# Numerical Modeling

## 2.1 Mathematical Formulation

The differential equations governing the laminar incompressible fluid motion has been represented in this chapter. Subsequently, the numerical modeling for the present work has been described.

Numerical analysis in fluid dynamics involves mathematical representation of the physical problem for which the solution is sought. Essentially they are the conservation laws for mass, momentum and energy respectively. Following the continuum approach, these governing equations are generated in the form of partial differential equations (PDE). The conservation equation for mass is referred to as continuity equation while the same for the momentum is known as the Navier-Stokes equation. Similarly, equations following conservation of energy may be expressed in terms of Temperature.

### *Continuity Equation*

$$\frac{\partial u}{\partial x} + \frac{\partial v}{\partial y} + \frac{\partial w}{\partial z} = 0 \dots\dots\dots (1)$$

### *X-Momentum Equation*

$$\rho \left( u \frac{\partial u}{\partial x} + v \frac{\partial u}{\partial y} + w \frac{\partial u}{\partial z} \right) = -\frac{\partial p}{\partial x} + \frac{\partial}{\partial x} \left( \mu \frac{\partial u}{\partial x} \right) + \frac{\partial}{\partial y} \left( \mu \frac{\partial u}{\partial y} \right) + \frac{\partial}{\partial z} \left( \mu \frac{\partial u}{\partial z} \right) \dots\dots\dots (2)$$

### *Y-Momentum Equation*

$$\rho \left( u \frac{\partial v}{\partial x} + v \frac{\partial v}{\partial y} + w \frac{\partial v}{\partial z} \right) = -\frac{\partial p}{\partial y} + \frac{\partial}{\partial x} \left( \mu \frac{\partial v}{\partial x} \right) + \frac{\partial}{\partial y} \left( \mu \frac{\partial v}{\partial y} \right) + \frac{\partial}{\partial z} \left( \mu \frac{\partial v}{\partial z} \right) \dots\dots\dots (3)$$

### *Z-Momentum Equation*

$$\rho \left( u \frac{\partial w}{\partial x} + v \frac{\partial w}{\partial y} + w \frac{\partial w}{\partial z} \right) = -\frac{\partial p}{\partial z} + \frac{\partial}{\partial x} \left( \mu \frac{\partial w}{\partial x} \right) + \frac{\partial}{\partial y} \left( \mu \frac{\partial w}{\partial y} \right) + \frac{\partial}{\partial z} \left( \mu \frac{\partial w}{\partial z} \right) \dots\dots\dots (4)$$

## 2.2 Numerical Algorithm

The mathematical models described above consist of sets of differential equations subjected to appropriate boundary conditions. To provide the algebraic form of the governing equations, a fully staggered grid system have been adopted for the velocity components and the scalar variables and these equations were discretized using a control volume formulation. The numerical solution in the present work is accomplished by using Semi implicit method for pressure linked equation revised (SIMPLER) and the power-law scheme proposed by Patankar.

### 2.2.1 Control- Volume Formulation

In the control volume formulation the calculation domain is divided into a number of non-overlapping control volumes surrounding each grid point. The differential equation is integrated over each control volume. Piecewise profiles expressing the variation of the variable between the grid points are used to evaluate the required integrals.

The most attractive feature of control volume formulation is that the resulting solution would imply that the integral conservation of quantities such as mass, momentum is exactly satisfied over any group of control volumes, and, of course, over the whole domain. This characteristic exists for any number of grid points. Thus even the coarse grid solution exhibits exact integral balances.

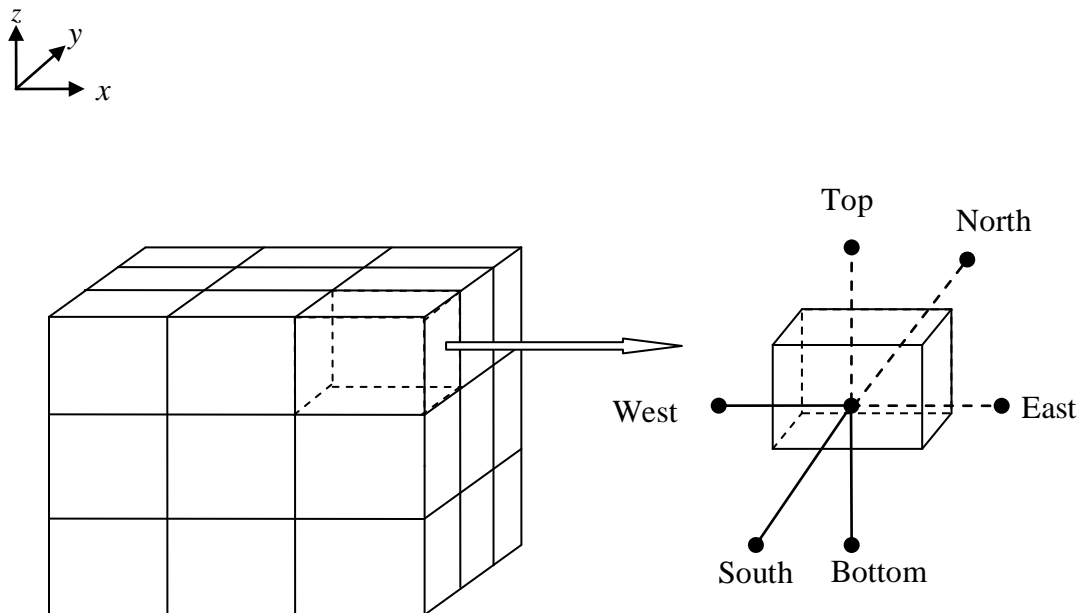


Fig.2.2.1, Control Volume Formulation

### 2.2.2 The Power Law Model

The power law model as described by Patankar has been used for the discretization of the flow governing equations in the present study. The Power-Law differencing scheme is more accurate approximation to the exact solution of the conduction –diffusion equation and produces better result than the Hybrid scheme by Patankar.

### 2.2.3 The Staggered Grid

To avoid the discrepancies related to the source pressure term and velocities in momentum equations, staggered grid arrangement has been considered. In the staggered grid, the

velocity components are calculated for the points lie on the faces of the control volumes. Thus  $x$ -direction velocity  $u$  is calculated at the faces that are normal to the  $x$ -direction. The main grid points are shown by small circles fig 2.2(b). The dashed lines indicate the control volume faces. The location for  $u$  lies on the  $x$ -direction link joining two adjacent main grid points. Whether the  $u$  location is exactly mid way between the grid points depends upon how the control volumes are defined. The  $u$  location must lie on the control volume face, irrespective of whether the latter happens to be mid way between the grid points. Similarly,  $v$  and  $w$  can be calculated.

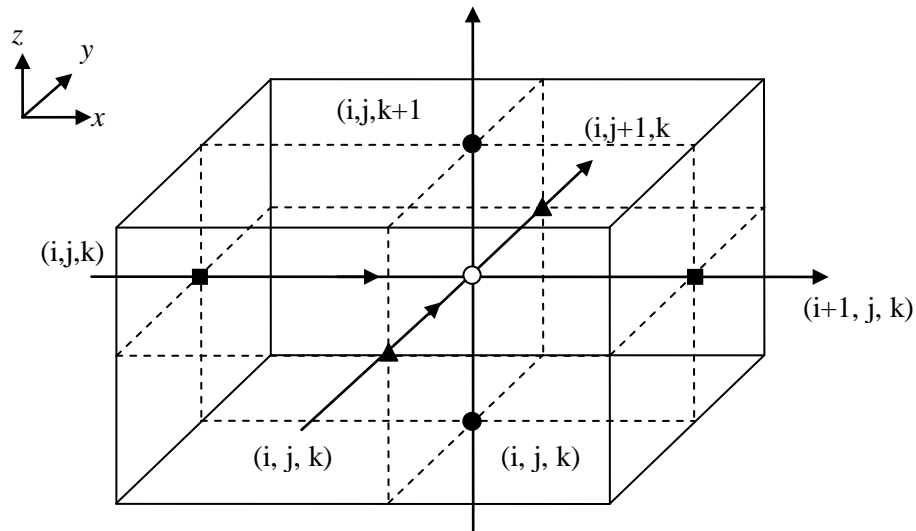


Fig. 2.2.2, staggered grid arrangements in three dimensions

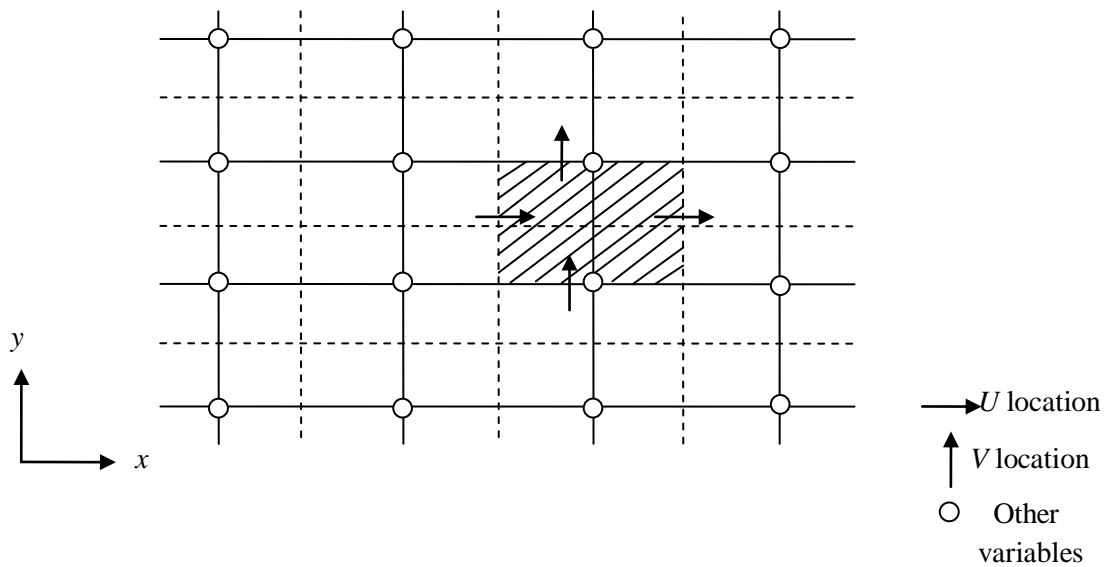


Fig.2.2.3, staggered grid in two dimensions

### 2.2.4 SIMPLE Algorithm

A Staggered control volume for the x-momentum equation is shown in figure 2.2(d). If the attention has been focused on the locations for  $u$  only, there is nothing unusual about this control volume. Its faces lie between the point  $e$  and the corresponding locations for the neighbor  $u$ 's. The control volume is staggered in relation to the normal control volume around the main grid point  $p$ . The staggering is in the  $x$ -direction only, such that the faces normal to that direction pass through the main grid points  $P$  and  $E$ . the difference  $p_P - p_E$  can be used to calculate the pressure force acting on the control volume for the velocity  $u$ .

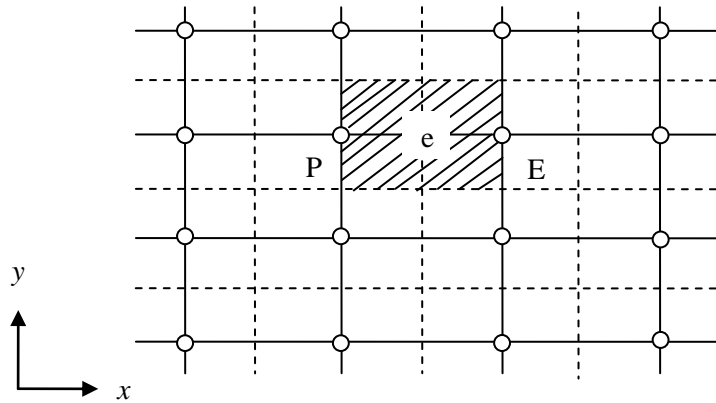


Fig. 2.2.4, Control Volume for  $u$

The calculation of the diffusion coefficient and the mass flow rate at the faces of the  $u$  control volume shown in Fig. 2.2(d) would require an appropriate interpolation. The resulting discretization equation can be written as,

$$a_e u_e = \sum a_{nb} u_{nb} + b + (p_P - p_E) A_e \dots \dots \dots (5)$$

Here the number of neighbor terms will depend on the dimensionality of the problem. For two dimensional situations, four  $u$  neighbors are shown outside the control volume and for three dimensional cases; six neighbor  $u$  would be included. The neighbor coefficient  $a_{nb}$  account for the combined convection-diffusion influence at the control volume faces. The term  $(p_P - p_E) A_e$  is the pressure force acting on the  $u$  control volume,  $A_e$  being the area on which the pressure difference acts. For two dimensions,  $A_e$  will be  $\Delta y \times 1$ , while in the three dimensional case  $A_e$  will stand for  $\Delta y \Delta z$ .

The momentum equation for the other directions is handled in a similar manner. Equation (6) shows the control volume for the  $y$ -direction momentum equation; it is staggered in the  $y$  direction. The discretization equation for  $v_n$  can be seen to be,

$$a_n v_n = \sum a_{nb} u_{nb} + b + (p_P - p_N) A_n \dots \dots \dots (6)$$

Where,  $(p_P - p_N) A_n$  is the appropriate pressure force. For the three dimensional case, a similar equation for the velocity component  $w$  can be written.

The momentum equations can be solved only when the pressure field is given or is somehow estimated. Unless the correct pressure field is employed, the resulting velocity field will not satisfy the continuity equation. Such an imperfect velocity field based on a guessed pressure field  $p^*$  will be denoted by  $u^*$ ,  $v^*$ ,  $w^*$ . These starred velocity field will result from the solution of the following discretization equations:

$$a_e u_e^* = \sum a_{nb} u_{nb}^* + b + (p_P^* - p_E^*) A_e \dots \dots \dots (7)$$

$$a_n v_n^* = \sum a_{nb} u_{nb}^* + b + (p_P^* - p_N^*) A_n \dots \dots \dots (8)$$

$$a_t w_t^* = \sum a_{nb} w_{nb}^* + b + (p_P^* - p_T^*) A_t \dots \dots \dots (9)$$

In these equations, the velocity components and pressure have been given the superscript  $*$ . The location  $t$ , can be noted, lies on the  $z$ -direction gridline between the grid points  $P$  and  $T$ .

### The pressure and Velocity Corrections

Our aim is to improve the guessed pressure  $p^*$  such that the resulting starred velocity field will progressively get closer to satisfying the continuity equation. The correct pressure  $p$  is obtained from,

$$p = p^* + p' \dots \dots \dots (10)$$

Where,  $p'$  will be called the pressure correction. The corresponding velocity corrections  $u'$ ,  $v'$ ,  $w'$  can be introduced in a similar manner:

$$u = u^* + u' \dots \dots \dots (11)$$

$$v = v^* + v' \dots \dots \dots (12)$$

$$w = w^* + w' \dots \dots \dots (13)$$

So we get,

$$a_e u_e' = \sum a_{nb} u_{nb}' + b + (p_P^* - p_E') A_e \dots \dots \dots (14)$$



Neglecting the term  $\sum a_{nb}u_{nb}'$  from the Eq. (14) we get,

$$a_e u_e' = (p_P^* - p_E') A_e \dots \dots \dots (15)$$

Or,

$$u_e' = (p_P^* - p_E') d_e \dots \dots \dots (16)$$

Where

$$d_e \equiv \frac{A_e}{a_e} \dots \dots \dots (17)$$

Equation (5) will be called the velocity correction formula. It can be written as,

$$u_e = u_e^* + d_e (p_P' - p_E') \dots \dots \dots (18)$$

This shows how the starred velocity  $u_e^*$  is to be corrected in response to the pressure corrections to produce  $u_e$ .

The corrections formula for the velocity components in other directions can be written similarly:

$$v_n = v_n^* + d_n (p_P' - p_N') \dots \dots \dots (19)$$

$$w_t = w_t^* + d_t (p_P' - p_T') \dots \dots \dots (20)$$

### The Pressure Correction Equation-

We shall now turn the continuity equation into an equation for the pressure correction. For the purpose of this derivation, we shall assume that the density  $\rho$  does not directly depend on pressure. The derivation is given here for the three dimensional situation. The continuity equation is,

$$\frac{\partial \rho}{\partial t} + \frac{\partial(\rho u)}{\partial x} + \frac{\partial(\rho v)}{\partial y} + \frac{\partial(\rho w)}{\partial z} = 0 \dots \dots \dots (21)$$

Now, it will be integrated over the shaded control volume shown in Fig. 2.2(c) for the integration of the term  $\frac{\partial \rho}{\partial t}$ , it is assumed that  $\rho_P$  prevails over the control volume. Also a velocity component such as  $u_e$  located on a control volume face will be supposed to govern the mass flow rate for the whole face. In conformity with the fully implicit practice, the new values

of velocity and density (i.e. those at time  $t + \Delta t$ ) will be assumed to prevail over the time step; the old density  $\rho_p^0$  (i.e., the one at time  $t$ ) will appear only through the term  $\frac{\partial \rho}{\partial t}$ .

With these decisions, the integrated form becomes,

$$\frac{(\rho_p - \rho_p^0)\Delta x\Delta y\Delta z}{\Delta t} + ((\rho u)_e - (\rho u)_w)\Delta y\Delta z + ((\rho v)_n - (\rho v)_s)\Delta z\Delta x + ((\rho w)_t - (\rho w)_b)\Delta x\Delta y = 0 \dots \dots \dots (22)$$

Now, substituting all the velocity components, the expression given by the velocity correction formula after rearrangement, the following discretization equation for  $p'$  can be obtained

$$a_p p'_p = a_e p'_e + a_w p'_w + a_n p'_n + a_s p'_s + a_t p'_t + a_b p'_b + b \dots \dots \dots (23)$$

Where,

$$a_e = \rho_e d_e \Delta y \Delta z \dots \dots \dots (24)$$

$$a_w = \rho_w d_w \Delta y \Delta z \dots \dots \dots (25)$$

$$a_n = \rho_n d_n \Delta z \Delta x \dots \dots \dots (26)$$

$$a_s = \rho_s d_s \Delta z \Delta x \dots \dots \dots (27)$$

$$a_t = \rho_t d_t \Delta x \Delta y \dots \dots \dots (28)$$

$$a_b = \rho_b d_b \Delta x \Delta y \dots \dots \dots (29)$$

$$a_p = a_e + a_w + a_n + a_s + a_t + a_b \dots \dots \dots (30)$$

$$b = \frac{(\rho_p^0 - \rho_p)\Delta x\Delta y\Delta z}{\Delta t} + ((\rho u^*)_w - (\rho u^*)_e)\Delta y\Delta z + ((\rho v^*)_s - (\rho v^*)_n)\Delta z\Delta x + ((\rho w^*)_b - (\rho w^*)_t)\Delta x\Delta y \dots \dots \dots (31)$$

Since the values of the density  $\rho$  will normally be available only at the main grid points, the interface densities such as  $\rho_e$  may be calculated by any convenient interpolation. Whatever the method of interpolation, the value of  $\rho_e$  must be consistently used for the two control volumes to which the interface belongs.

The pressure-correction equation derived as above is prone to divergence unless some under relaxation is used. We under relax  $u^*$ ,  $v^*$  and  $w^*$  while solving the momentum equations (with a relaxation factor  $\alpha$ , set equal to about 0.5); further we add only a fraction of  $p'$  to  $p^*$ . In other words, we employ,

$$p = p^* + \alpha_p p' \dots \dots \dots (32)$$

With  $\alpha_p$  set equal to 0.8. The task is to calculate  $p$ , which will be used as  $p^*$  in the next iteration. The values of the relaxation factors that are mentioned here, namely  $\alpha = 0.5$  and  $\alpha_p = 0.8$ , have been found to be satisfactory in a large number of fluid flow computations.

### SIMPLE Algorithm

The SIMPLE stands for Semi Implicit Method or Pressure Linked Equations.

The sequences of operations are

- 1) Start with a guessed pressure field,  $p^*$
- 2) Solve the momentum equations, such as Eqns. (7) to (9) to obtain  $u^*$ ,  $v^*$  and  $w^*$ .
- 3) Solve the  $p'$  equation.
- 4) Calculate  $p$  from equation (10) by adding  $p'$  to  $p^*$ .
- 5) Calculate the  $u, v, w$  from their starred values using the velocity-correction formulas (18-20).
- 6) Treat the corrected pressure  $p$  as a new guessed pressure  $p^*$ .
- 7) Repeat the steps from step two till the converged solution is obtained

### 2.2.5 SIMPLER Algorithm

The SIMPLER stands for “Semi Implicit Method or Pressure Linked Equations Revised”. This method is an improved version of SIMPLE. The steps for calculation are as follows.

- 1) Start with a guessed velocity field.
- 2) Calculate the coefficients of the momentum equations. Hence, calculate the pseudo velocities  $\hat{u}, \hat{v}$  and  $\hat{w}$  by using the values of the neighbor velocities,  $u_{nb}$

$$\hat{u}_e = \frac{\sum a_{nb} u_{nb} + b}{a_e} \dots\dots\dots(33)$$

$$\hat{v}_n = \frac{\sum a_{nb} v_{nb} + b}{a_n} \dots\dots\dots(34)$$

$$\hat{w}_t = \frac{\sum a_{nb} w_{nb} + b}{a_t} \dots\dots\dots(35)$$

- 3) Calculate the coefficients of the pressure equation and solve it to obtain the pressure field.

$$a_p p_p = a_E p_E + a_W p_W + a_N p_N + a_S p_S + a_T p_T + a_B p_B + b \dots\dots\dots(36)$$

Where,  $a_E, a_W, a_N, a_S, a_T, a_B, a_P, b$  are as given in equation (24) to (31)

4) Treating this field as  $p^*$ , solve the momentum equation to obtain  $u^*, v^*$  and  $w^*$ .

$$a_e u_e^* = \sum a_{nb} u_{nb}^* + b + (p_P^* - p_E^*) A_e \dots \dots \dots (37)$$

$$a_n v_n^* = \sum a_{nb} v_{nb}^* + b + (p_P^* - p_N^*) A_n \dots \dots \dots (38)$$

$$a_t w_t^* = \sum a_{nb} w_{nb}^* + b + (p_P^* - p_T^*) A_t \dots \dots \dots (39)$$

5) Calculate the mass source term  $b$ , and hence solve the  $p'$  equation.

6) Correct the velocity field but do not correct the pressure.

$$u_e = u_e^* + d_e (p'_P - p'_E) \dots \dots \dots (40)$$

$$v_n = v_n^* + d_n (p'_P - p'_N) \dots \dots \dots (41)$$

$$w_t = w_t^* + d_t (p'_P - p'_T) \dots \dots \dots (42)$$

## REFERENCES

- 1) Anderson, J. D., "Computational Fluid Dynamics: The Basics with Applications", McGraw-Hill Publisher, 1976
- 2) Patankar, S. V., "Numerical Heat Transfer and Fluid Flow", Taylor and Francis Publisher, 1980

## Chapter 3

---

# Experimental Setup and Procedure

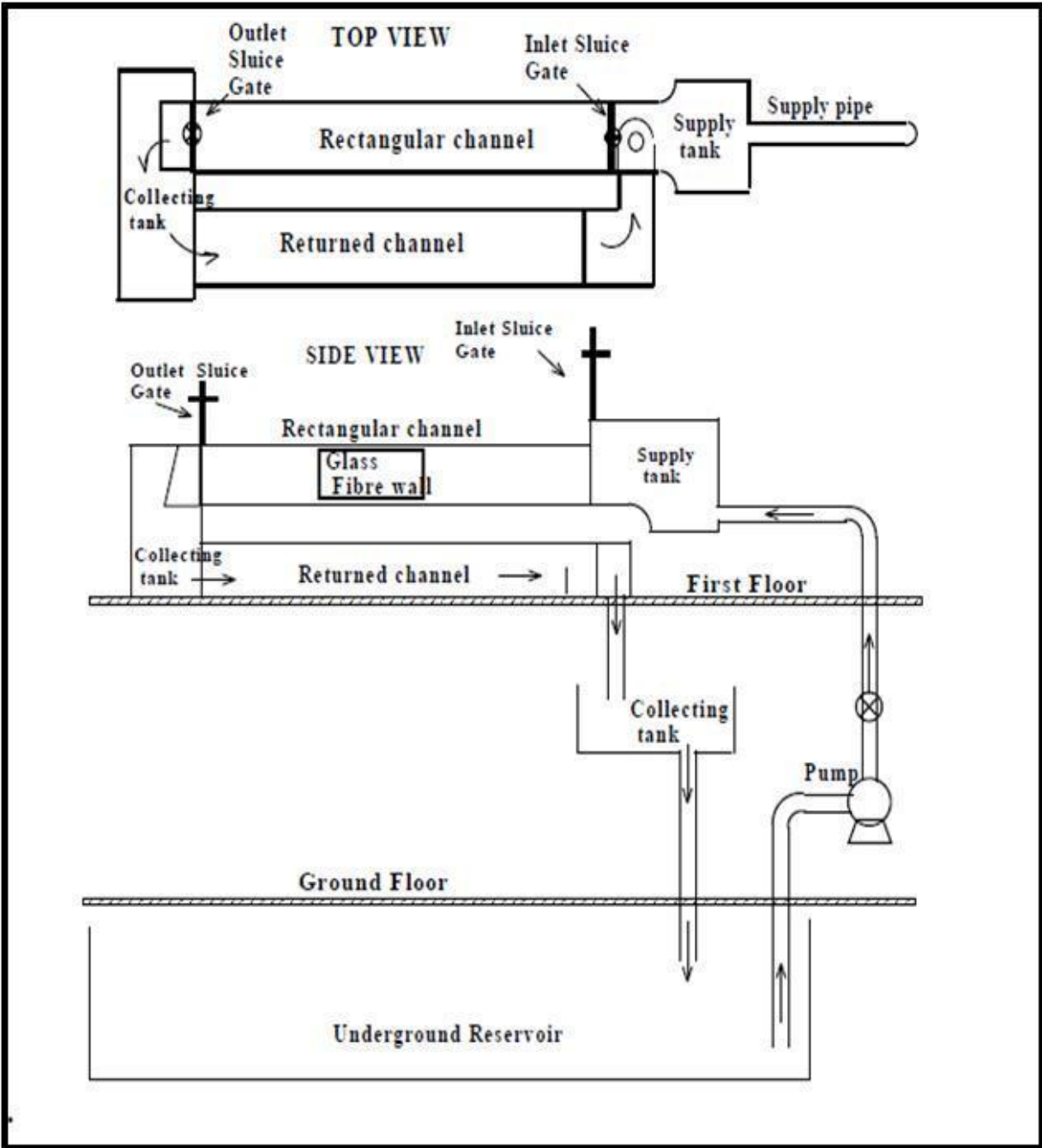
### 3.1 General description of Experiment

The setup of hydraulic jump experiment, on which the hydraulic jump experiment is performed, is in the hydraulics laboratory of Jadavpur University. The setup contains a big rectangular channel in which the water is supplied by a pump. The channel setup is 8.00 m long, 0.45 m in width and 0.53 m in height. The channel is metallic and side walls of mid channel are made of glass, which is 2.3 m in length. The advantage of this glass channel is that jump can easily be observed in a better way because of transparent glass side walls.



*Fig 3.1.1, Rectangular Channel Setup*

The channel is provided with two gates, one at the start of the channel and the other one at the end of the channel. By controlling these gates, the location of hydraulic jump and other phenomenon can be adjusted. Like if we close the inlet gate, the velocity at inlet will be more and jump goes away from the inlet gate and if we open the inlet gate, the jump will come towards the inlet gate. Same condition is with outlet gate, if we decrease the outlet gate opening, the jump will go away from outlet gate. It means the jump will shift towards the inlet gate and if we open the outlet gate opening, the jump will come towards the outlet gate. After this channel, there is a return channel which is made of brick. It returns the water which comes out of the setup channel. At the end of the return channel, a rectangular notch is there. By using this notch, we can calculate velocity. This whole setup is on the first floor of hydraulics laboratory. After the notch, there is a pipe which takes the water to the reservoir which is on the ground floor. Water is supplied to the setup by a pump which is on the ground floor and it takes water from the reservoir. The water recirculates again and again. There are two valves after pump which controls the discharge in the setup, one is bypass valve which bypasses the flow directly, means if the opening of the bypass valve is more, more water will be bypassed and less water is available for the setup. There is one more valve which is main valve. It directly connects the pipe carrying flow to the setup thus it also controls the discharge in the setup. On rectangular channel, one moving trolley is mounted which moves on the channel by help of rollers. A point gauge is mounted on this trolley which can move vertically. A scale is attached by it which will tell the vertical movement of the point gauge. By using this point gauge, the water height of upstream and downstream can be measured easily.



3.1.2, Schematic Diagram of the Rectangular Channel Set Up

The water issuing out from downstream sluice gate was collected in a collecting tank as shown in figure. The collecting tank was connected to returned channel 0.54m wide, 0.53m deep and 8.00m long. The depth of flow in the flume channel was measured by point gage mounted on a travelling trolley as shown in the figure. Supercritical flow is obtained by an adjustable sluice



gate at the entrance of the channel i.e. the channel is between sluice gates. The maximum Froude number obtained by controlling inlet sluice gate was 5.3. Corresponding to maximum feasible water flow rate. Higher Froude number was not possible as the inlet tank would overflow.

Water is supplied to a tank from underground reservoir by using centrifugal pump through a pipe. There is no constant head tank. The discharge is controlled by sluice gate such that if the sluice gate opening is less, the depth of water in the inlet tank becomes higher. If the inlet sluice opening is less than 6.5cm, the water will overflow in the tank.

### 3.2 Experimental Setup



*Fig 3.1.3, Point gauge mounted on moving trolley*



*Fig. 3.1.4, end of Channel*



*Fig 3.1.5, A view of pump system in ground floor*

### **3.3 Measurements of different experimental quantities:**

The discharge through the flume had been constant during the experiment with a fixed setting of the pump delivery valve. The setting has been fixed based on occurrence of hydraulic jump formation with different openings of the inlet sluice valve. During the course of the experimentation the quantities that were measured had been velocity of flow, depths of flow at various locations, also velocity at different location. A travelling point gauge assembly with option for moving both across the flume and along the flume has been designed, fabricated and installed in the course of the present work. The pointer is fitted with a measuring scale for indicating the depth of flow

### **3.4 Measurement of average velocity and flow rate through the channel**

Beside the rectangular channel, there is a returning channel made of brick which takes the water coming out of the channel and returns it to the reservoir. There is a rectangular notch fixed in the returning channel whose width is 53.5 centimeter and height is 35.5 centimeter. Flow passes over the notch and the height of water above the notch is measured and by using Current meter.



*Fig 3.1.6, Rectangular notch in return channel*

Thus with the help of current meter, the velocity can be calculated for both upstream and downstream.



*(a) Near the Inlet Sluice Gate*



*(b) Near the Outlet Gate*

*Fig. 3.1.7, Top view of Rectangular Channel bed (on which the experiments were done) at Fluid Mechanics & Hydraulic Lab, Jadavpur University, Kolkata*

## 3.5 Measurement of velocity through the channel with Current Meter

### 3.5.1 Current Meter

It is a device measuring stream flow velocities

#### Feature

- Accurate measurement
- Permanent magnet mounted on its shaft
- Equipped with water velocity indicator.
- Simple and rugged design
- Rust free surface
- Highly durable and require negligible maintenance
- User friendly menu driven system function.

### 3.5.2 Types of Current Meters

Current meters are available in two styles. The **bucket wheel current meters** look very much like anemometers, which are used to measure air speed. Bucket wheel current meters are of stainless steel, brass and bronze construction. The AA Current Meter is used for water velocities above 3.0 feet per second. The Mini Current Meter is used for slower water, and is slightly smaller in size. Bucket wheel meters have a tail fin to keep the meter pointed directly into the current. This style of meter produces a signal which can be used with headphones, or a digital counter. The second type of meter uses a **propeller / impeller**, which rotates as the water moves past the unit. There are several styles available which work on this principle. The Scoffers hand held current meters use a propeller which can be used in water ranging from 0.1 fps to 25 fps. A choice of rods and computer console displays is available. The Handheld Flow meter with low speed impeller can measure current as slow as 2 cm per second. A standard impeller is also available for current speeds above 10 cm/sec. These products are available as mechanical or electronic units.



*Fig 3.1.8, Bucket wheel current meter*



*Fig 3.1.9, Propeller type current Meter*



### **3.5.3 Current Meter working principle**

- Current meter counters

The signal from the sensors or current meter can read in one of several ways. The simplest set has a mechanical counter which tracks revolutions of the impeller. The counter begins as soon as the sensor meets the water and continues until the unit is lifted clear again. To determine velocity, a stopwatch is used in order to plot revolutions against time. A chart is then used to determine velocity. This is the least expensive set. Other units use an audio signal sent to headphones. Each revolution produces a tone. The tones are counted and recorded against time as in the previous system to determine velocity. The more advanced current meter systems include a digital counter or computer. These counters track the revolutions electronically. The best units will directly convert the revolutions to a velocity which is displayed on screen. Some will store minimum / maximum readings in memory. Some models are true data loggers which time stamp the data for downloading to a computer via RS-232 output.

- Electromagnetic Induction

The physics behind: Charged particles (the ions in seawater) are moving with the ocean currents in the magnetic field of the Earth which is perpendicular to the movement. Using Faraday's law of induction (the third of Maxwell's equations), it is possible to evaluate the variability of the averaged horizontal flow by measuring the induced electric currents. The

method has a minor vertical weighting effect due to small conductivity changes at different depths.

- Tilt

Tilt current meters operate under the drag-tilt principle. They consist of a sub-surface buoy that is anchored to the sea floor with a flexible line or tether. The float tilts as a function of its shape, buoyancy and the water velocity. Once the characteristics of a given buoy are known, the velocity can be determined by measuring the angle of the buoyancy. The buoyancy contains a data logger that records the orientation (angle from vertical and compass bearing) of the Tilt Current Meter. A Tilt Current Meter is typically deployed on the bottom with an anchor but may be deployed on lobster traps or other convenient anchors of opportunity. A TCM has the advantage over other methods of measuring current in that they are generally relatively low-cost instruments and the design and operation is relatively simple. The low-cost of the instrument may allow researchers to use the meters in greater numbers (thereby increasing spatial density) and/or in locations where there is a risk of instrument loss.

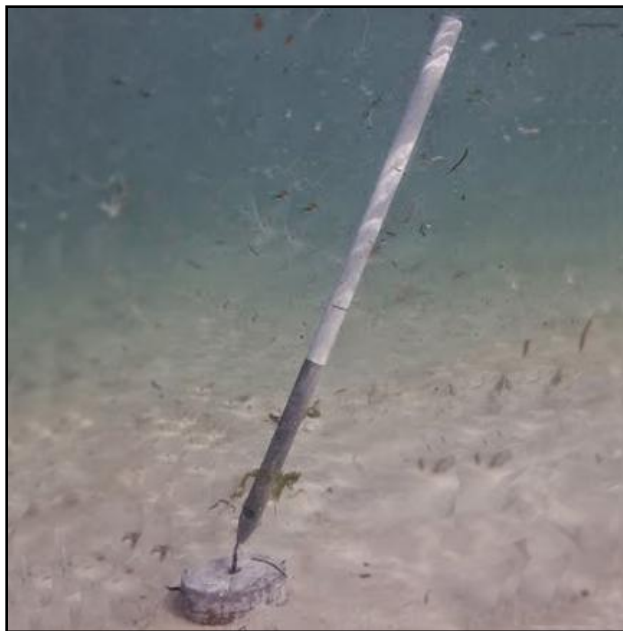


Fig 3.1.10, Tilt current meter

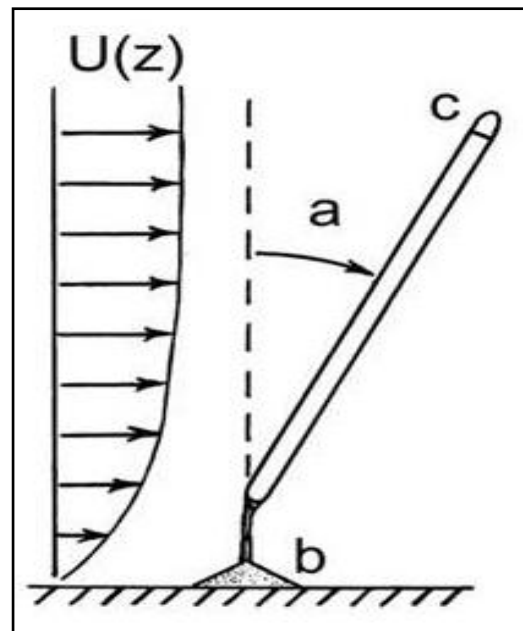
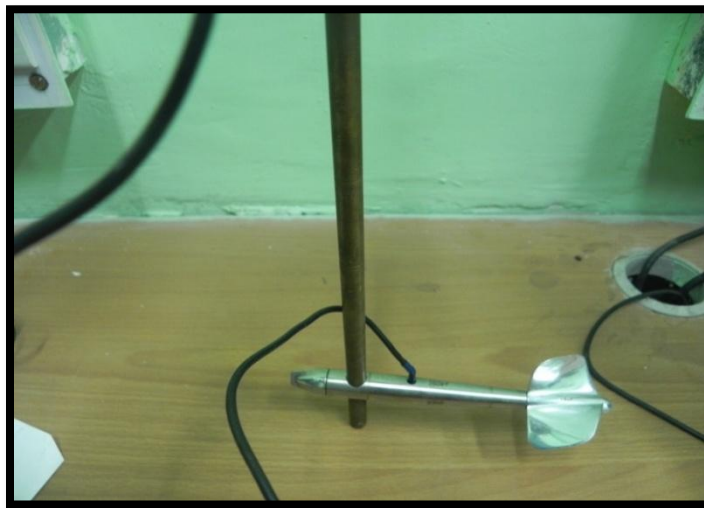


Fig 3.1.11, mechanism of tilt current meter

### 3.5.4 Measurement of velocity and flow rate through the channel with Propeller type Current flow meter

The flow rate through the channel during the experiments was obtained using a propeller type current flow meter, which records the mean velocity of flow on a small region in the cross section plane of the flow in the channel. During experimentation, the flow rate is controlled by the pump delivery valve and is kept fixed for a particular experiment run. Before the experimental run, the flow is allowed into the channel and out of it by keeping both the inlet and outlet sluice gates wide open. After the flow has reasonably stabilized the velocity of flow at different small region at the mid section of the channel is measured using the current meter (fig 3.13). The current meter gives as output the number of revolution over a given period of time measured by stopwatch (fig 3.17c). The revolution per minute thus obtained is used in the calibration correlation (N vs. V) supplied with the instrument to determine the flow rate. Once this is done subsequent experiment continue by controlling the sluice gate for this setting of discharge through the channel.

We use propeller type current meter in our experiment. In our college laboratory we have a current meter picture below. In that current meter we have some propellers, the no is - 1, 2, 3, 4, 3a, 4-2, 4-3, 2-2, 2-3. Each and every propeller has a unique specification. In our experiment we use propeller no 3a. The other equipment used in this experiment are revolution counter box, 1m long scale stopwatch, and three types baffles.



*Fig 3.1.12, propeller 3a used in our experiment*



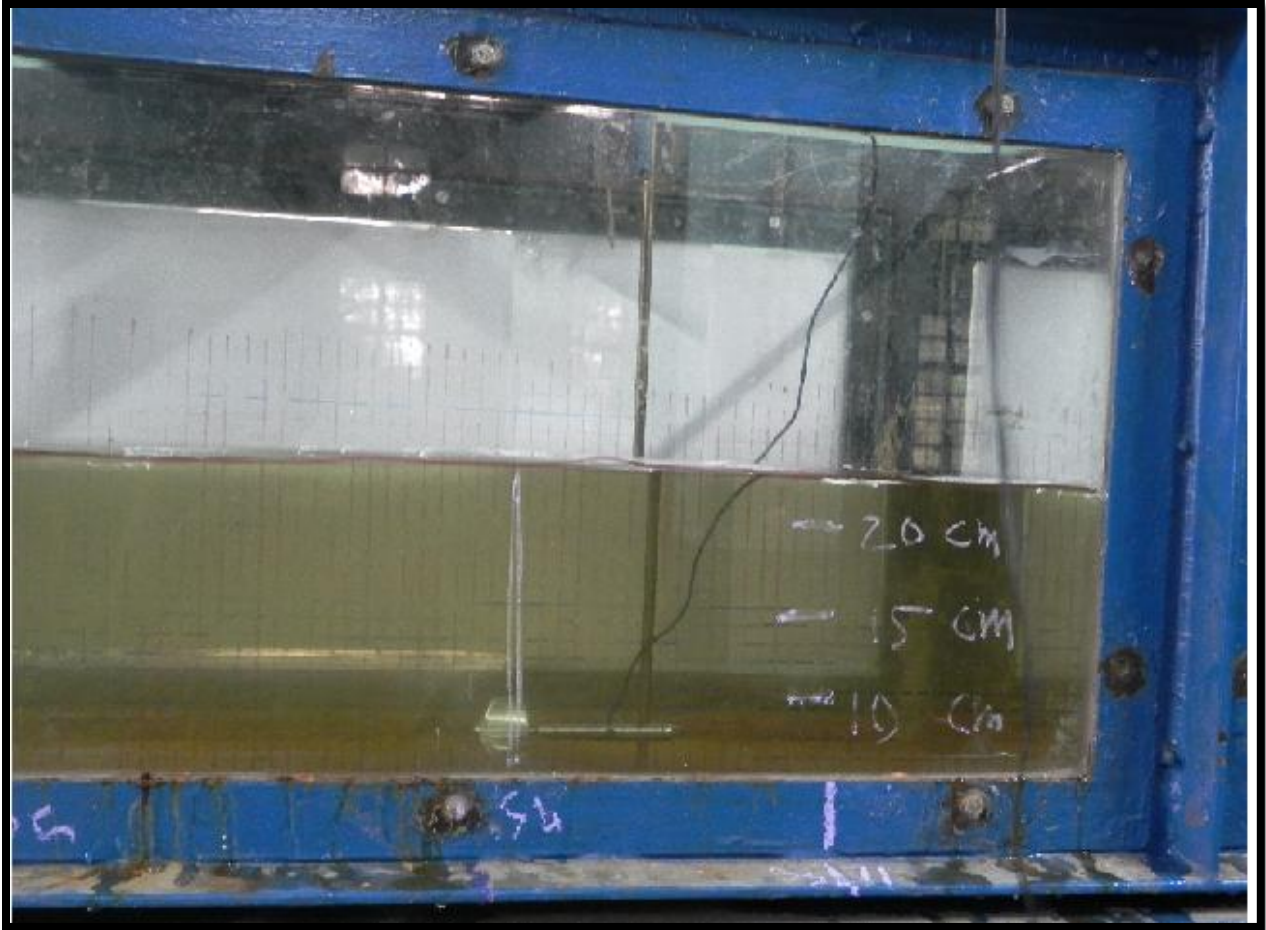


*Fig 3.1.13, view of current meter placed in open channel*

On the setup that is a rectangular channel a moving trolley is there which is in Fig 3.1.3. It is a point gauge which can move vertically & also horizontally with the help of hand screw. Trolley can move along the length of the channel. Current meter propeller 3a is used in our experiment, this is attached to the rod and this rod was fixed with the trolley and there was a screw which controls the vertical motion of the rod. Weir was connected with the propeller which was joining to the revolution current box. This propeller was then dip into the flowing water in the channel and the height of the propeller from the base was measured by point gauge. So this propeller from the base was measured by point gauge, so this propeller revolves by the impact of water. If the velocity of water is moving the revolution in the box given at Fig 3.17 moves also. Counter

box gives the revolution and it is counted in the unit time. For set of experiment 10sec time is taken to measure the rotation in the counter box. The height of propeller is changed by the help of a screw and it is taken as different placed as shown in Fig 3.3.

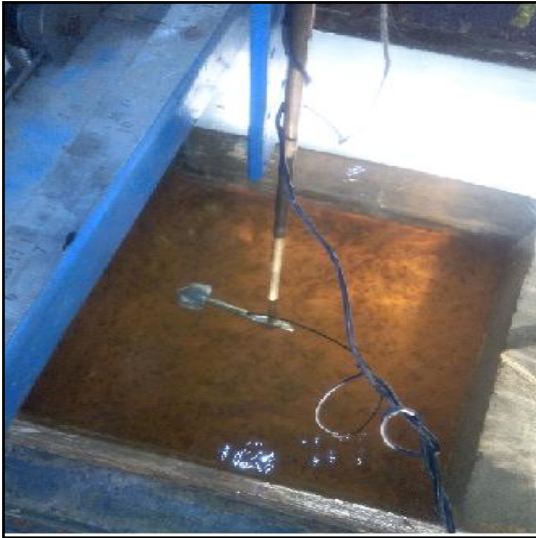


*Fig 3.1.14, top view of current meter*

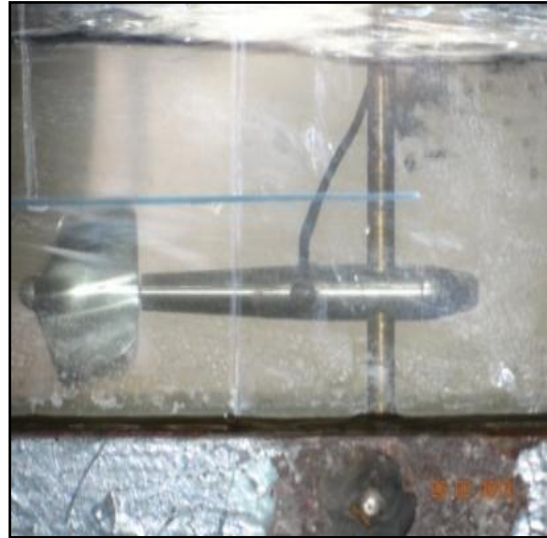


*Fig 3.1.15, close up view of propeller*



*Fig 3.1.16, different type of propeller and instruments*



(a) Revolution Counter box(Close)



(b) Revolution Counter box(Open)



(c) Stopwatch



(d) Port of current meter



(e) Port of the box



(f) Light



(g) Cannon EOS DSLR camera

Fig 3.1.17, instrument that are used in the Experiment

## Chapter 4

---

### Result and Discussion

## 4.1 Numerical Result and Discussion

In the fig 4.1.1 a grid independent study has been shown. Though there is an under shoot near the surface but 80-90% places has been shown to collapse on one another. These prove that the grid independent study has been done effectively.

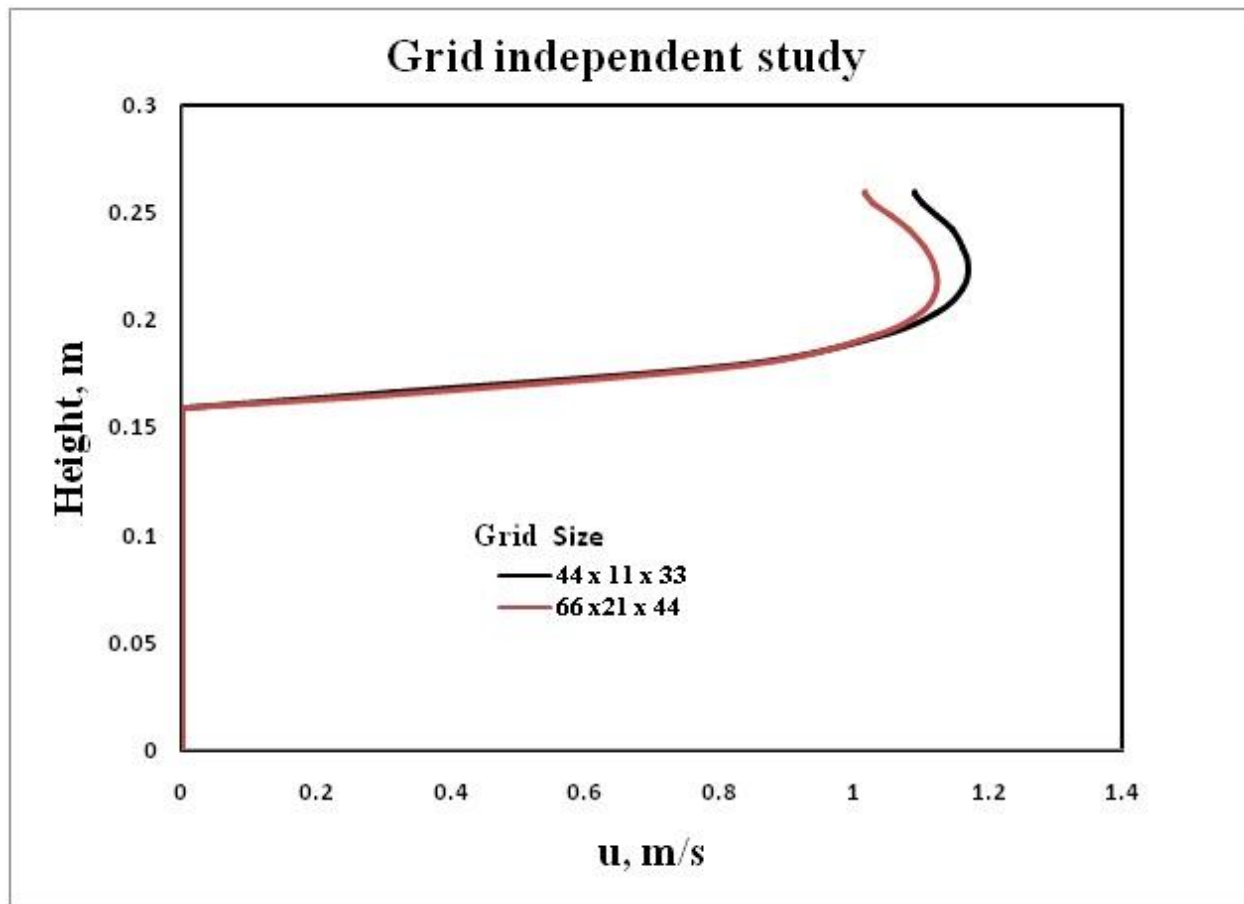
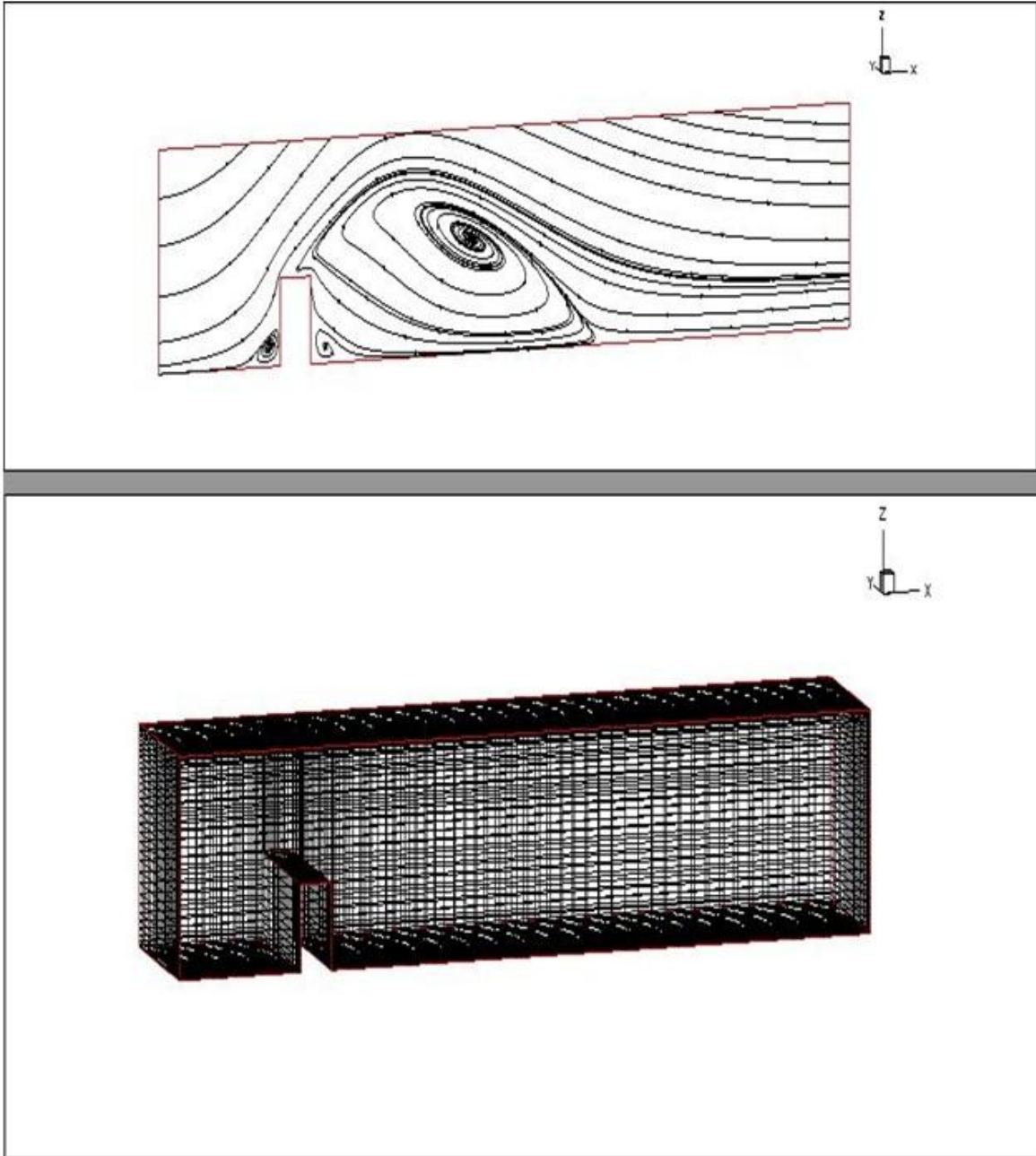


Fig 4.1.1, grid independent study

In reality we have accepted the  $44 \times 11 \times 33$  as our basic structure of the numerical methodology. The grid structure has been shown in the figures 4.1.2 and 4.1.3. It should be noted that the grids are non-uniform in structure with logarithmic variations. The grids are so made to capture the steep variations of the flow variables particularly near the walls.



*Fig. 4.1.2, flow and grid structures with single baffle*

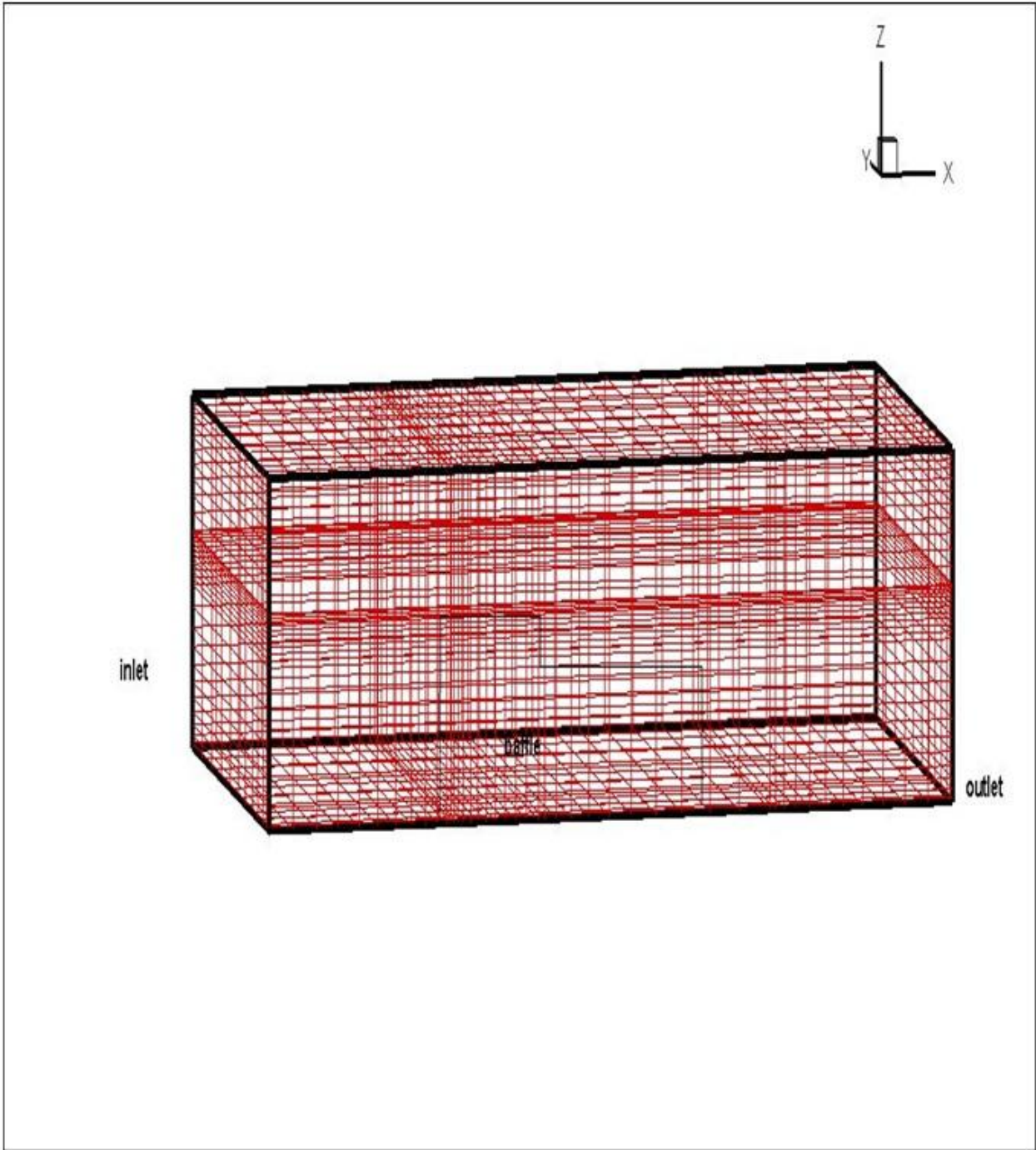
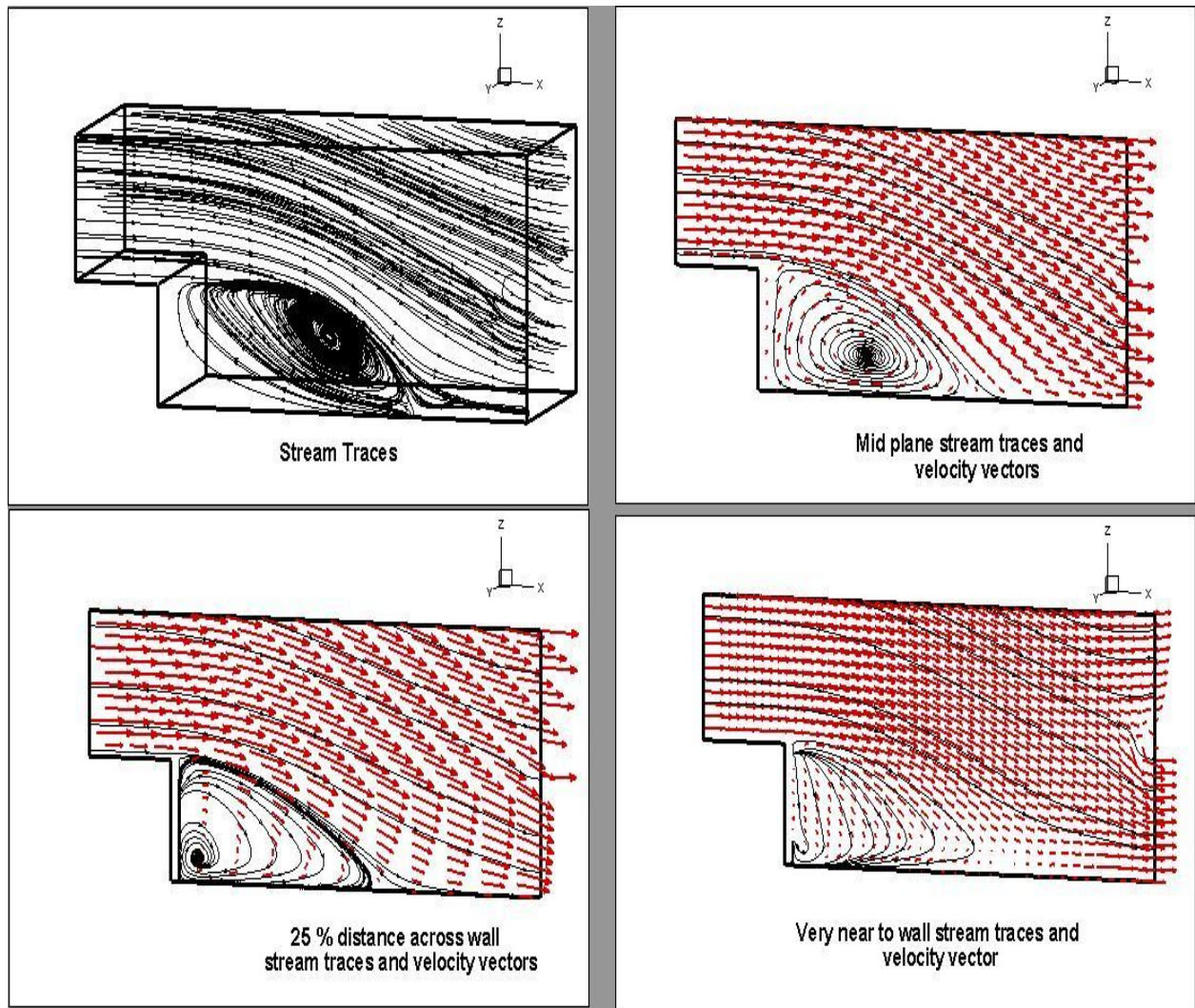


Fig. 4.1.3, flow and grid structures with single baffle



*Fig 4.1.4, 3-Dimensional Back step flow analysis*

In fig 4.1.4, we have observed that the 3 dimensional flow situations are very complicated. This is due the fact that through the surface interaction with the atmosphere shows general tendency but the expansion point and beyond that while passing through the passage of the wall the boundary conditions changes abruptly. The flow becomes sluggish at those zones and there is back flow showing an adverse pressure gradient. This adverse pressure gradient causes a buffer zone where the velocity is low and residence time for any fluid or other particle is more at that place. This means a generation of a cylindrical vortex extended from one wall to the other is present there. Though the middle plane the recirculation bubble and the reattachment point at the middle plane is very much organized & discipline, however, as



we go through the wall these vortices reduce in size and very near to the wall. This means there are intense boundary layer effects particularly the laminar sub-layer is very much effective at those region. If the side wall roughness is very much high then this effects are much more dominant. Due to this boundary layer effects the vortex structure becomes very much complicated and intense 3-d structures are chaotic in nature. This can be absolutely understandable by the stream trace plotting as shown in the figure. This is due to the fact that the wall effect dominates near the end or near the vertical surfaces. This explanation is very much clear from the figures.

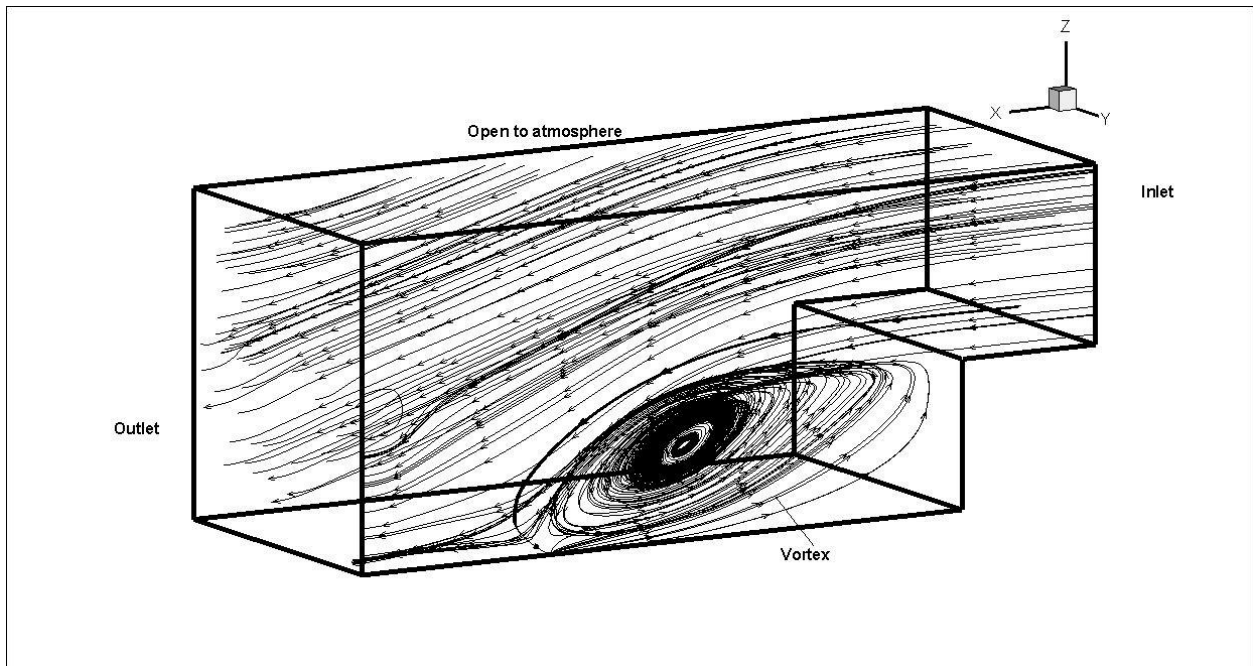


*Fig. 4.1.5, 3-Dimensional back step result*

In the fig 4.1.5, a very well posed vortex generated anticlockwise to the axis. These vortices are very important from the point that they produce low pressure zone, thus recirculation bubbles are generated. This recirculation but bubbles are cylindrical in nature.

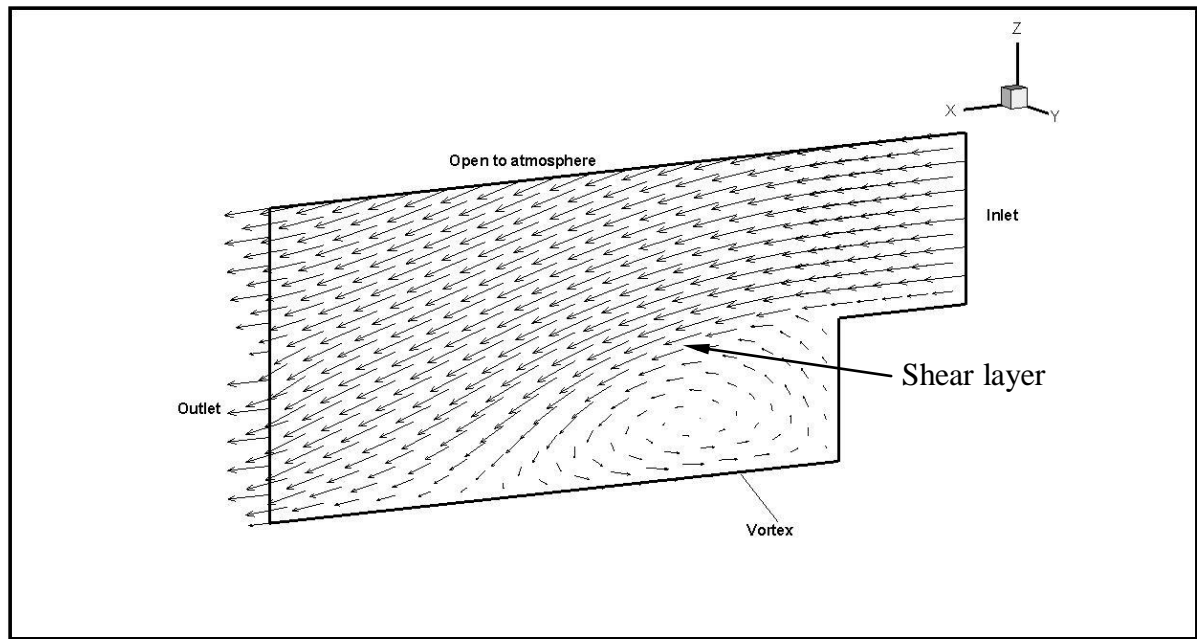


*Fig. 4.1.6, mid plane back step result*

In fig. 4.1.6 we can see that at all the mid plane there exist two distinct velocity zones, one is the vortex generated at the bottom which is enveloped by the incoming flow negotiating recirculation bubble and go passed towards the end. The vortex is counter clockwise rotating one and there has been a very good interaction between the bubble and the main flow culminating into free shear layer type flow happen there through near the side wall and effects are very much active. These phenomena can be further corroborated from the fig 4.1.4 below which is nothing but placement of a baffle in the form of English letter 'L'. Here the fluid has to negotiate sharply.

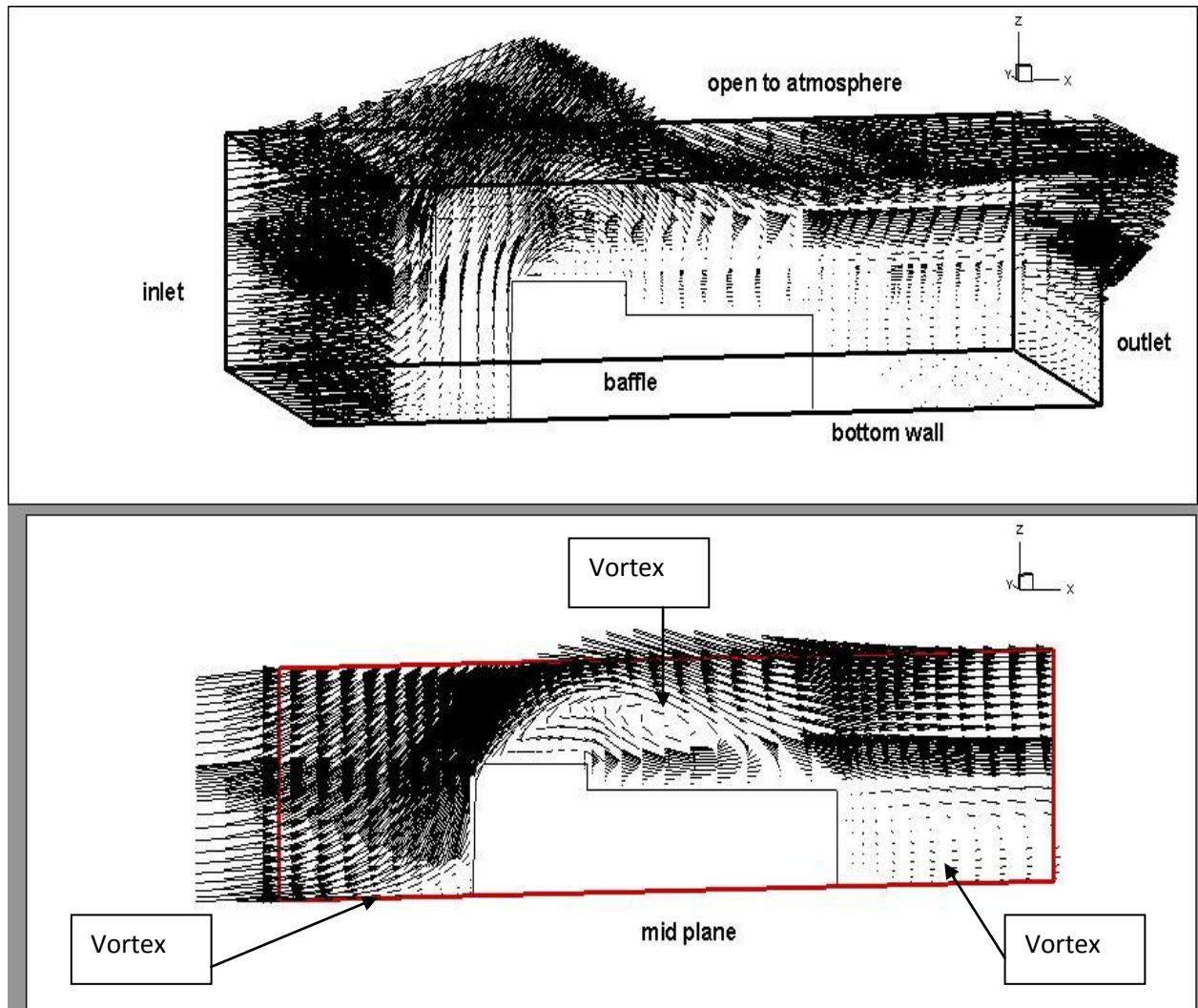


*Fig. 4.1.7, 3-D and 2-D velocity vector result*

At the upper corner of the baffle in fig 4.1.7, the moment it goes beyond the height of the baffle at the corner a sudden change in boundary condition causes a recirculation at the first roof of the baffle, followed by generation of smaller bubbles at the downstream of the baffle. However it is very clear that at the mid plane of the recirculation bubble behaves in such a way that there is inevitably presence of a counter clockwise rotation vortex. However at the end of this complex baffle there exists a very fee able recirculation. This recirculation extends up to the ends.

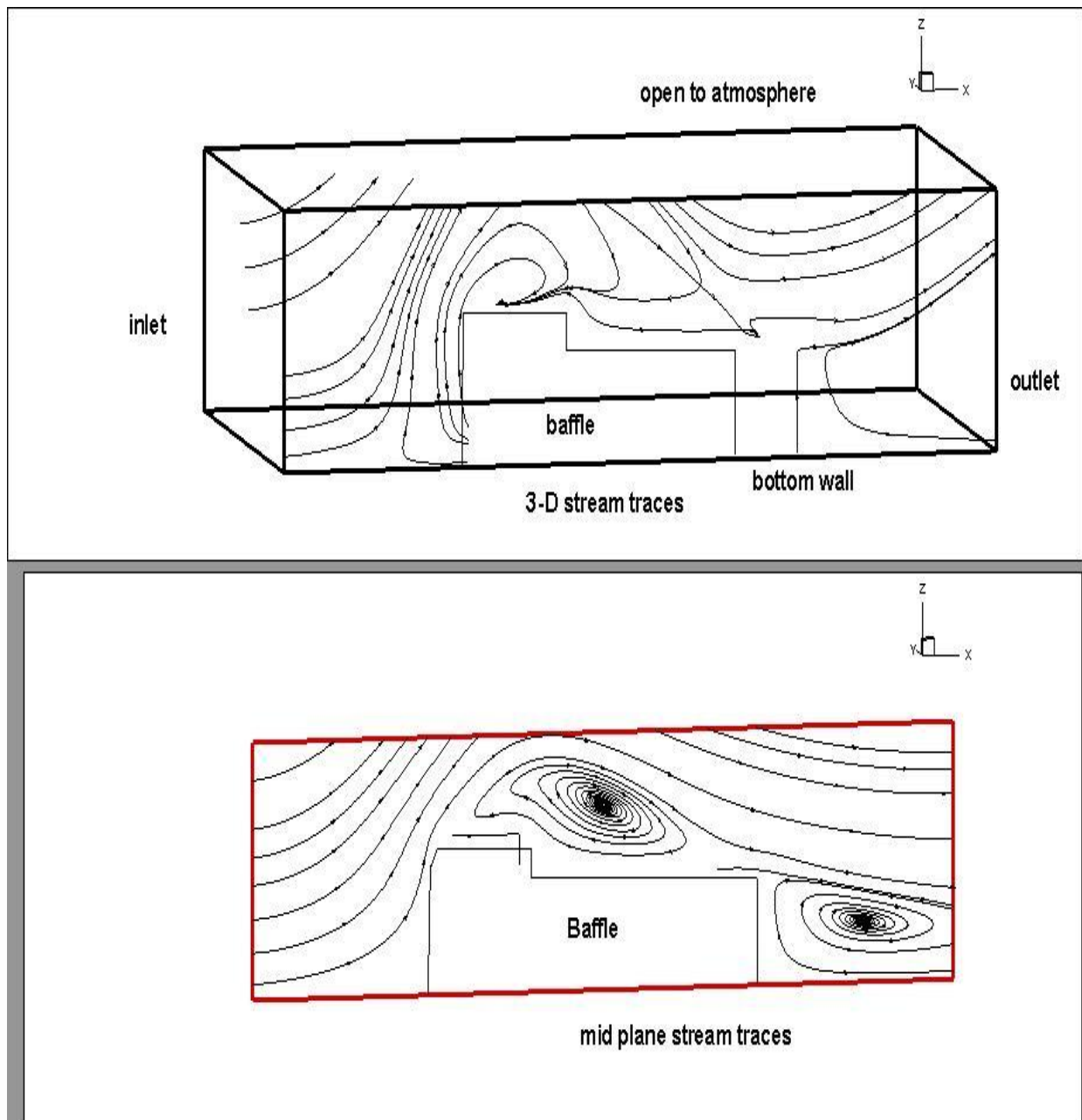





*Fig 4.1.8, Stream traces result*

In fig 4.1.8, the first picture is a 3 dimensional view of flow through open channel and the 2<sup>nd</sup> fig. represent the 2 Dimensional view of the open channel .From this two fig. we see it has two recirculation zones. First one is upper the baffle and second one is after the baffle i.e. downstream position. For the upper part of baffle there is a possibility to reform adverse pressure gradient is negative that why the recirculation zone comes here and also the same conclusion draw here for downstream cases.

## 4.2 Experimental result and Discussion

We use three types of baffle into the channel as barrier.

	A Type
	B Type
	C Type

*Fig. 4.2.1, Different types of Baffle*



Fig. 4.2.2 flow pattern of water in the channel

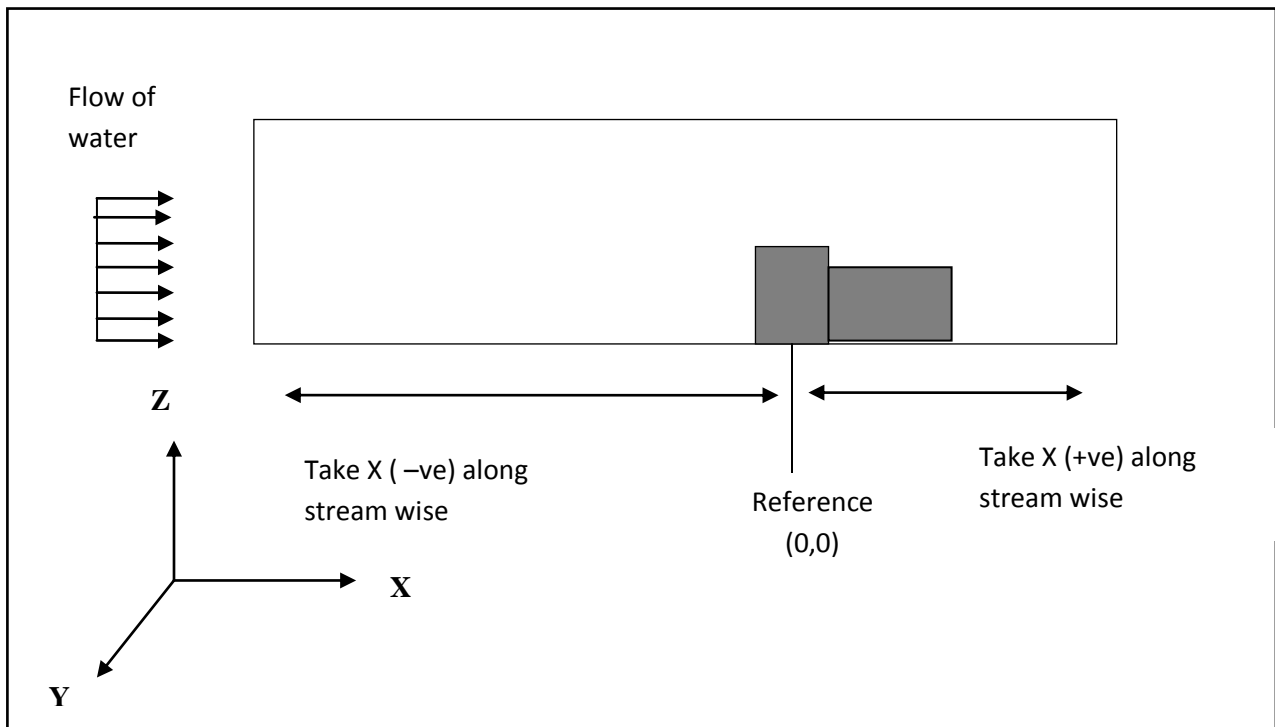
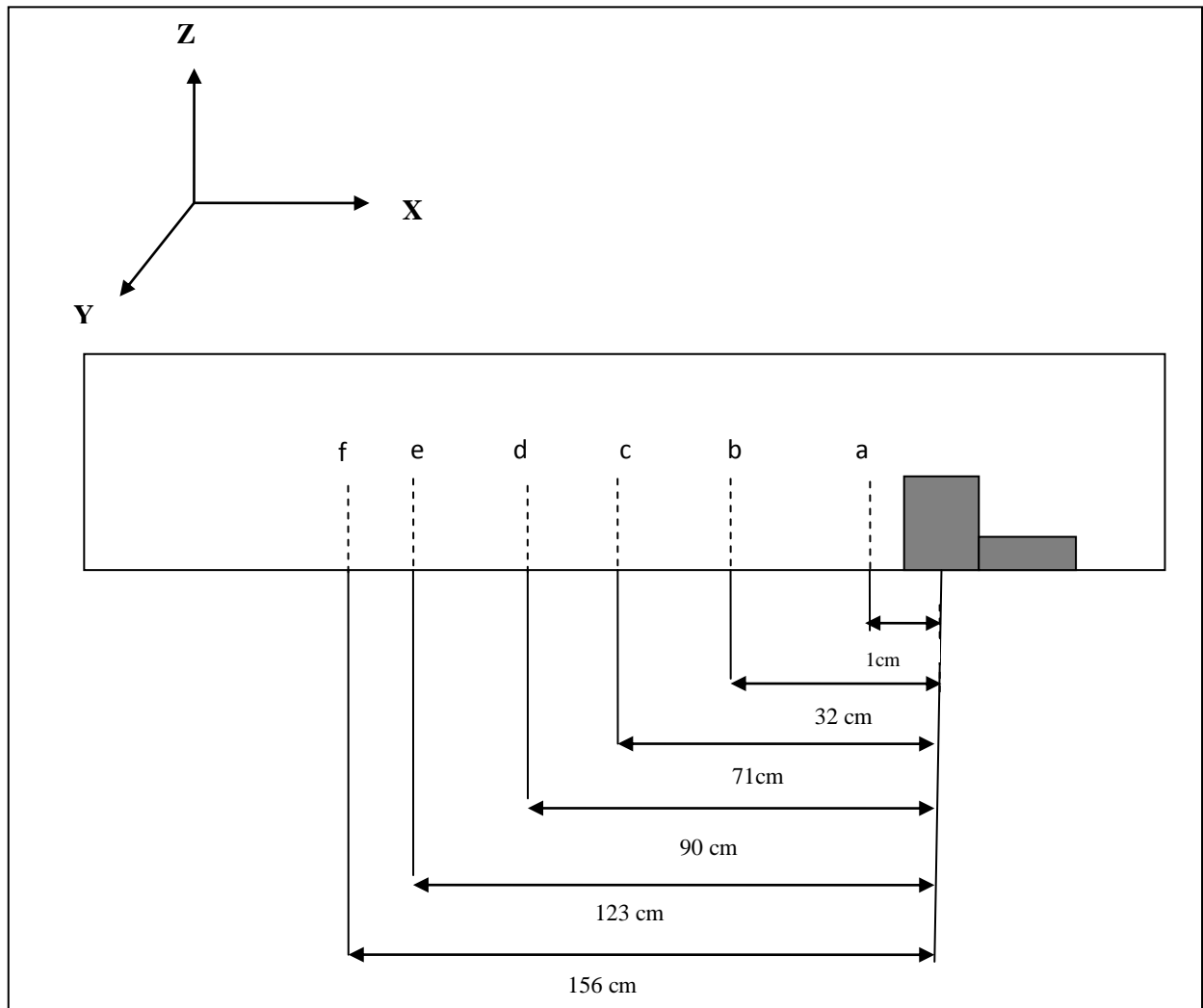
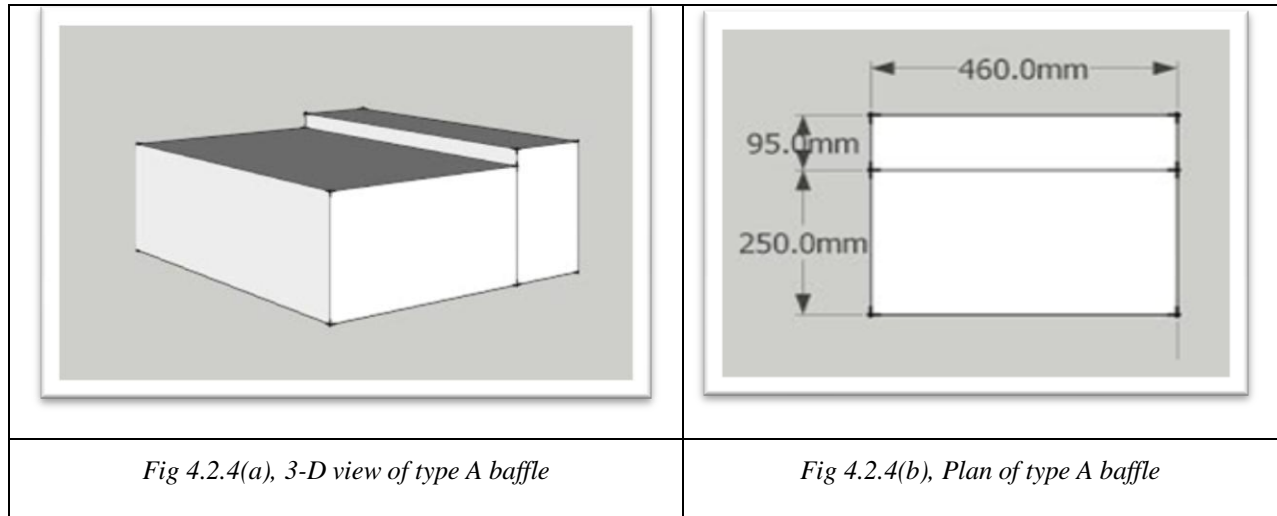
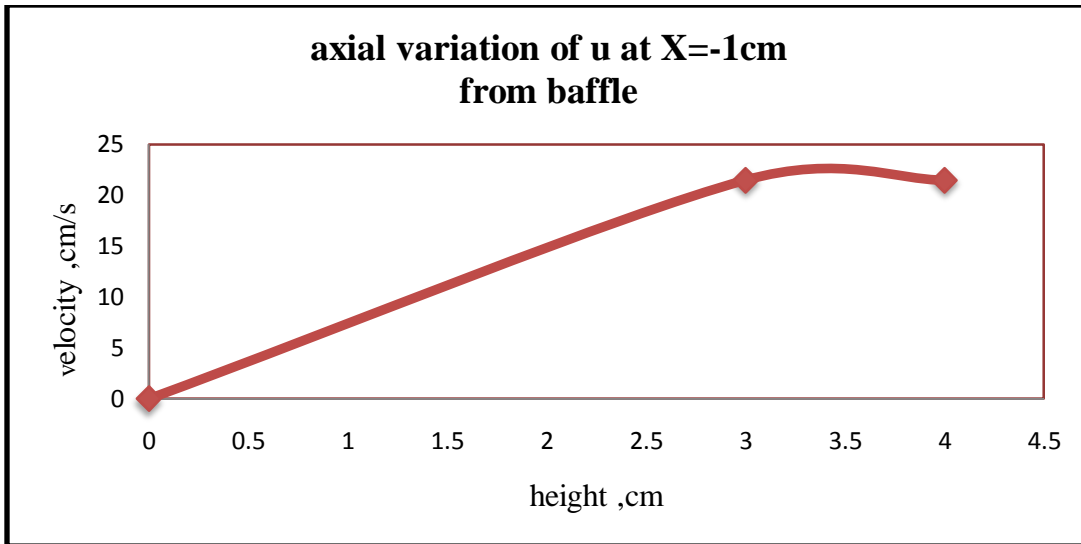


Fig. 4.2.3, a sketch of side view channel with baffle

**Upstream result of type A baffle:**



*Fig. 4.2.5, a typical geometric drawing for type A shown the position of measurement*



*Fig 4.2.6, Velocity Distribution at X= -1 cm*

In above fig 4.2.6 on the baffle at a position of X=1 cm a very natural tendency abiding all the physical law, yet obeying the interfacial phenomena reduces the velocity.

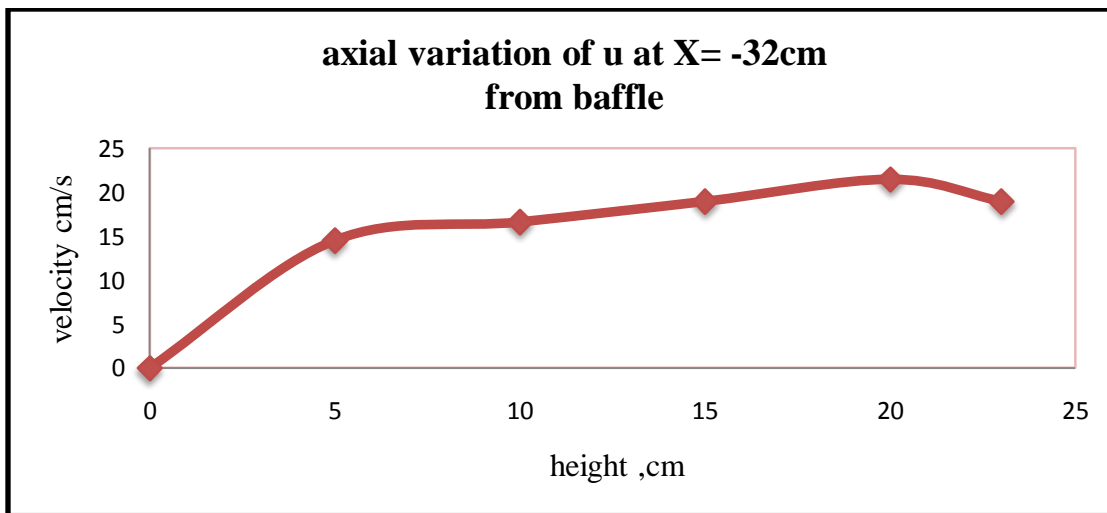


*Fig 4.2.7, Velocity distribution at X=-32cm*

In the fig 4.2.7 , the velocity increases right from the wall to a height of 5 cm, then it remain straight up to=20cm. however the interfacial phenomena bring down its velocity as depicted from the figure.



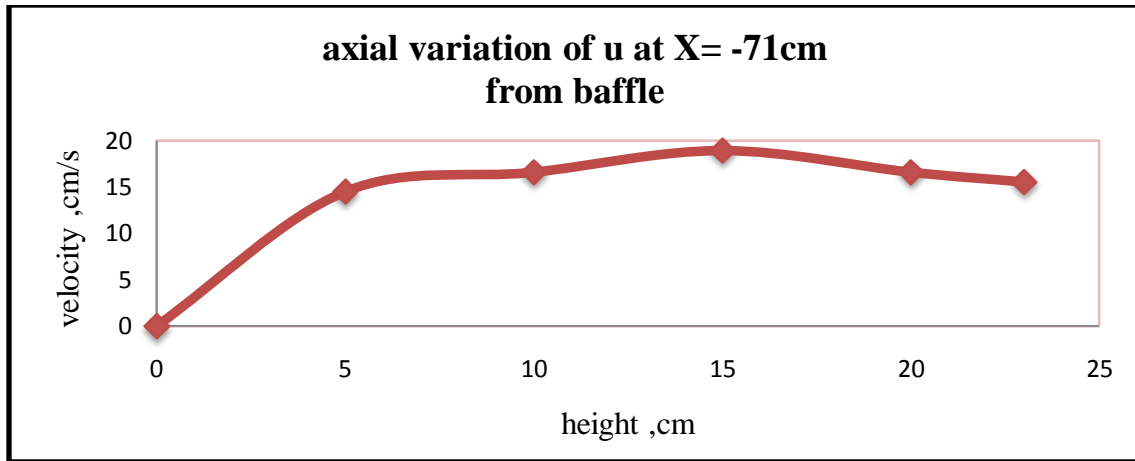


*Fig 4.2.8, Velocity distribution at X= -71cm*

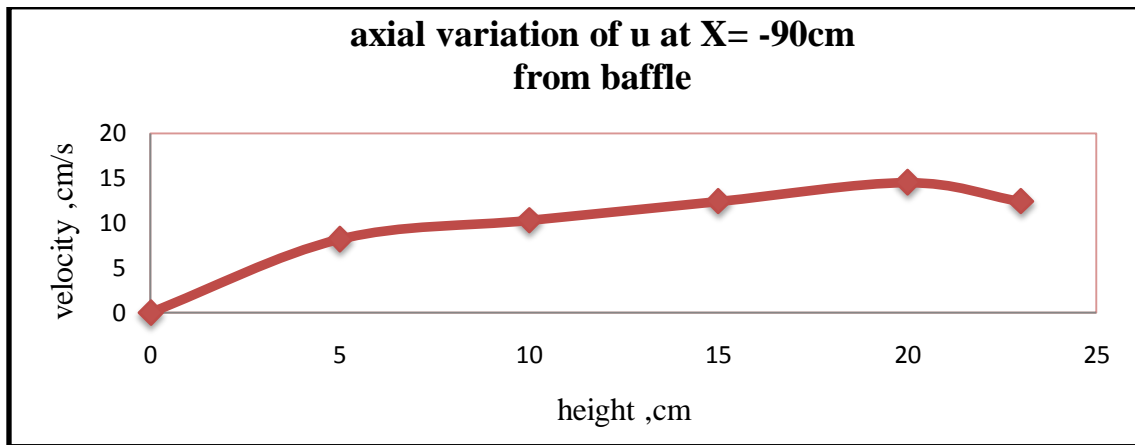


*Fig 4.2.9, Velocity distribution at X= -90cm*

From fig 4.2.8 and 4.2.9 looks like almost similar pattern. But in fig 4.2.8 the maximum velocity is at the height of 15cm and in fig 4.2.9 the maximum velocity is at the height of 20cm.

The fig 4.2.8 graph is higher ,the variation of velocity is increases more.

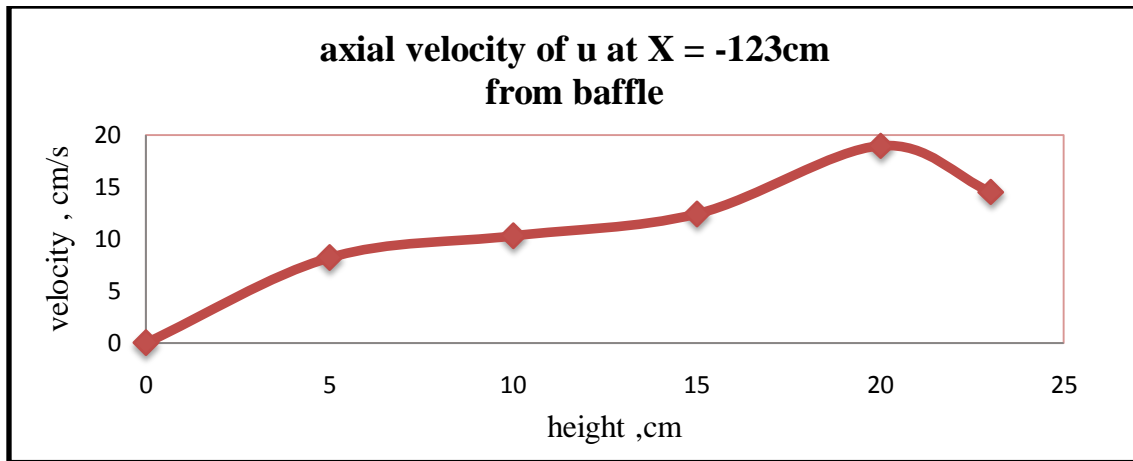


*Fig 4.2.10, Velocity distribution at X= -123cm*

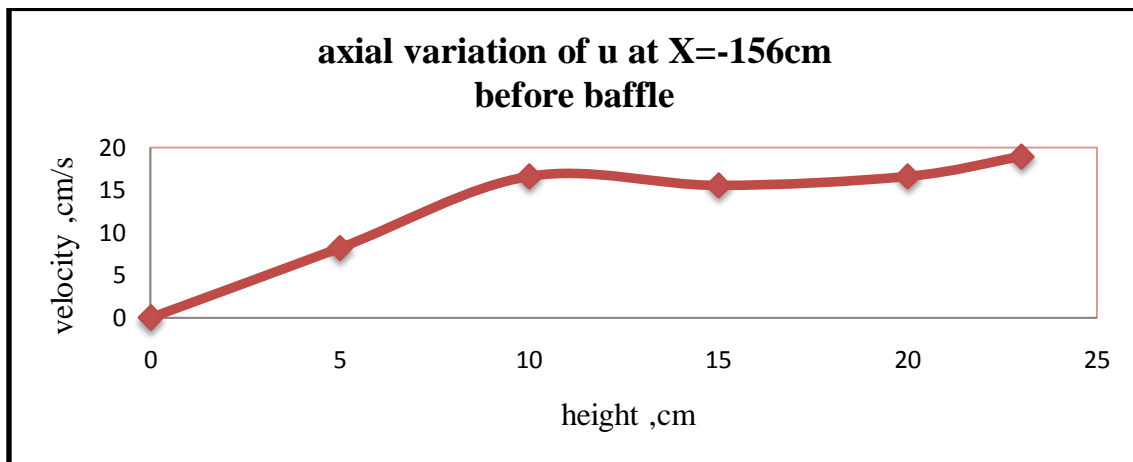


*Fig 4.2.11, Velocity distribution at X= -156cm*

From fig 4.2.10 the nature of graph gradually increases but at the point of 20cm its get the highest value and after that it again increases.

From fig 4.2.11 the distribution graph is varied with height increasing but at the height of 15cm its decreases a little. As this is in type A baffle so the water is not logged or getting obstacles much.

**Upstream result of type B baffle:**

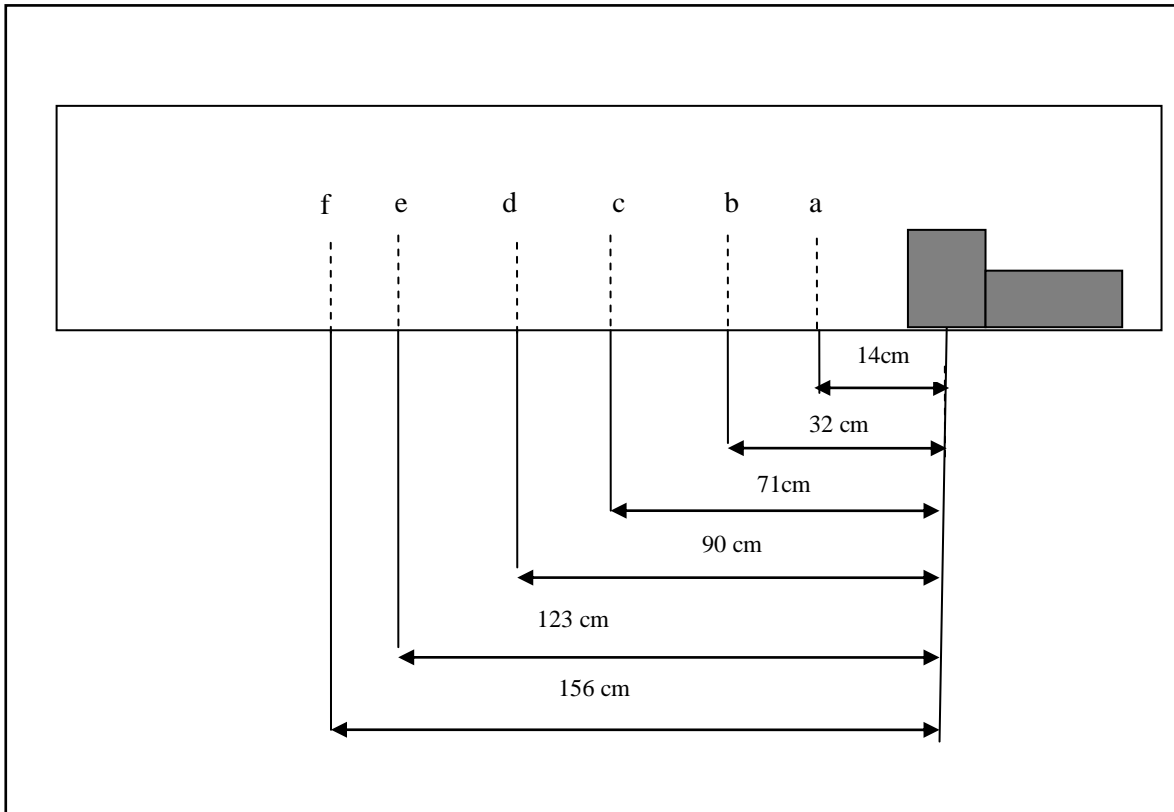


*Fig. 4.2.12, a typical geometric of type B drawing shown the position of measurement*

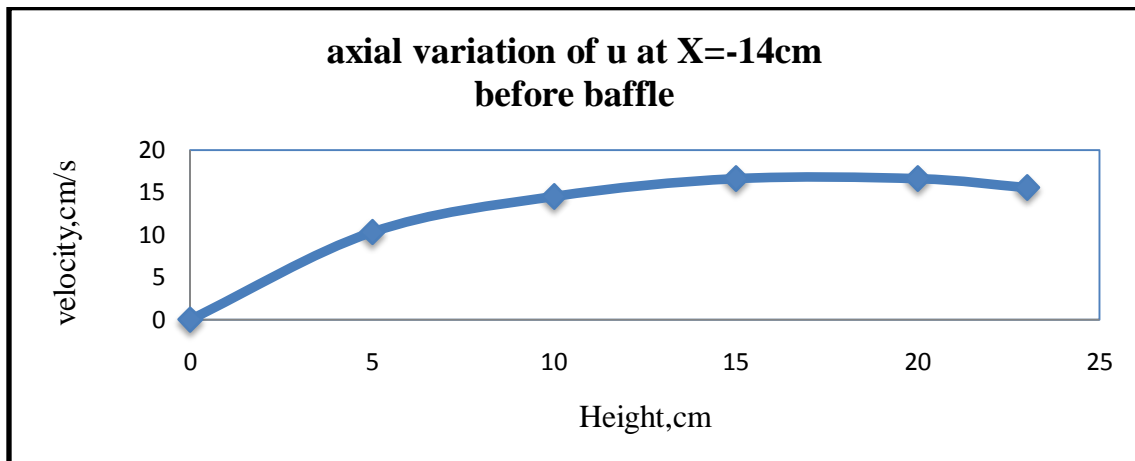


*Fig. 4.2.13, velocity distribution at X= -14 cm*

From fig 4.2.13, we see that the velocity distribution is parabolic type. However near the surface of the water the velocity reduces slightly. Actually from this graph we get that maximum

velocity is at a height of 20cm and the surface velocity is little bit less. These means that the velocity gradient increases from the bottom wall and becomes maximum at little bit deep from the free surface. The velocity gradient reduces at the free surface. This is very peculiar phenomenon with the interaction of water and atmosphere. Actually, at the interface of water and air there is a sharp change in fluid properties. The density of the water is 1000 kg/m<sup>3</sup>, but at the free surface after the extend of the water we reach to the air which density is 1.25 kg/m<sup>3</sup> nearly at 20°C. So there is a jump in the density from 1000 to 1.25kg/m<sup>3</sup>. Similarly viscosity also reduces from 10<sup>-4</sup> to 10<sup>-5</sup> pa-sec. These means, there is a discontinuity at the surface. All these interactive phenomena causes reduction in the velocity of water at the free surface and this is clearly visible from fig 4.2.13.

On above fig 4.2.14, which is X=32 cm distance from the mid of the baffle. From these figure a similar physical phenomena has been observed. However in between the free surface and the little bit higher than the bottom surface, the velocity shows little reduction in value in the earlier trend but ultimately achieved the velocity at the height of 20 cm, which we already observed.

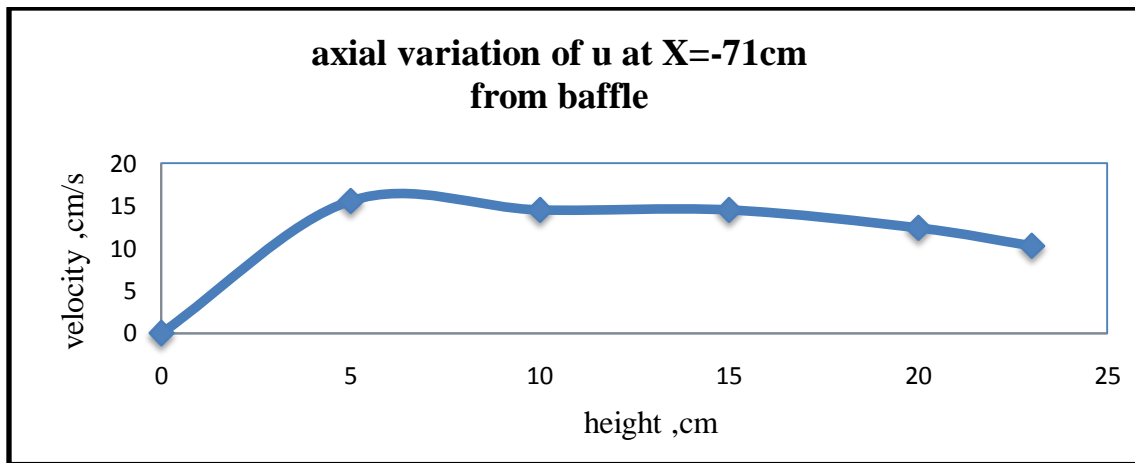
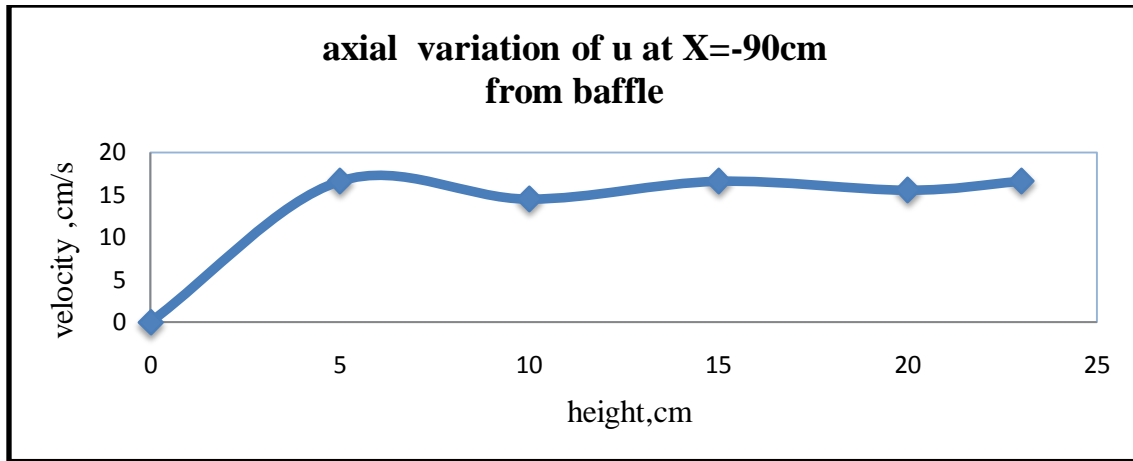


Fig4.2.15, velocity distribution at X=-71cm

From above fig 4.2.15, at the axial position of X=71cm the initial velocity gradient has been observed to be very sharp but after a certain distance of 5 cm from the bottom the velocity reduces and this trend is found to be true up to the surfaces, but the phenomena that the surface velocity is lower than at a little depth from the surface that phenomena still true here also.



*Fig 4.2.16, Velocity distribution at X= -90cm*

In the fig 4.2.16, similar tendency is observed though a little waviness in the velocity is observed.

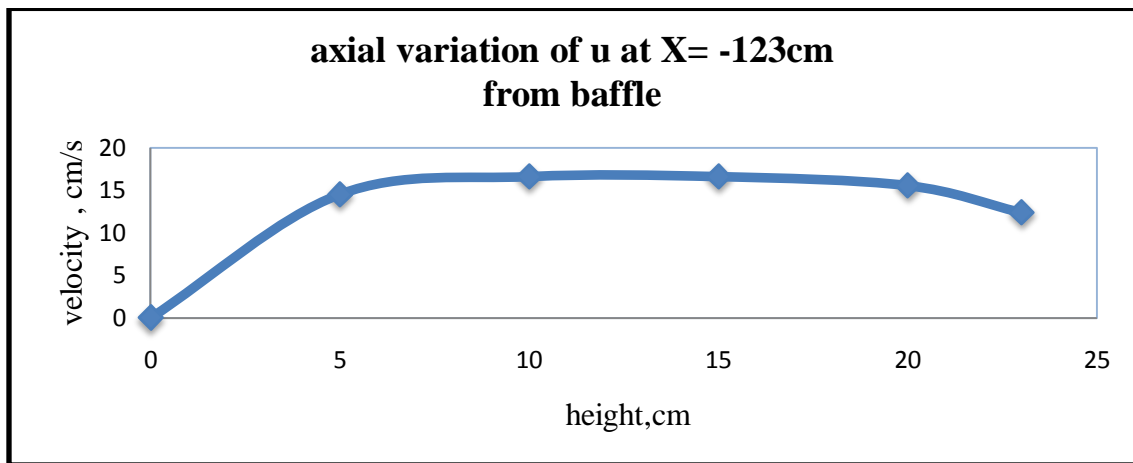


*Fig 4.2.17, velocity distribution at X= -123cm*

In fig 4.2.17, a very well structure streamwise velocity profile at a distance of X=123 cm has been observed and here also all the physical phenomena are present. The velocity profile is very much smooth, no undulation waviness in it. The final velocity at the surface once again reduces due to interaction between fluid & air properties.

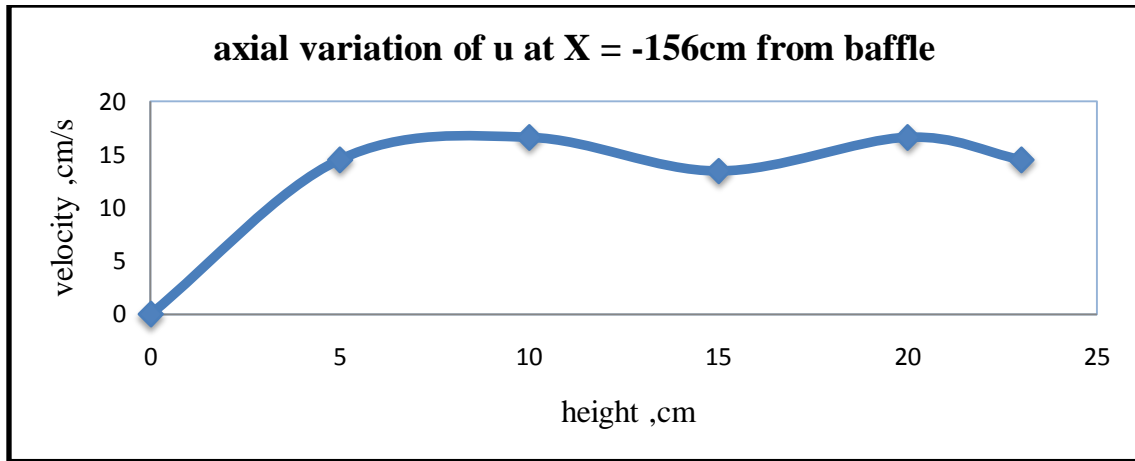


Fig 4.2.18 velocity distribution at X= -156cm

**Upstream result of type C baffle:**

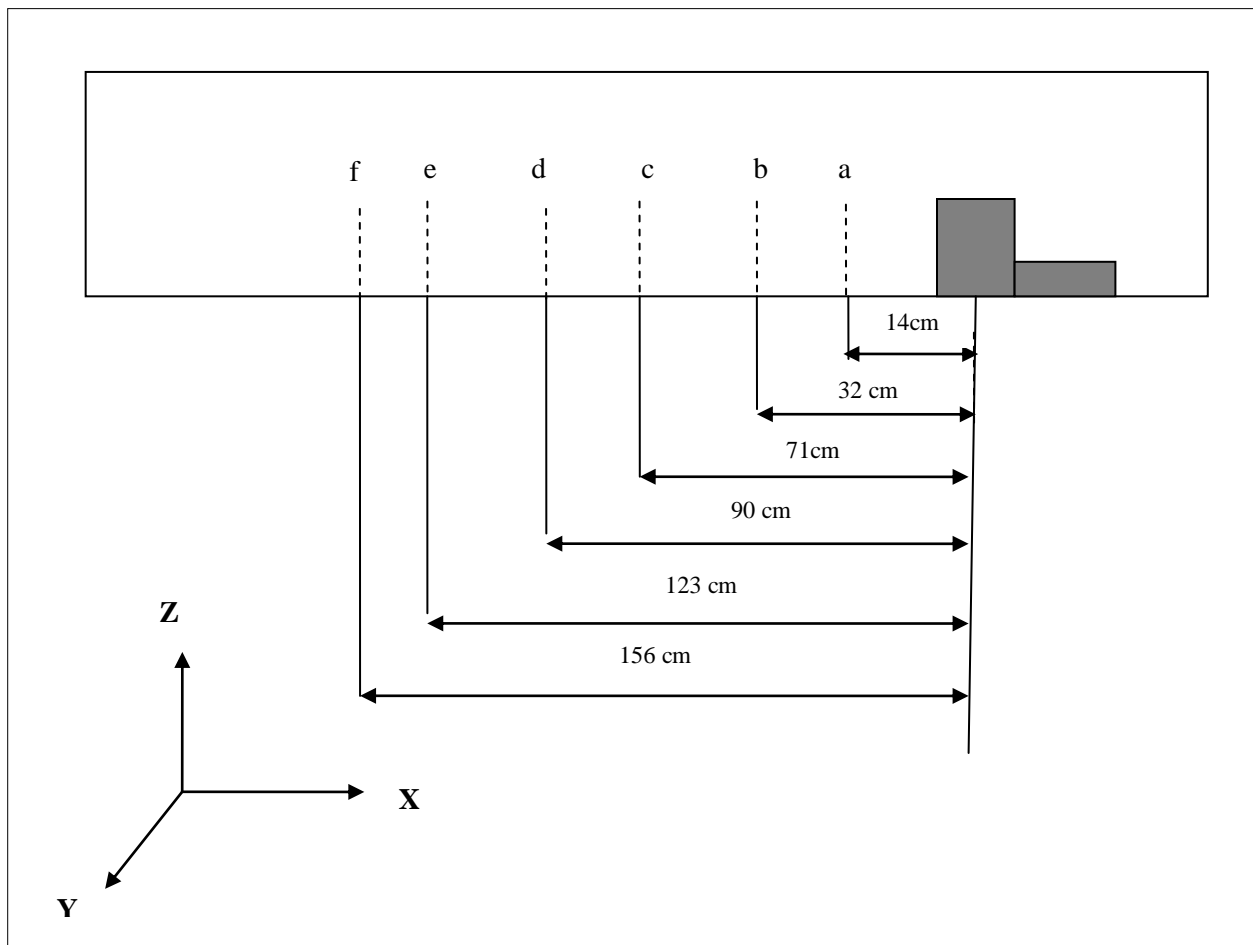


Fig 4.2.19, A typical geometric drawing shown the position of measurement

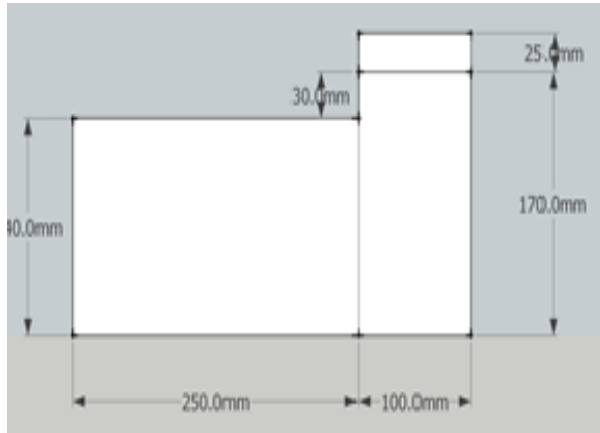


Fig 4.2.20, Side view of type C baffle

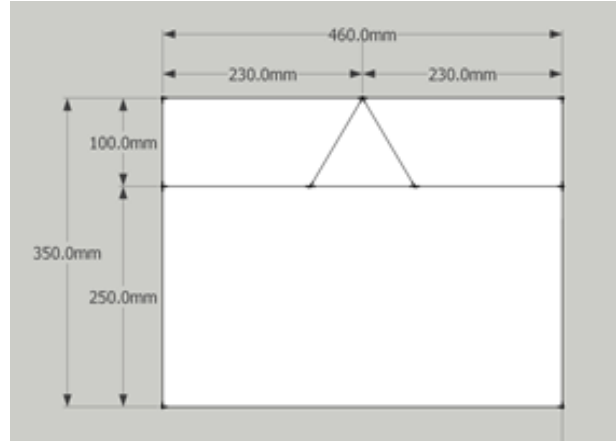


Fig 4.2.21, Plan of type C baffle

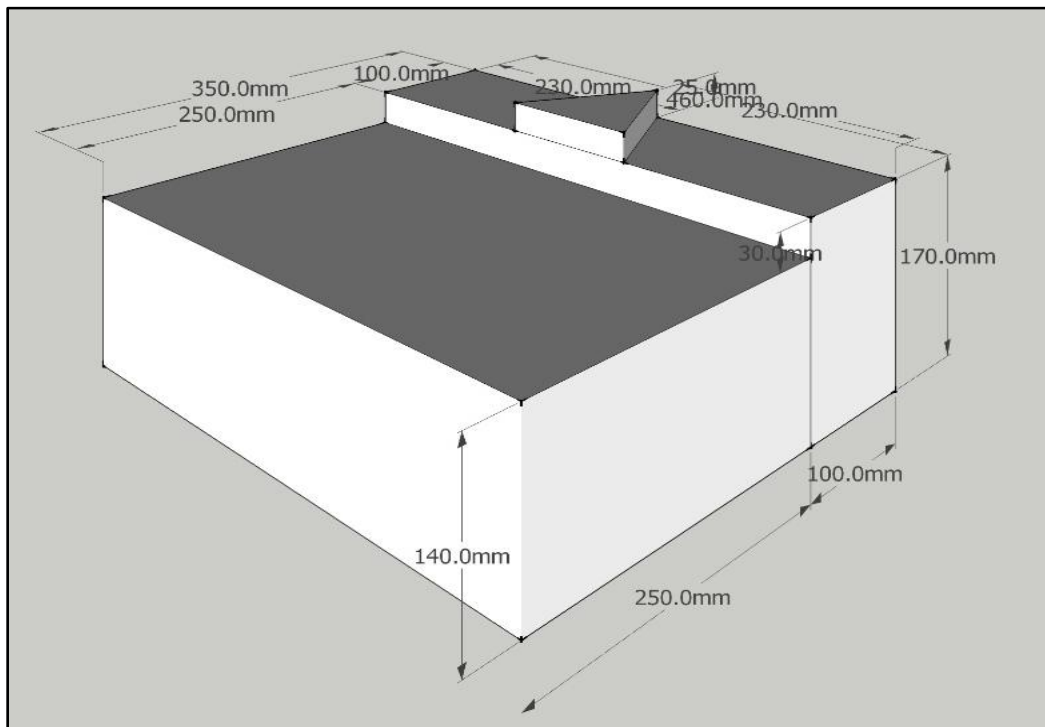
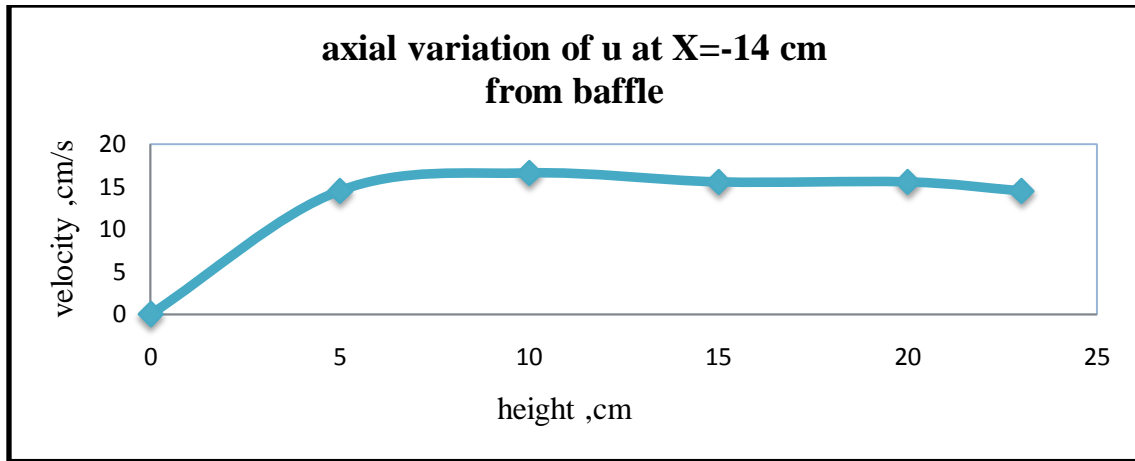
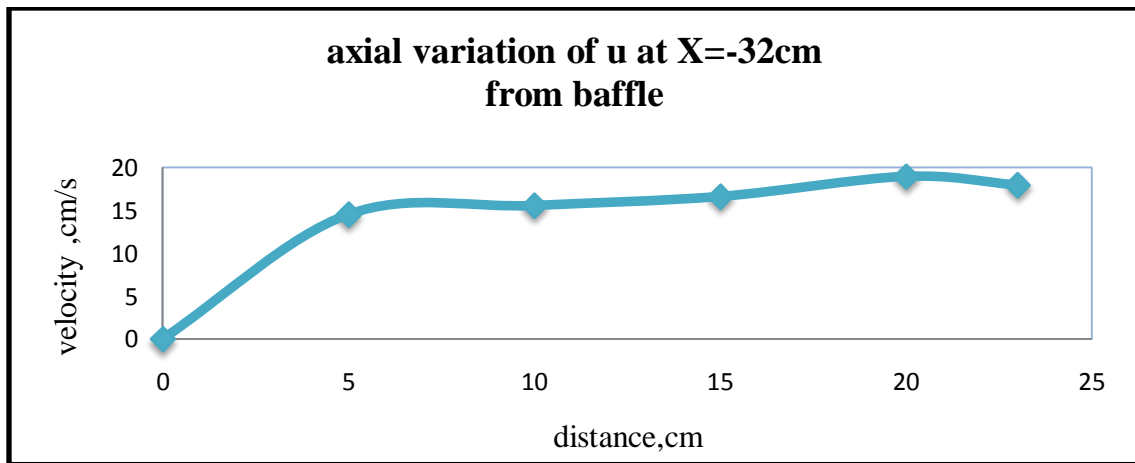


Fig 4.2.22, 3 dimensional view of C Type Baffle



*Fig 4.2.23, velocity distribution at X=-14cm*



*Fig 4.2.24, velocity distribution at X= -32cm*

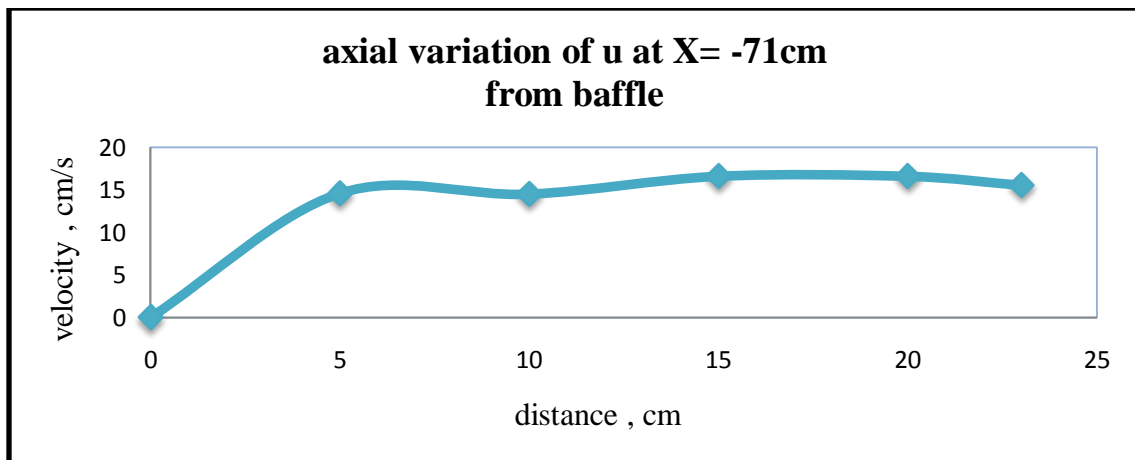


*Fig 4.2.25, velocity distribution at X= -71cm*



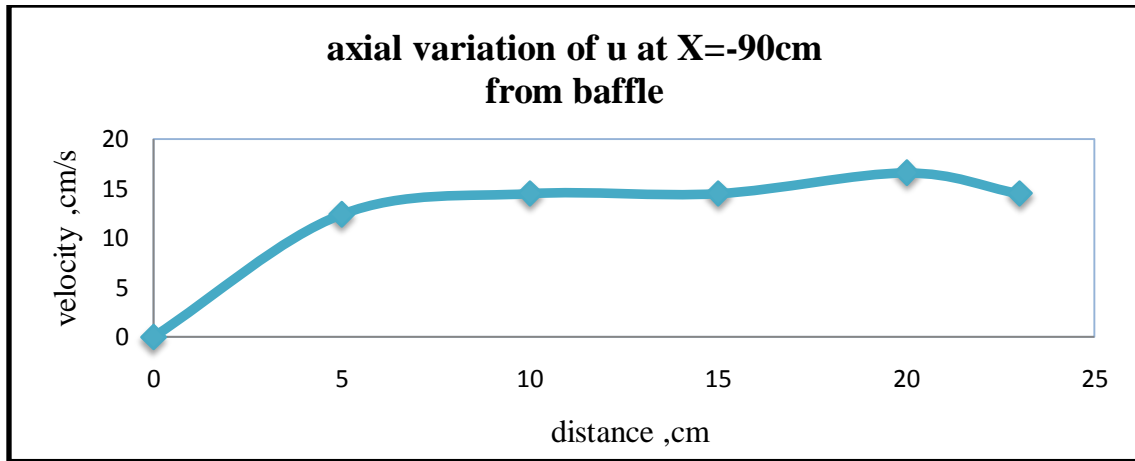


*Fig 4.2.26, velocity distribution at X= -90cm*

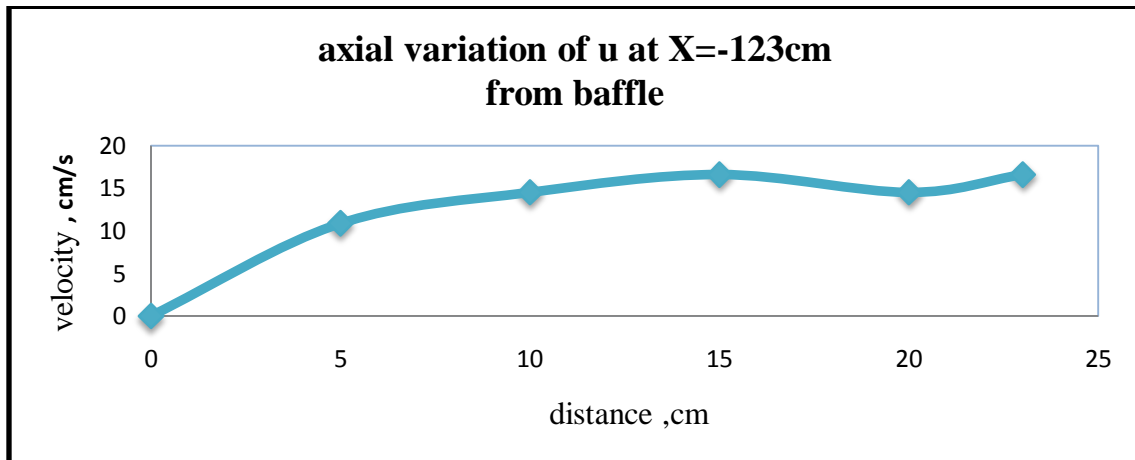


*Fig 4.2.27, velocity distribution at X=-123cm*

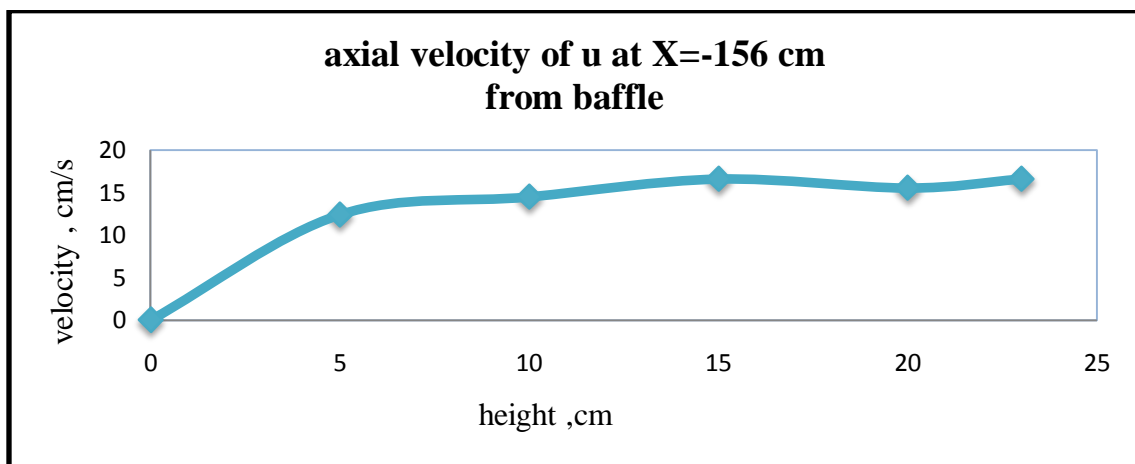


*Fig 4.2.28, velocity distribution at X=-156cm*

**Fig 4.2.23, 4.2.24, 4.2.25, 4.2.26, 4.2.27, 4.2.28** owe the similar description as we have done to the upper discussion, the velocity profile along stream wise increases gradually with height.

**Reading above the type B baffle**

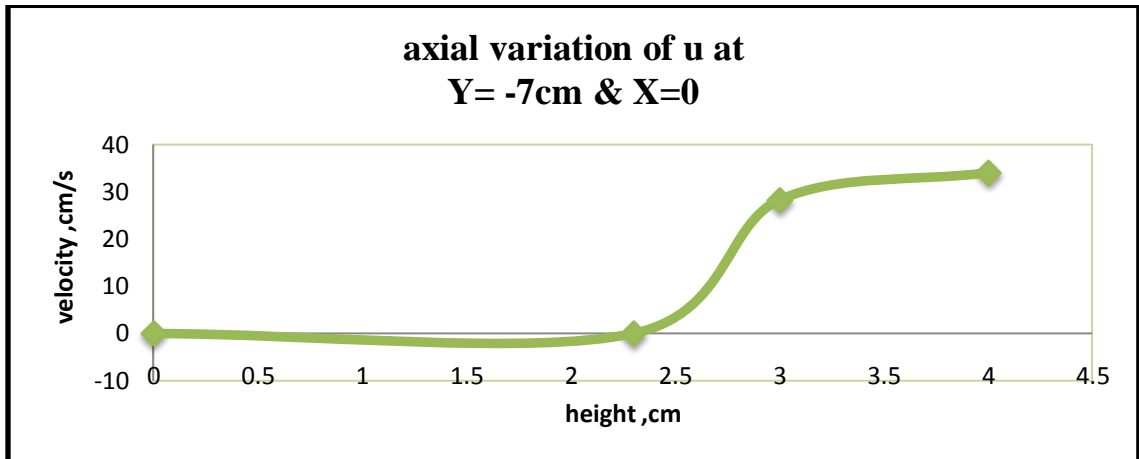


*Fig 4.2.29, velocity distribution at y= -7cm*

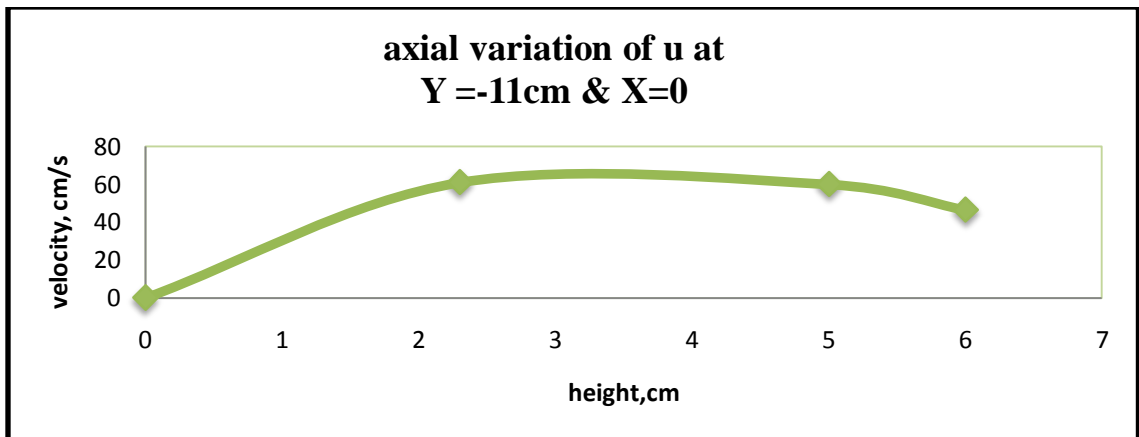


*Fig 4.2.30, velocity distribution at y= -11cm*

From fig 4.2.29 the axial variation is different. Up to the height of near about 2.5cm there are no such increases in velocity profile. But from 2.5cm the velocity starting increases. As it is type B baffle, the surface is not smooth it's like channel type so the at the distance of 7cm (i.e. from

midpoint of baffle) there is very little bit recirculation creates and so after that increase in height the velocity increases.

From fig 4.2.30 the variation of velocity profile is normal its gradually increases but at the end of it decreases little bit.

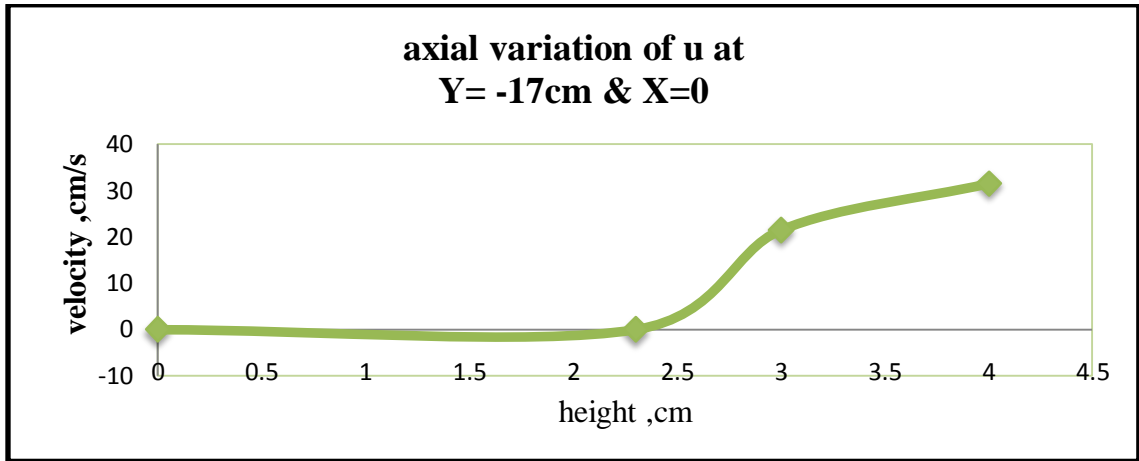


Fig 4.2.31, velocity distribution at y= -17cm

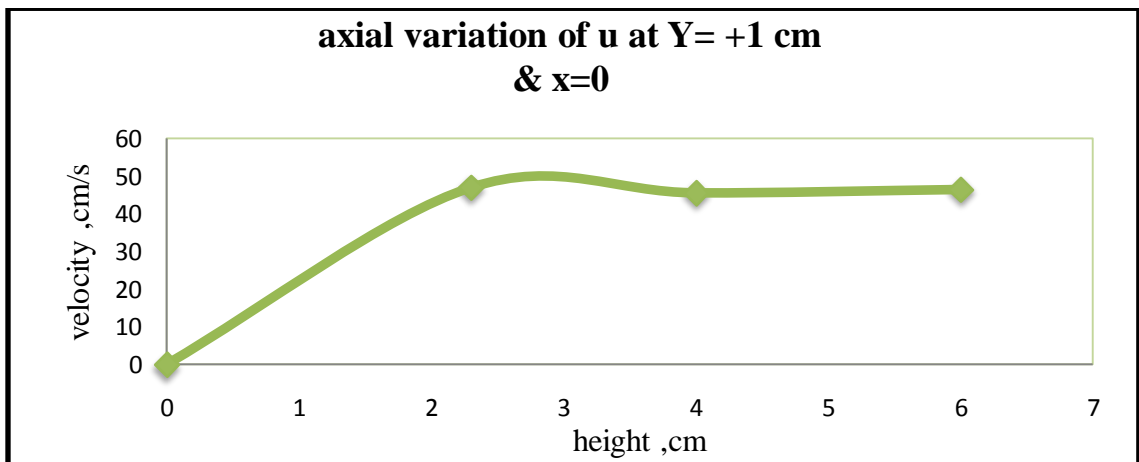


Fig 4.2.32, velocity distribution at y=1cm

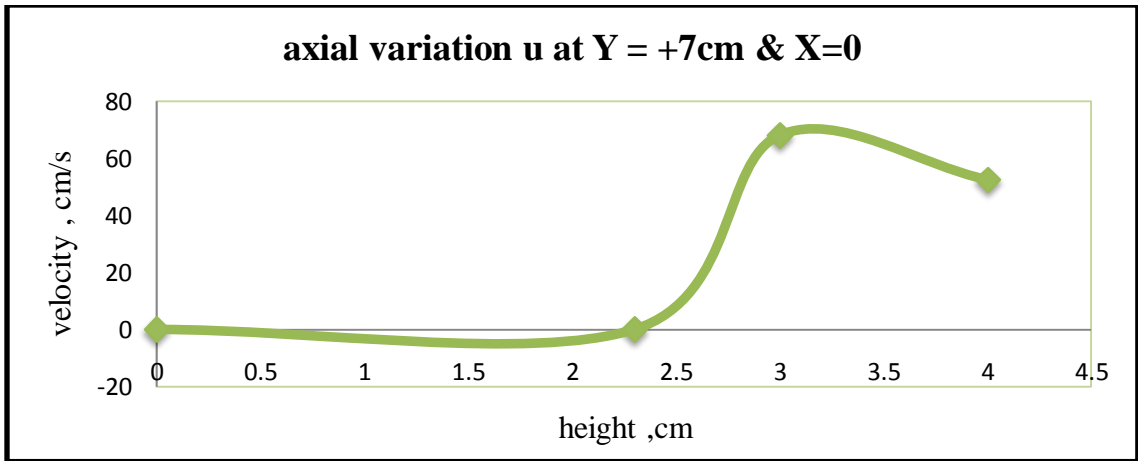


Fig 4.2.33, velocity distribution at y=7cm

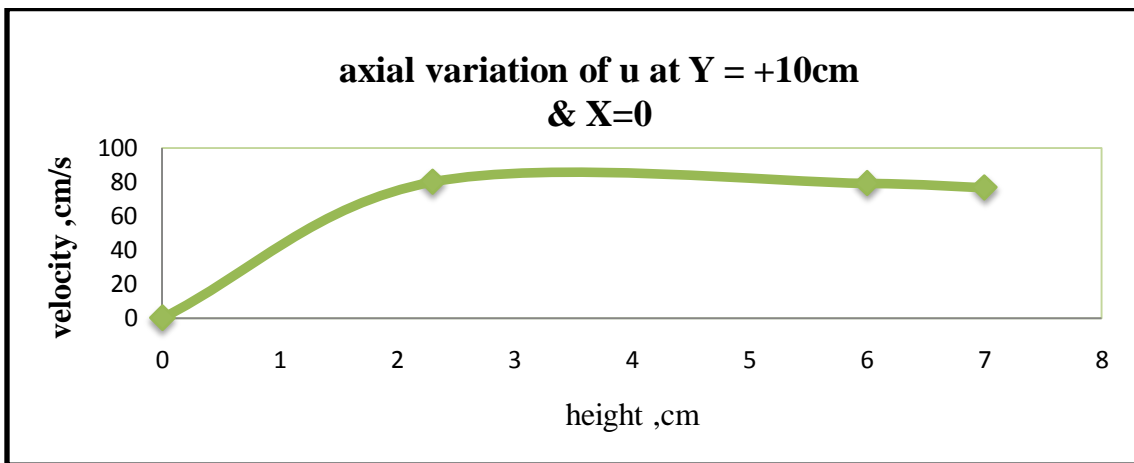


Fig 4.2.35, velocity distribution at y=10cm

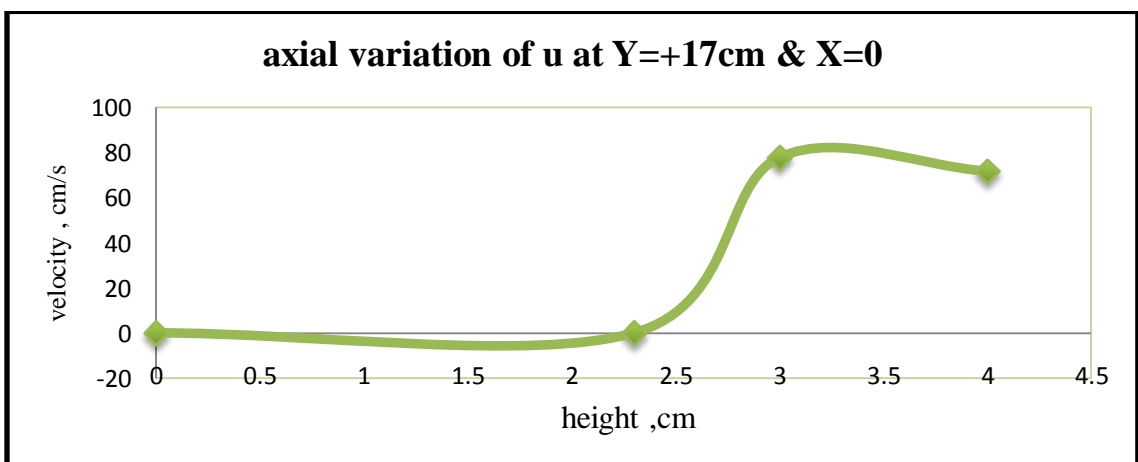
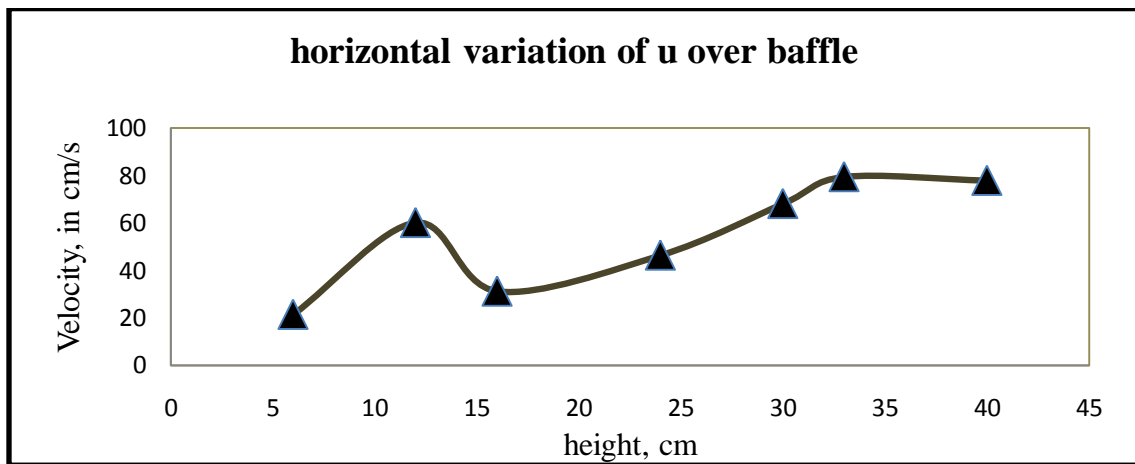


Fig 4.2.35, velocity distribution at y=17cm

Fig 4.2.31 is alike with fig 4.2.29. In fig 4.2.32 is different it increases the velocity gradually. At the height of near about 3cm its velocity is highest after that it increases little and at end it gradually follows straight. Fig 4.2.33 is near like fig 4.2.31 but its variation at the point of 2.5cm is more. Fig 4.2.35 is almost same like fig 4.2.33. So the variation in the graph shows that when water passes through the channel it's behave a abnormal nature means some recirculation may present there but when the water passes through plane surface its behave normal.

**Horizontal variation of velocity along the width of Type B baffle:**



*Fig 4.2.36, Horizontal variation of velocity along the width of type B*

In above fig the nature of graph is very peculiar type. The highest point is in between 30 to 40cm. But the nature of graph is changes suddenly at the height near about 20cm. first it increases then decreases again smoothly increases to the end. As this is type B baffle so the variation looks like this.

**Horizontal variation of velocity along the width of type A baffle:**

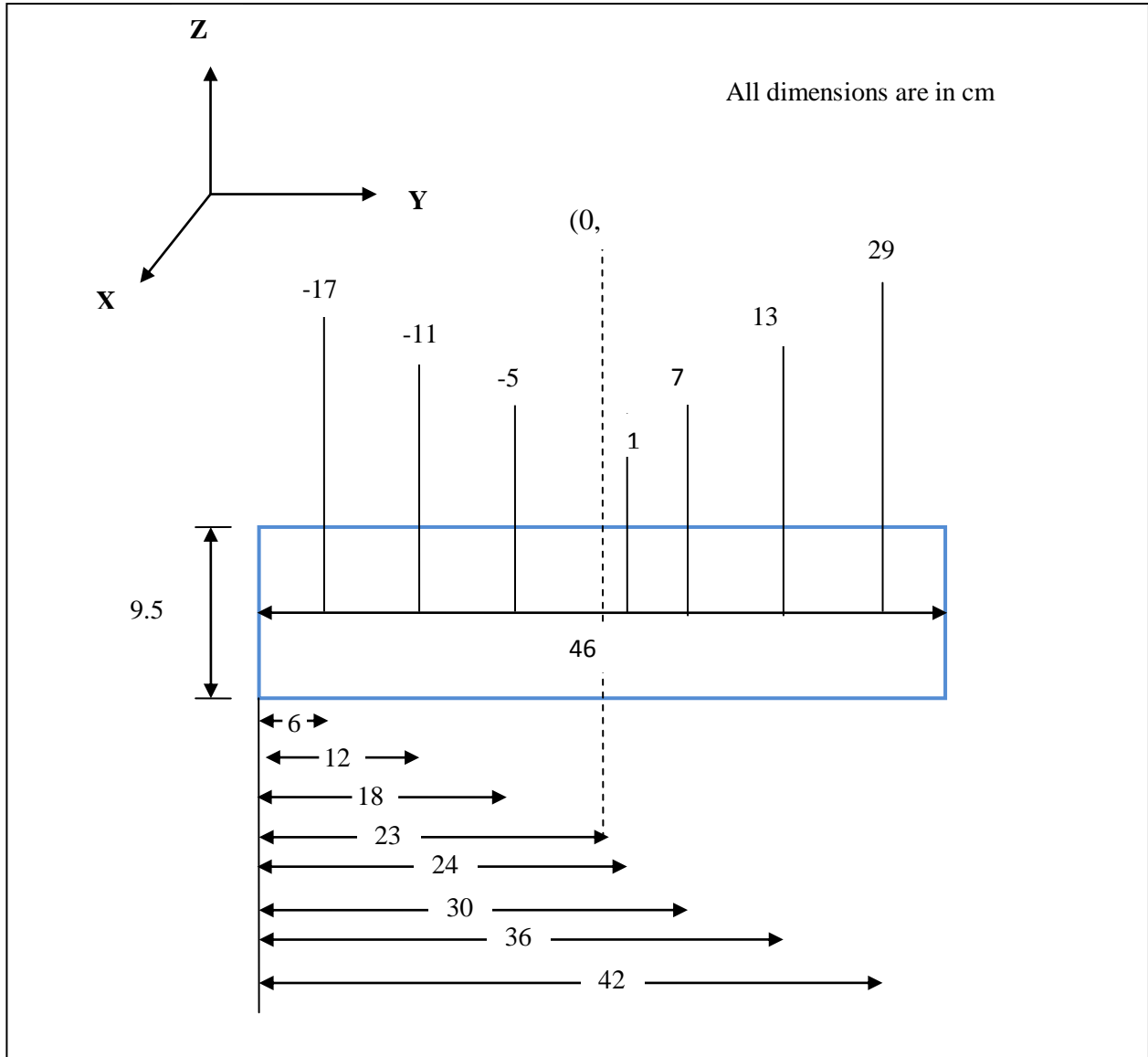


*Fig 4.2.37, Plan view of the measurement of type A baffle*

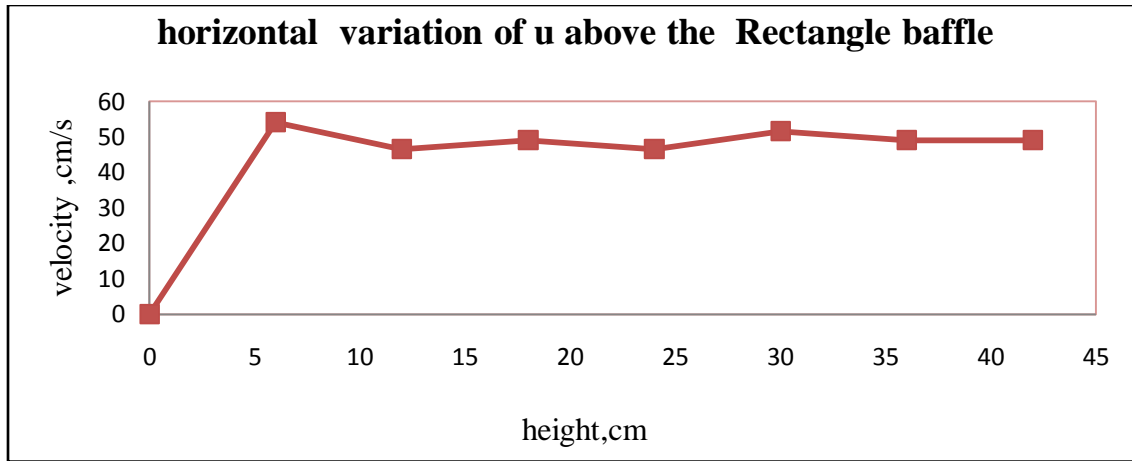


Fig 4.2.38, Horizontal variation of velocity along the width of type A

**Reading above the baffle type C:**

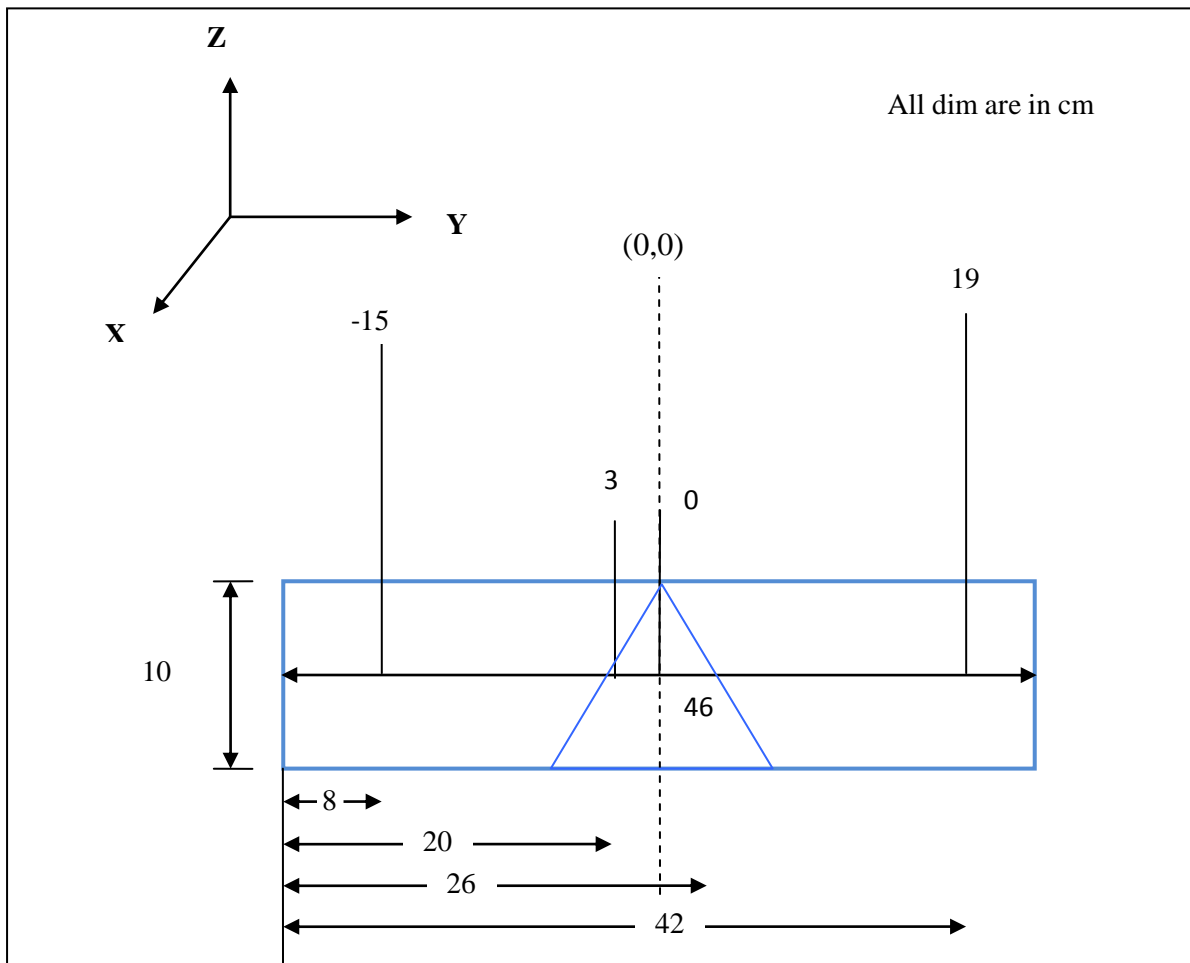


Fig 4.2.39, plan view of measurement

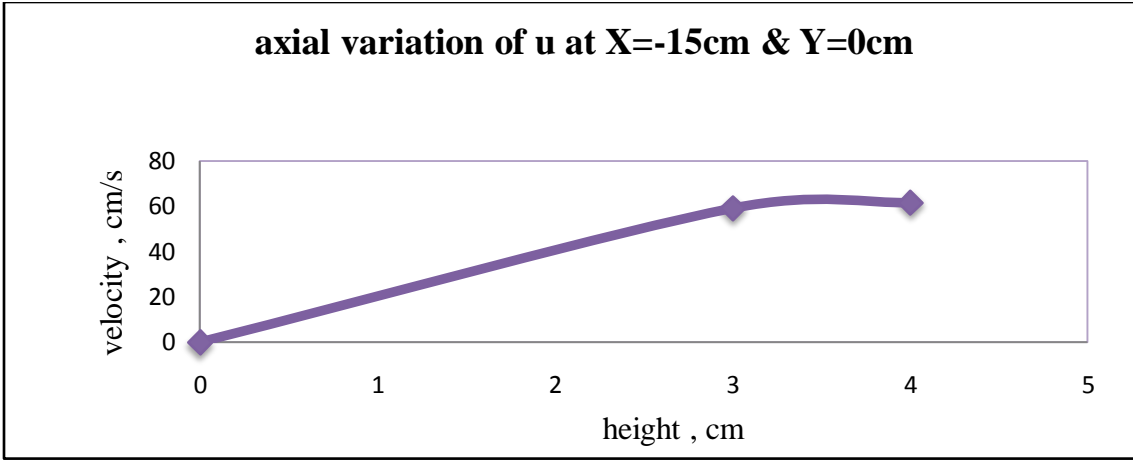


Fig 4.2.40, velocity distribution at  $x=-15\text{cm}$

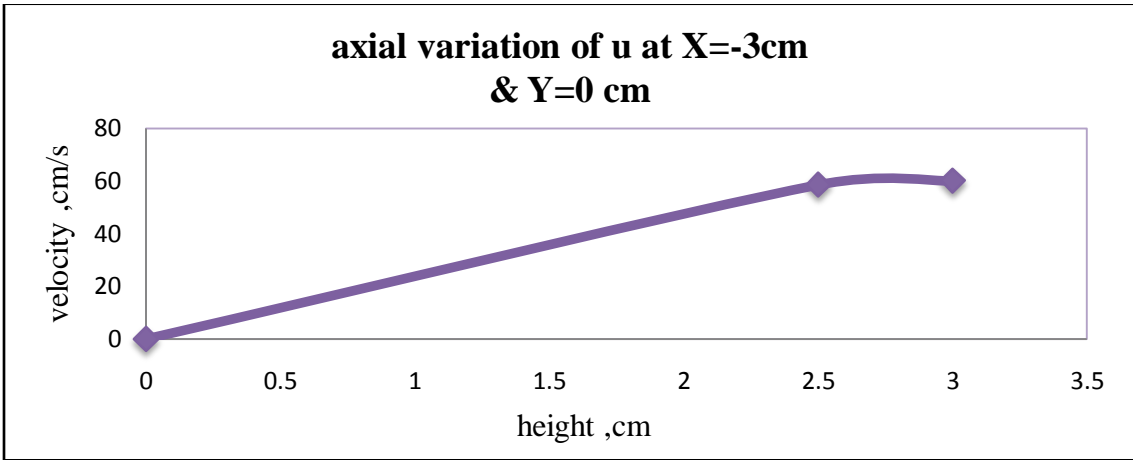
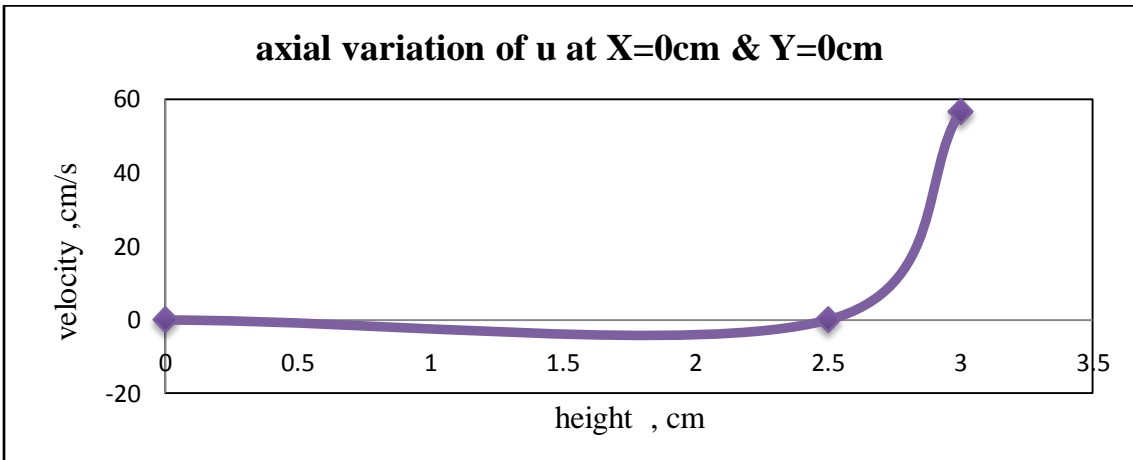


Fig 4.2.41, velocity distribution at  $x=-3\text{cm}$

Fig 4.2.40 and 4.2.41 are very similar. It is semi parabolic and changes are straight.



Fig, 4.2.42, velocity distribution at  $x=0$



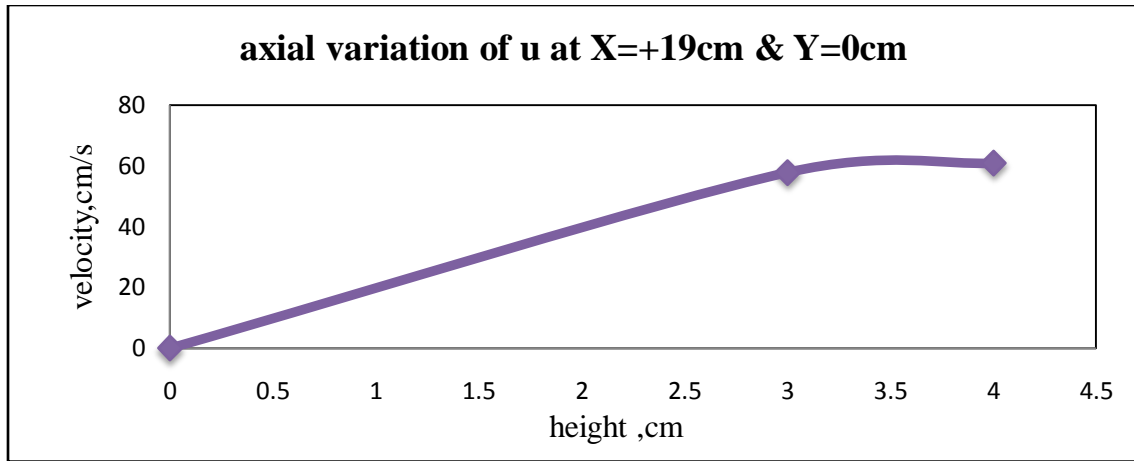


Fig 4.2.43, velocity distribution at  $x=+19\text{cm}$

**Reading of Type C baffle at downstream:**

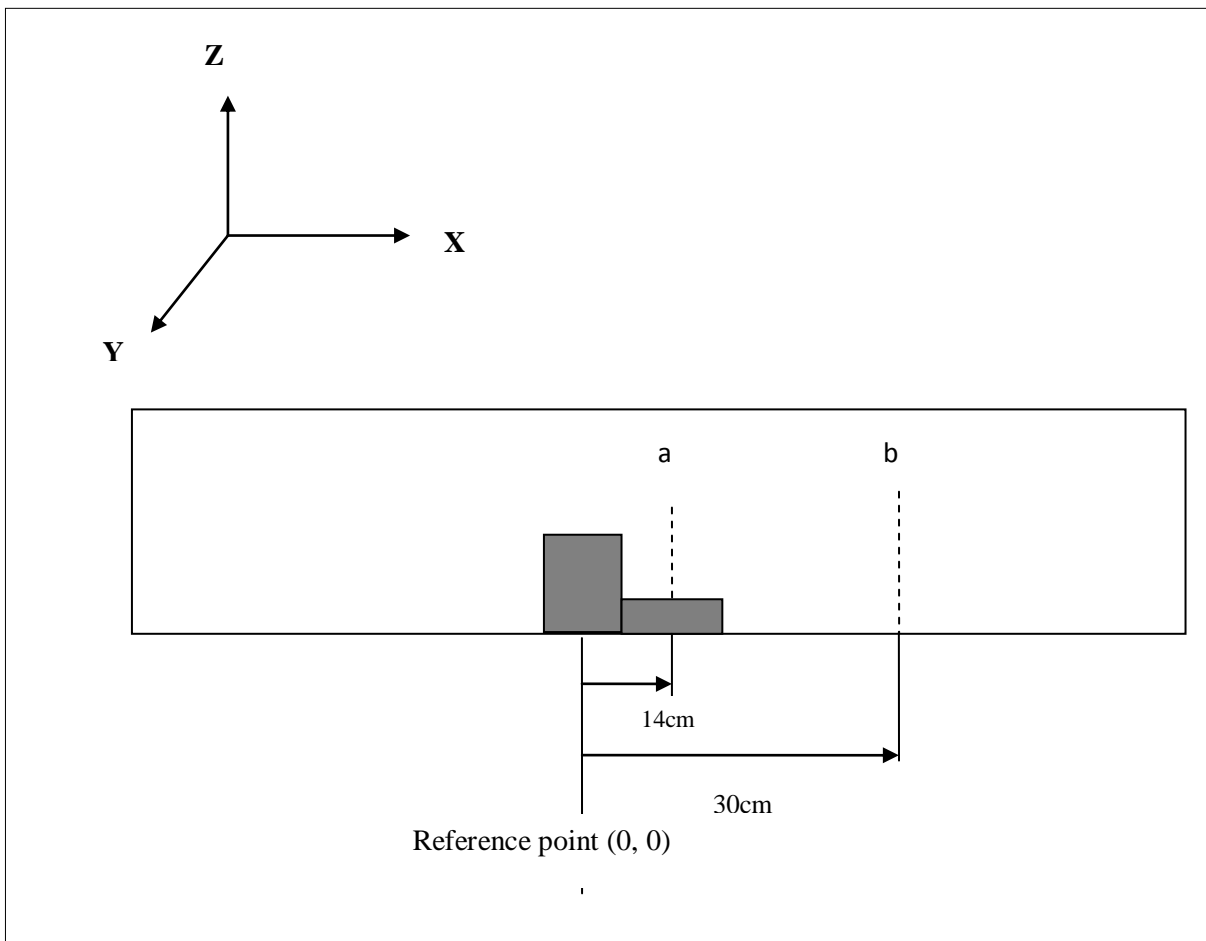
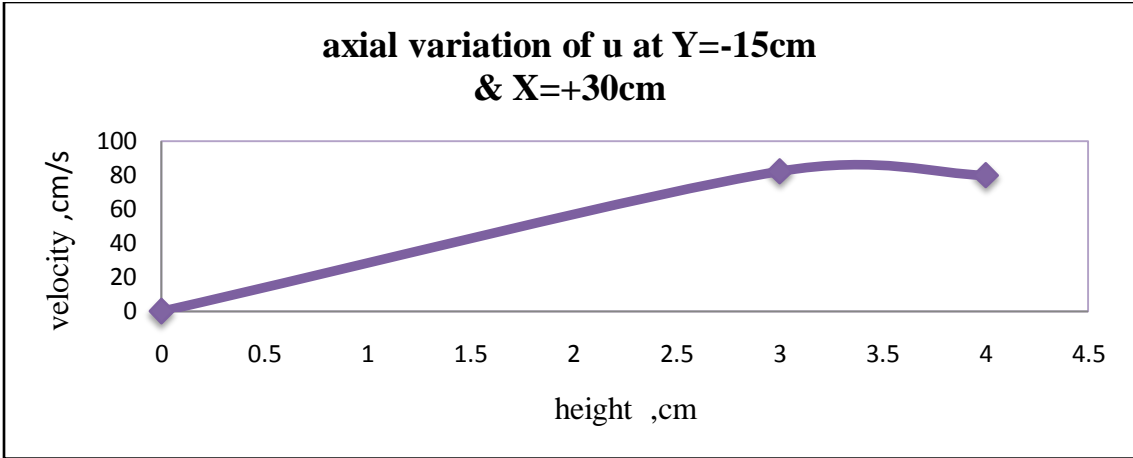
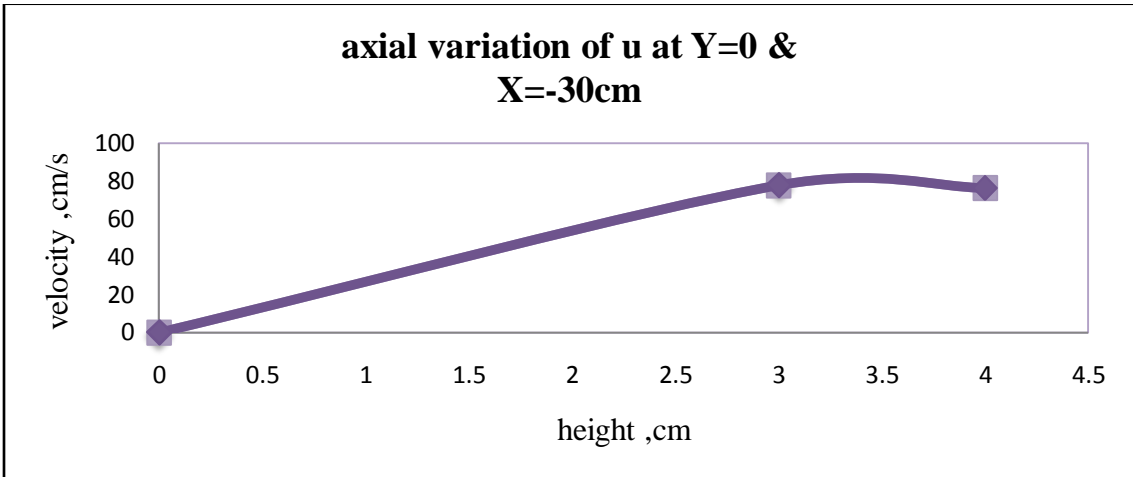


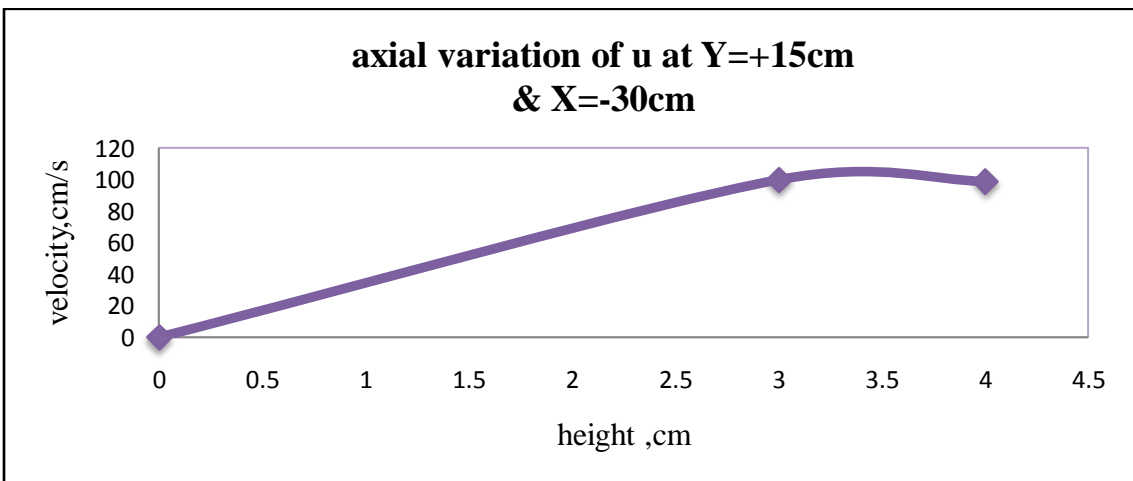
Fig 4.2.44, typical geometric drawing shown the position of measurement



Fig, 4.2.45, velocity distribution at y=-15cm



Fig, 4.2.46, velocity distribution at y=0



Fig, 4.2.47, velocity distribution at y=+15cm

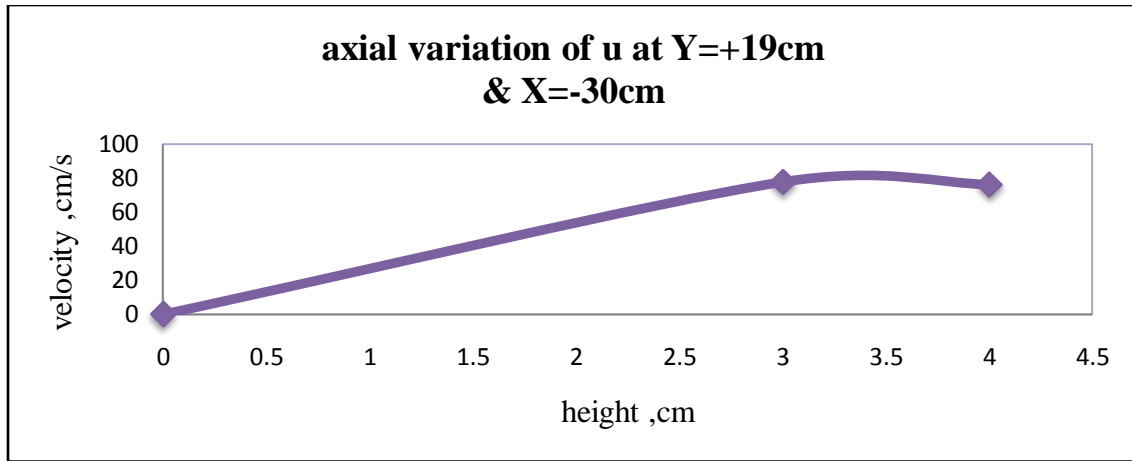


Fig. 4.2.48, velocity distribution at y=19cm

The fig 4.2.45, 4.2.46, 4.2.47, 4.2.48 are similar type looks alike pattern. The velocity distribution is parabolic type. From above graphs the velocity increases approx at the height of 3cm maximum and reduces after that.

**Reading of Type B baffle at downstream:**

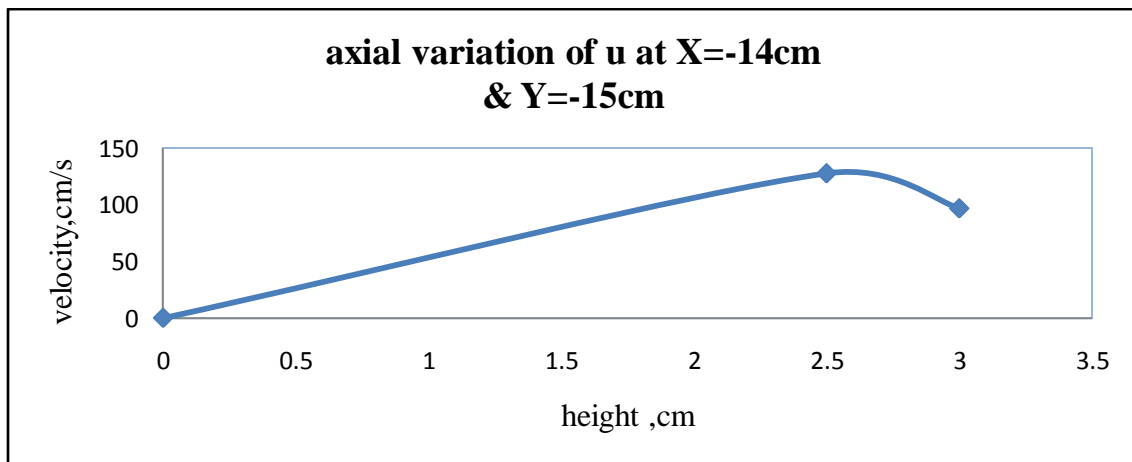
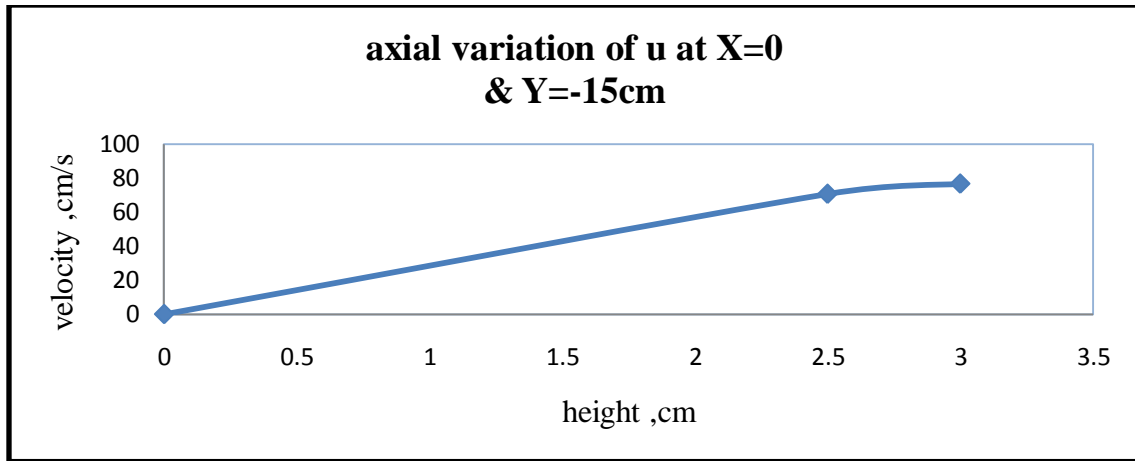
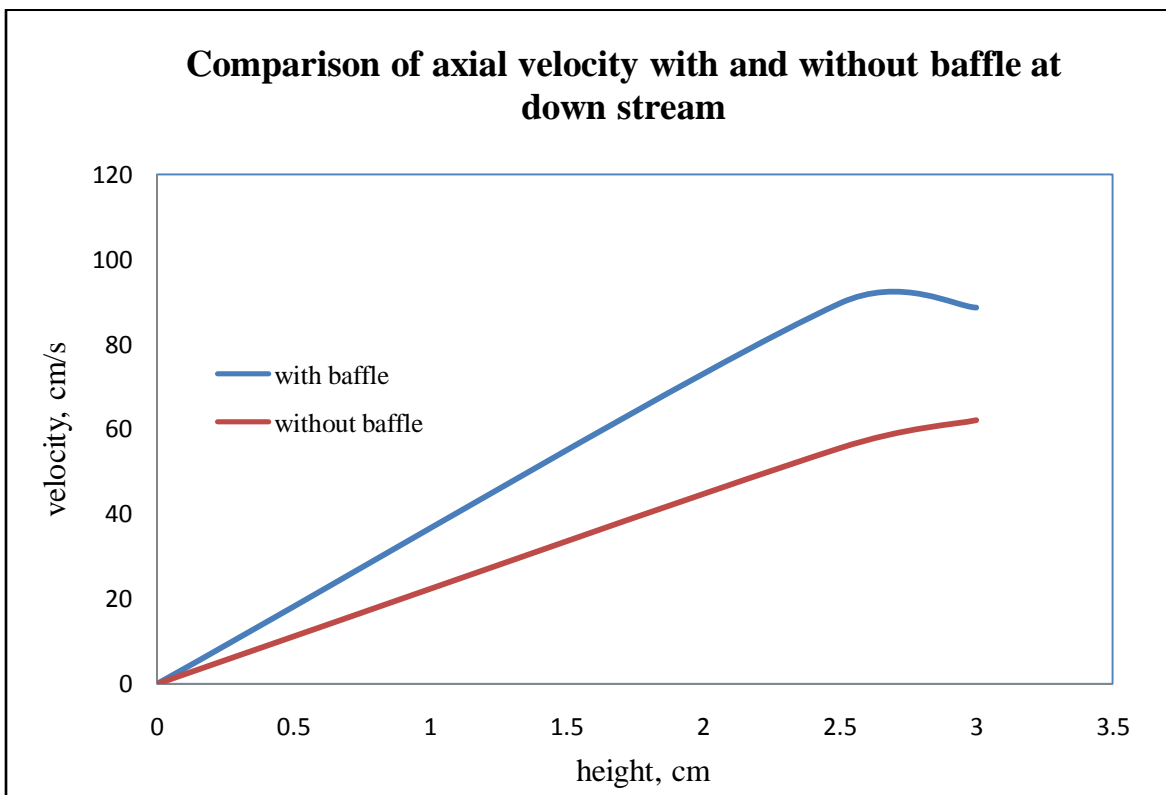


Fig 4.2.49, velocity distribution at X= -14cm

For type B baffle the velocity distribution graph is almost same for fig 4.2.49 & fig 4.2.50. That means in downstream the profile are same. For almost near to baffle the highest velocity is about 2.5cm and for 15cm away from baffle it is little bit less.



*Fig. 4.2.50, velocity distribution at X= 0*



*Fig.4.2.51, Comparison of velocity profile for flow with and without baffle*

In this figure above we observed that the variation of stream wise velocity is linear up to the point little below from the free surface. However the slope of the curve is more for with baffle.

This is due to the fact that the area decreases with the baffle so to obey the conservation of mass law. The velocity with the baffle must increase. However there is an undershoot near the free surface. This undershoot is more prominent for the case of open channel flow with baffle. This may be attributed due to the fact that with the baffle the shear stress generated at the free surface is much more than without baffle. Therefore, the resistance is more for the presence of baffle this causes more reduction of velocity for decreases of with baffle producing higher undershoot.

# Conclusion

---

## **CONCLUSION**

An experimental and numerical study of the open channel flow in a rectangular channel with and without baffle has been performed. The current meter has been used for measuring the velocity field. It was found that the measurement follows physics of the flow satisfactorily. The recirculation and effect of baffle has been observed accurately. From the numerical study it has been observed that there are several low pressure zones before, on and after the baffle respectively. The size of the recirculation bubble on the baffle is maximum or comparable with the same one after the baffle. It has been noted that the velocity at the free surface is not maximum and the maximum velocity is observed to be resided a few distance below. Both numerical and experimental results show this tendency. Though different shapes of the baffle were used, but the subtle differences are yet to be determined with better accuracy. However, an attempt has been taken to identify which shape to be the best possible for better open channel flow for the aquatic life such as fish etc. for their movement in rivers, streams etc.

## **FUTURE SCOPE OF WORK**

The boundary condition taken was laminar and steady fluid flow conditions. However there are enough scopes for measuring such a flow under turbulent condition. Also using different types of baffle with different roughness and introducing transitional flow would be very challenging future scope of work. A numerical study with k-e model or LES would have been a better option under such turbulent flow conditions. The author wishes to do these works in future as further research work if funding is available.

## References

---



## **REFERENCES**

- [1] Pandtl, L., (1933) “Recent Results of Turbulent Research”, translation by National Advisory Committee for Aeronautics, TM 720.
- [2] Von Karman, T., (1921) “On laminar and Turbulent Friction”, translation by National Advisory Committee for Aeronautics, TM 1092.
- [3] Von Karman T., (1930) “Mechanical Similitude and Turbulence”, translation by National Advisory Committee for Aeronautics, TM 611.
- [4] Nikuradse, J., (1950) “Laws of Turbulent Flow in Rough Pipes”, translation by National Advisory Committee for Aeronautics, TM 720.
- [5] Vanoni, V.A, (1941) “Velocity Distribution in Open channels”, Civil Engineering, **11**(6), pp. 356-357.
- [6] Tracy, H.J., and Lester, C.M., (1961) “Resistance Coefficients and velocity Distribution- Smooth Rectangular Channel,” Water Supply Paper 1592-A, U.S Geological Survey.
- [7] Launder, B.E., Spalding D.B, (1974) “The numerical computational of turbulent flow”, computer methods in Applied mechanics and Engineering **3**(2), pp. 269-289.
- [8] Perkins H.J., (1970) “The formation of stream wise vorticity in turbulent duct flow”, Journal of Fluid Mechanics **44**(4), pp. 721-740.
- [9] Yan. J, Wu Tang.H, Xiao.Y, Li.K,Jun Tian.Z, (2011) “Experimental Study on Influence of Boundary on Location of Maximum Velocity in Open Channel flows”, Water Science and Engineering, **4**(2), pp. 185-191
- [10] Bonakdari .H, Lipeme Kouyi .G, Asawa .G, (2014), “Developing Turbulent Flows in Rectangular Channels: A Parametric Study”, Journal of Applied Research in Water and Waste Water, **1**(2), pp. 53-58.
- [11] Burger, J., Haldenwang, R. and Alderman, N., (2010) “Experimental database for non-Newtonian flow in four channel shapes”, Journal of Hydraulic Research, **48**(3), pp. 363-370,

- [12] Gandhi .B.K., Verma, H.K., Abraham, B., (2010), “Investigation of Flow Profile in Open Channels CFD”, IGHM-2010, Oct. 21-23, 2010, IIT Roorkee, India.
- [13] Schlichting, H., “Boundary Layer Theory”, McGraw Hill, 1979
- [14] Sooky, A. A., (1969) “Longitudinal dispersion in Open Channels”, Journal of Hydraulic Division of American Society of Civil Engineering, Engineering, **95**(4), pp. 1327-1346.
- [15] Bogle, G. V., (1997), “Stream Velocity Profiles and Longitudinal Dispersion”, Journal of Hydraulic Engineering Trans ASCE, **123**(9), pp. 816.
- [16] Deng, Z., Singh, V. P. and Bengtsson, L., (2004) “Longitudinal Dispersion Coefficient in Straight Rivers”, Journal of Hydraulic Engineering Trans ASCE, **127**(1), pp. 919-927.
- [17] Seo, Won II and Baek, K.O., (2004) “Estimation of the longitudinal dispersion coefficient using the velocity profiles in natural streams”, Journal of Hydraulic Engineering Trans ASCE, **130**(3), pp. 227-236.
- [18] ABSI, R., (2011) “An ordinary differential equation for velocity distribution and dip-phenomenon in open channel flows”, Journal of Hydraulic Research, IAHR, Taylor and Francis, **49**(1), pp. 82-89.
- [19] Mohanta<sup>1</sup>, A., Naik, B., Patra, B.K., and Khatua, B.K., (2014) ”Experimental and Numerical Study of Flow in Prismatic and Non-prismatic Section of a Converging Compound Channel”, International Journal of Civil Engineering Research, **5**(3), pp. 203-210.
- [20] Patil, S., Kostic, M., and Majumdar.P. (2009) “Computational Fluid Dynamics Simulation of Open-Channel Flows Over Bridge-Decks Under Various Flooding Conditions”, Proceedings of the 6th WSEAS International Conference on FLUID MECHANICS.
- [21] Razmi, A.M., Bakhtyar, R., Firoozabadi, B., and Barry, D.A., (2013) “Experiments and numerical modeling of baffle configuration effects on the performance of sedimentation tanks”, Canadian Journal of Civil Engineering, **40**(2), pp. 140-150.

- [22] Tamayol, A., Firoozabadi, B., and Ahmadi, G., (2008) "Determination of settling tanks performance using an Eulerian-Lagrangian method", *Journal of Applied Fluid Mechanics*, **1**(1), pp. 43–54.
- [23] Ekama, G.A., Barnard, J., and Gunthert, F., (1997) "Secondary settling tanks: Theory, modeling, design and operation", IWA Scientific and Technical Rep. No. 6, International Water Association, London, UK.
- [24] Shahrokhi, M., Rostami, F., Md Said, M.A., Sabbagh-Yazdi, S., Syafalni, S., and Abdullah, R. (2012) "The effect of baffle angle on primary sedimentation tank efficiency", *Canadian Journal of Civil Engineering*, **39**(3), pp. 293-303.
- [25] Shahrokhi, M., Rostami, F., Md Said, M.A., Sabbagh-Yazdi, S., and Syafalni, S., (2011) "The effect of number of baffles on the improvement efficiency of primary sedimentation tanks", *Applied Mathematical Modelling*, **36**(8), pp. 3725-3735.
- [26] Rostami, F., Shahrokhi, M., Md Said, M.A., Abdullah, R., and Syafalni, S., (2011) "Numerical modeling on inlet aperture effects on flow pattern in primary settling tanks", *Applied Mathematical Modelling*, **35**(6), pp. 3012-3020.
- [27] Jamshidnia, H., Takeda, Y., Firoozabad, B., (2011) "Effect of a standing baffle on the flow structure in a rectangular open channel", *Journal of Hydraulic Research*, **48**(3), pp. 400-404.
- [28] Pu, J.H, (2013) "Universal Velocity Distribution for Smooth and Rough Open Channel Flows", *Journal of Applied Fluid Mechanics*, **6**(3), pp. 413-423.
- [29] Karimi, M, Theuri, D, Kinyanjui M, (2014) "Modeling Fluid Flow in an Open Rectangular Channel with Lateral Inflow Channel", *International Journal of Sciences: Basic and Applied Research*, **17**(1), pp. 186-193.
- [30] Fan, P. and Li, J.C., (2006) "Diffusive wave solutions for open channel flows with uniform and concentrated lateral inflow", *Advances in Water Resources*, **29**(7) pp. 1000-1019.
- [31] Henderson, F.M., "Open Channel Flow. Macmillan Publishing Company", New York, 1966.

- [32] Bilgil, A., (1998) “The effect of wall shear stress on friction factor in smooth open channel flows”, Ph. D. Thesis, Karadeniz Technical University, Trabzon, Turkey.
- [33] Chadwick, A. and Morfett, J., (1993) “Hydraulics in Civil Engineering and Environmental Engineering”, Chapman and Hall, pp. 187-200.
- [34] .Lee, Y. S. and Smith, L. C., (1986) “Analysis of power-law viscous materials using complex stream, potential and stress functions”, in Encyclopedia of Fluid Mechanics, vol.1, Flow Phenomena and Measurement, ed. N. P. Chermisinoff, pp. 1105-1154.
- [35] Moffatt, H. K., (1964) “Viscous and resistive eddies near a sharp corner”, Journal of Fluid Mechanics, **18**(1), pp. 1-18.
- [36] Roache, P. J., (1972), Computational Fluid Dynamics, Hermosa, New Mexico, pp. 139-173.
- [37] Taylor, T. D., and Ndefo, E., (1971) “Computation of viscous flow in a channel by the method of splitting”, Proc. of the Second Int. Conf. on Num. Methods in Fluid Dynamics, Lecture Notes in Physics, vol. 8, pp. 356–364, Springer Verlag, New York.
- [38] Durst, F., and Peireira, J. C. F., (1988) “Time-dependent laminar backward facing step flow in a two-dimensional duct”, Journal of Fluids Engineering, **110**(3), pp.289-296.
- [39] . Alleborn, N., Nandakumar, K., Raszillier, H., and Durst, F., (1997) “Further contributions on the two-dimensional flow in a sudden expansion”, Journal of Fluid Mechanics, **330**, pp. 169-188.
- [40] Kim, J., and Moin, P., (1985) “Application of a fractional-step method to incompressible Navier-Stokes equations”, J. Computer. Phys., **59**(2), pp. 308–323.
- [41] Armaly, B. F., Durst, F., Peireira, J. C. F., Schonung, B., (1983) “Experimental and theoretical investigation of backward-facing step flow”, J. Fluid Mech., **127**, pp. 473-496.
- [42] Gartling, D. K., 1990, “A test problem for outflow boundary conditions-flow over a backward-facing step”, Int. J. Numer. Methods Fluids **11**(7), pp. 953-967.

- [43] Lee, T., and Mateescu, D., (1998) “Experimental and numerical investigation of 2D backward-facing step flow”, *J. Fluids Structures*, **12**(6), pp. 703-716.
- [44] Le, H., Moin, P., and Kim, J., (1997) “Direct numerical simulation of turbulent flow over a backward-facing step”, *Journal of Fluid Mechanics*, **330**, pp. 349-474.
- [45] Heenan, A. F., and Morrison, J. F., (1998) “Passive control of back step flow”, *Experimental Thermal and Fluid Science*, **16**(1-2), pp. 122-132.
- [46] Williams, P. T., and Baker, A. J., (1997) “Numerical simulations of laminar flow over a 3D backward-facing step”, *Int. J. Numer. Methods Fluids*, **24**(11), pp. 1159-1183.
- [47] Barkley, D., Gomes, M. G. M., and Henderson, R. D., (2002) “Three dimensional instability in flow over a backward-facing step”, *Journal of Fluid Mechanics*, **473**, pp. 167-190.
- [48] Biswas.G.,Breuer.M., Durst.M.,(2004) “Backward-Facing Step Flows for Various Expansion Ratios at Low and Moderate Reynolds Numbers”, *Journal of Fluids Engineering*, Vol. 126.
- [49] Fan, P. and Li, J.C., (2006) “Diffusive wave solutions for open channel flows with uniform and concentrated lateral inflow”, *Advances in Water Resources*, **29**(7), pp. 1000-1019.
- [50] White, F. M., “Fluid Mechanics”, McGraw-Hill Publication, Fifth edition, 2003.
- [51] Salami, L.A., “On velocity-area methods for asymmetric profiles”, University of Southampton Interim Report V, 1972.
- [52] Barkley, D., Gomes, M. G. M. and Henderson, R.D., (2002) “Three-dimensional instability in flow over a backward-facing step”, *Journal of Fluid Mechanics*, **473**, pp. 167-190.
- [53] Lyn, A and Rodi, W, (1990) “Turbulence measurements in model settling tank”, *Journal of Hydraulic Engineering*, **116**(1), pp. 3-21.
- [54] Anadromous Salmonid Passage Facility Design, National Marine Fisheries Service Northwest Region, February 2008.

## Annexure I

### The Empirical Formula for the Propeller Type Current meter

Current Meter No. 11449 Type :Lab

V = water velocity in ft per sec

n = Number of Revolutions per sec

<b>Propeller No. 1</b>		<b>Propeller No. 1-2</b>	
n = for all	$V = 0.1804n + 0.105$	n < 5.00	$V = 0.1508n + 0.380$
		n > 5.00	$V = 0.1738n + 0.295$
<b>Propeller No.2</b>		<b>Propeller No. 2-2</b>	
n < 1.30	$V = 1.2952n + 0.115$	n < 4.39	$V = 0.2939n + 0.380$
n > 1.30	$V = 0.3329n + 0.066$	n > 4.39	$V = 0.3313n + 0.328$
n < 2.80			
n > 2.80	$V = 0.3411n + 0.043$	n < 7.69	$V = 0.3411n + 0.253$
		n > 7.69	
<b>Propeller No.3</b>		<b>Propeller No. 1-3</b>	
n < 0.97	$V = 0.7324n + 0.141$	n < 3.41	$V = 0.1670n + .203$
n > 0.97	$V = 0.8233n + 0.052$	n > 3.41	$V = 0.1804n + 0.157$
n < 4.33			
n > 4.33	$V = 0.8311n + 0.010$		
<b>Propeller No. 4</b>		<b>Propeller No. 2-3</b>	
n < 0.53	$V = 1.415n + 0.203$	n < 5.00	$V = 0.1508n + 0.380$
n > 0.53	$V = 1.6761n + 0.066$	n > 5.00	$V = 0.1738n + 0.295$
n < 2.00			
n > 2.00	$V = 1.7056n + 0.007$		
<b>Propeller No. 3a</b>			
n < 0.64	$V = 0.6908n + 0.111$		
n > 0.64	$V = 0.8233n + 0.046$		
n < 2.50			
n > 2.50	$V = 0.8364n + 0.013$		